Simple Yet Versatile Fluorescent Labeling Methods for Advanced Microscopy Techniques

Chenyi Mao

A dissertation

submitted in partial fulfillment of the

requirements for the degree of

Doctor of Philosophy

University of Washington

2021

Reading Committee:

Dr. Joshua C. Vaughan, Chair

Dr. Bo Zhang

Dr. Dan Fu

Program Authorized to Offer Degree:

Chemistry

University of Washington

Abstract

Simple Yet Versatile Fluorescent Labeling Methods for Advanced Microscopy Techniques

Chenyi Mao

Chair of the Supervisory Committee:
Dr. Joshua C. Vaughan
Departments of Chemistry and Physiology & Biophysics

Advanced microscopy techniques have undergone rapid development in recent years and now enable the comprehensive 3-dimensional analysis of intact biological specimens over a wide range of length scales. Despite these advances, the technologies for labeling specimens and which are critical to their success have developed at a slower pace. Immunofluorescence and fluorescent protein tags that have been used for decades are still the two dominant methods in use today. Although powerful, they still face several limitations such as slow labeling speed due to the antibody's large size (particularly for thick specimens), inconsistent reproducibility due to antibody variability, and complicated processing due to the required genetic manipulation of the specimen (if possible) when using fluorescent proteins. In addition, the labeling efficiency is challenging for both approaches because many antibodies are unable to bind heavily fixed or processed specimens, and fluorescent protein can dimerize or otherwise perturb the normal function of the organism and may become nonfluorescent due to denaturation and/or dissociated during potentially harsh sample processing conditions. Here, I present a new labeling method that is inspired by well-established histological staining. The new labeling method uses commercially

available reagents to efficiently map the distributions of proteins and oxidized carbohydrates of various specimens, so it is simple, versatile, and easily accessible. I also demonstrate its powerful utility when combining with advanced microscopy techniques and/or immunofluorescence. Additionally, I provide step-by-step procedures for a range of specimens and address ways to customize and troubleshoot to help disseminate this method.

Table of Contents

List of Figures, Tables, and Video Captions

Acknowledgements

When starting this journey at UW, no one ever probed me what I was about to get into. Over the past six years, I have experienced far more highs and lows, both professionally and personally, than I could ever have imagined. Standing at this point and reflecting on any of these events, I am fortunate enough that I did not give up yet have gained unique experience that shaped me into the person I am today. I would like to take this opportunity to recognize and thank some of the individuals who share and play indispensable role throughout my journey.

I would not be where I am today without having Joshua Vaughan agreed to take me as his first transferred graduate student. When I met Josh for the first time, I was struggling with my previous research group and was trying to identify a new direction I can embark on. Acknowledging my lack of relevant research background, Josh was willing to invest in my enthusiasm, and offer me an opportunity. My time in his lab witnesses his unmatched dedication to his students and his rigorous professional acumen as a scientist. Not only does he constantly discuss projects with me on a weekly basis, but he also offers help whenever needed. Josh is also an amazing teacher who always shows extreme patience. He guides me to think critically and encourages me to test preliminary hypotheses. As a scientist, Josh keeps challenging us to be better and to ensure that we do succeed. I have learned tremendous amount of knowledge from Josh, and I can certainly say that I would not keep pursuing science without getting well-trained in his lab. Josh, I truly thank you for being a fantastic mentor and I hope I can be a scientist as good as you are one day.

I also would like to give special thanks to Aaron Halpern, Tyler Chozinski, and Min Yen Lee. Aaron and Tyler are like big brothers to me. They taught me expansion microscopy, immunolabeling, confocal microscopy, and other skills so I can pick up and adapt these skills to my projects as soon as possible. In addition, they have always made themselves available to lend a hand, to troubleshoot experiments, and to share their wisdom. Min Yen is a great lab partner I have had the privilege of working closely with. We formed an alliance that went through plenty of weekly meetings with Josh, tried to convince josh to forego certain experiments that we want to deprioritize, and spent many hours in the microscope room to acquire nice images even during the pandemic. Min Yen, I am grateful for having someone to bounce ideas off and having a lab partner to work together with.

My thanks also extend to other current and former members of the Vaughan lab: Marcus Woodworth, Adilijiang Ali, Ziyu Guo, Chetan Poudel, Madeline Wong, Lauren Gagnon. Marco Howard, Danying Lin, Ethan Vo, Jonathan Perr, Zachariah Fincher, Jing-Ru Jhan, and Leonard Shin. All of you make the working environment feels a lot like family. I am going to miss working with you all. Moreover, I would like to recognize the labs of Dr. Jonathan T.C. Liu, Dr. Stuart Shankland, Dr. Charles Alpers, and Dr. Lih Lin for collaboration on various projects.

Last but not least, I would like to thank two special friends and my family. Zonglong and Jun, who encouraged me to switch to a new research group and offered insightful opinions. I thank you for all your supports throughout the years. I would be regretful if I did not mention my parents who express unconditional love and believes in me. Mom and Dad, there are not enough pages for me to fill in all the details you have done for me, but I wanted to particularly thank you for sending me across the Pacific Ocean while you are bearing missing. I also want to thank my relatives who have taken good care of my parents while I was away. Thank you and I love you all!

Dedication

This thesis is dedicated to my mother.

Chapter 1
Introduction

1.1 Confocal Microscopy

Microscopy enables the visualization of complex biological systems and their associated activities that are too small to be clearly seen by the unaided eye. For example, scientists discovered cells are the fundamental units of all known biological systems, and a cell is made up of various components that work together to generate energy, synthesize proteins, and accomplish other functions. Thus, microscopy offers the ability to decode the mysteries of life. Moreover, Marqués et al. recently reported that in a survey of 240 research articles from eight major biomedical research journals, 77% of articles reported microscopy data, and 50% of figures included at least one microscopy image[1]. Most images were acquired by optical microscopy, but a small fraction were recorded with electron microscopes or other non-optical methods. Microscopy is thus an indispensable tool of modern biomedical research.

Fluorescent probes are substances that absorb a specific wavelength of light and emit light of a longer wavelength generating fluorescence emission with high contrast over their surroundings. Because of this unique property, a subclass of optical microscopy, called fluorescence microscopy, uses fluorescent probes to highlight specific structures of interest so the fluorescence emission from a labeled target can be revealed with high contrast over background signal and with good signal to noise. Furthermore, multiple targets may be studied simultaneously by labeling them with fluorescent probes that have different absorption and/or emission wavelengths. Given the complexity of biological specimens that involve hundreds and thousands of molecular mechanisms, being able to achieve multiplexed readout with a superb specificity is a powerful capability that is widely used in the biomedical research community.

Although fluorescence micrographs are often displayed as two-dimensional images on a computer screen or sheet of paper, biological specimens are in fact three-dimensional objects. Most fluorescence microscopes excite fluorescence from the full depth of a sample and, particularly for thick samples, it can be a challenge to detect light from one focal plane while out-of-focus fluorophores also emit fluorescence that decreases contrast and can obscure signals of interest. Confocal microscopy was designed to remove the out-of-focus fluorescence. Although confocal microscopy has other advantages, being able to remove the out-of-focus fluorescence remains a major advantage and makes it one of the most important tools used to study complex biological systems[2].

1.1.1 A Brief Introduction to Laser-Scanning Confocal Microscopy

Ever since the invention of the first confocal microscope by Marvin Minsky[3], several types of confocal microscopy have been introduced that include laser-scanning confocal microscopy, slit-scanning confocal microscopy, and spinning disk confocal microscopy[2]. This chapter confines the discussion to laser-scanning confocal microscopy for its major role in this thesis. A simplified scheme of a laser-scanning confocal microscopy system is shown in **Figure 1.1**. An excitation beam from a laser light source is focused to a point by the objective lens and laterally scanned within the specimen in order to excite fluorophores within the sample. The emission light from the fluorophores labeling the specimen is brought to focus by the same objective lens and detected by a photomultiplier tube. Since the emitted fluorescence is usually several orders of magnitude weaker than the excitation beam, it is essential to carefully remove scattered

or reflected excitation light from the emission light. This task is achieved using a combination of a dichroic mirror and an emission filter. The dichroic mirror serves as a beam splitter that reflects excitation light but allows emission light to be transmitted. Typical dichroic mirrors can do this with ~95% efficiency (**Figure 1.1**). An emission filter is placed in the detection path between the dichroic mirror and detector (**Figure 1.1**) and, when properly configured, can suppress excitation light approximately one million-fold while transmitting 80% or more of the fluorescent signal. Together the dichroic mirror and emission filter enable the sensitive and robust detection of small numbers of photons. The excitation light can then be raster-scanned throughout the sample in two or three dimensions in order to capture images.

A key feature of the confocal microscope, in particular, is the pinhole aperture in the detection path (**Figure 1.1**). It is able to block most light from fluorophores coming from above and below the focus plane in order to eliminate out-of-focus light. Doing so substantially reduces background, improves the contrast difference between the focused object and its surroundings, and greatly improves image quality. A narrow pinhole also helps to improve lateral and axial spatial resolution, but it comes at the cost of detection efficiency, and practitioners therefore must generally strike a compromise between resolution and signal levels.

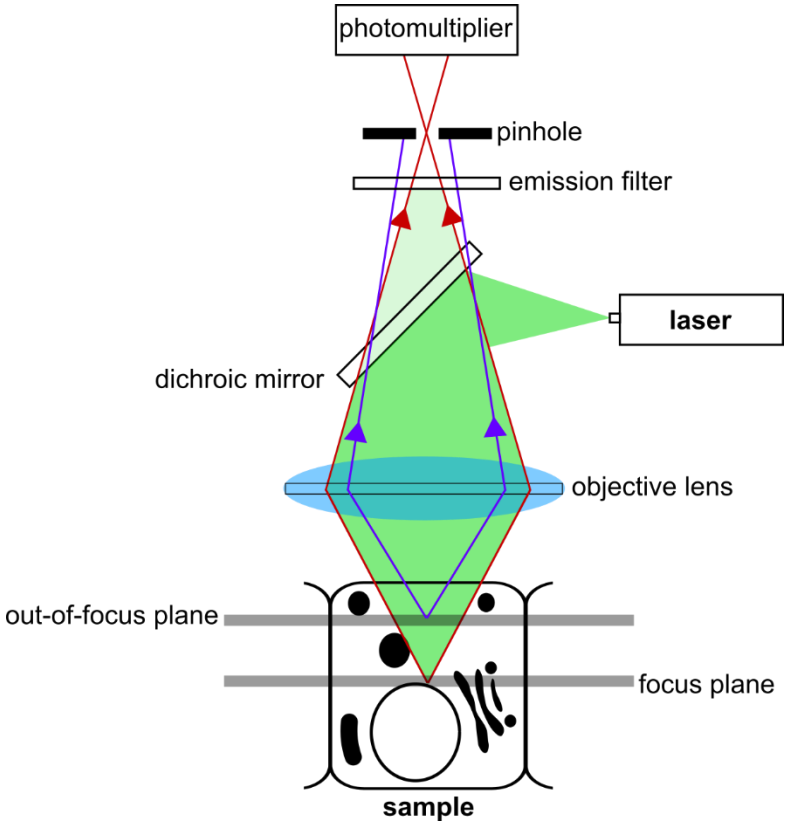

Figure 1.1 | Schematic illustration of a laser-scanning confocal microscope. The excitation light from the laser is shown in green and emission light generated from the focal plane and an out-of-focus plane is shown in red and purple, respectively. A small portion of the excitation light (light green) is blocked by the emission filter.

When the dynamics of a live specimen are being studied, the imaging mode can be further extended to a fourth dimension to capture multiple snapshots in time. Although extremely powerful, laser-scanning confocal microscopy suffers several key drawbacks that will be discussed further in the following sections. These include a limited spatial resolution and poor performance in thick specimens that scatter light[4,5].

1.1.2 Limitations of Laser-Scanning Confocal Microscopy

1.1.2.1 Spatial Resolution

Spatial resolution is usually defined as how closely two objects can be positioned but still be recognized as two separate objects. For the laser-scanning confocal microscope, the focal point illuminating the sample has a finite size that is determined primarily by the objective lens. While the lateral resolution is better than the axial resolution, the limiting factors are similar for both and this discussion will focus on lateral resolution.

When light emitted by a small fluorescent spot is collected by an objective lens and imaged onto a detector, it forms an image in the shape of an Airy disk (**Figure 1.2**). This occurs due to the diffraction of light at the pupil of the objective lens. According to Huygens's principle, waves that are in phase interfere constructively, whereas waves that are out phase interfere destructively. Most light will eventually arrive at the bright focal point of the Airy disk in phase, generating the brightest spot in the center, but dim rings are also observed surrounding the central spot. The radius of the first minimum of Airy disk is given by:

$$r = \frac{0.61\lambda}{NA} \quad [1]$$

where λ is the light wavelength, NA is the numerical aperture of the objective lens given by $NA = n \sin\theta$ for the index of refraction *n* (between the specimen and objective lens), and the half-angle θ for collection of light by the objective lens[2]. Equation [1] shows that a microscope's lateral spatial resolution is ultimately dependent upon the wavelength of light and the *NA* of the objective lens.

In 1873, Ernst Abbe described the lateral spatial resolution (minimum resolvable distance) of an optical microscope *d* using:

$$d = \frac{\lambda}{2NA} \quad [2]$$

where λ is the light wavelength and *NA* is the numerical aperture of the objective lens[6]. For laser-scanning confocal microscopy using visible light, the best achievable spatial resolution is ~200 nm along the lateral dimensions and ~500 nm along the axial dimension[7]. This limitation arises because the wavelengths of visible light are limited to ~400-700 nm and the *NA* of an objective lens cannot easily exceed ~1.4. Because of this intrinsic challenge, subcellular structures inside cells that are less than ~ 200 nm apart and their associated activities cannot be revealed, hindering scientists from a wide range of disciplines making fundamental biological discoveries. Therefore, in response to this resolution limit, there have been intense efforts over the past decades to reach the theoretical limits and to develop super-resolution microscopy techniques that can surpass this diffraction limit of visible light (see **Chapter 1.2.1**).

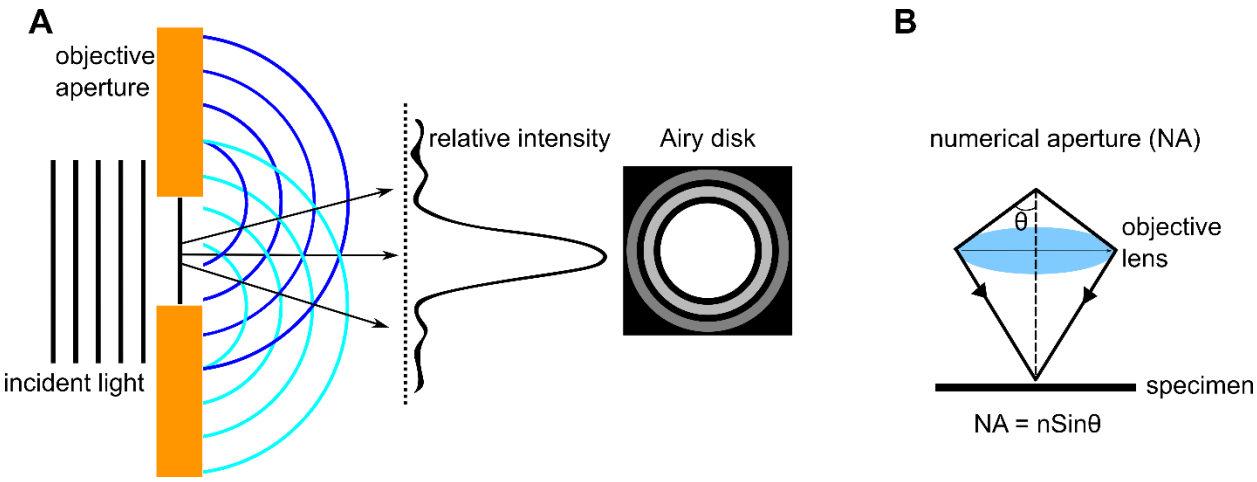

Figure 1.2 | (A) A demonstration of the formation of Airy disk pattern and a plot of its intensity profile along one direction. (B) An illustration of the half-angle θ of the incident light that determines the numerical aperture NA of the objective lens together with the index of refraction *n*.

1.1.2.2 Deep Imaging of Thick Specimens

Although laser-scanning confocal microscopy has contributed substantially to study complex biological systems, the imaging of most specimens thicker than ~100 µm is very challenging due to the scattering of light primarily caused by naturally occurring variations of refractive index within the specimen. When the excitation light illuminates a specimen, in addition to exciting fluorophores, the light wave also interacts with the specimen itself, and refractive index inhomogeneities within most samples ultimately lead to substantial scattering of the incident light in all directions so that the confocal excitation spot becomes much larger than it otherwise would. Scattering also occurs for the emitted fluorescence, and the net effect of scattering for excitation and emission is a hazy image with poor contrast, compromised spatial resolution, and low signal. Scattering is more prominent for thicker samples and for samples with larger inhomogeneities in the index of refraction.

To bypass the aforementioned limitations, biologists have utilized difficult volumetric reconstruction techniques that use manual sectioning of a thick specimen, imaging of all consecutive sections, and stitching the sequential images together[8,9]. Unfortunately, this approach is labor-intensive and frequently encounters artifacts due to sectioning and/or computational stitching distortions. Over the past decade, however, optical clearing techniques aiming to improve sample homogeneity via matching refractive index have been developed and demonstrated to be able to render 1 mm or thicker specimens highly transmissive[10–14]. Since sample refractive inhomogeneity can substantially degrade volumetric imaging, the combination of confocal microscopy with optical clearing techniques is particularly useful for the visualization of large intact specimens. Three groups of optical clearing techniques and the application of each group in kidney study are discussed in **Chapter 1.2.2** and **Chapter 1.3.3**, respectively.

1.1.3 A Brief Overview of Fluorescent Probes for Confocal Microscopy

To maximize the capabilities of confocal microscopy, it is imperative to have specimens fluorescently labeled. An ideal probe should, therefore, at least contain a targeting moiety that specifies the probe to the structure or molecule of interest, and a reporter group consisting of a fluorophore that indicates its location with high contrast. In the following, three fluorescent probes[15] – fluorophore-antibody conjugates, small-molecule probes, fluorescent proteins – that have been coupled with confocal microscopy to study live and fixed specimens for decades are briefly discussed.

1.1.3.1 Fluorophore-antibody Conjugates

Immunofluorescence is a labeling technique that uses fluorophore-antibody conjugates to label a specimen where the antibody functions as a targeting moiety against an antigen on a biological specimen and the fluorophore functions as a reporter group. The structural unit of an antibody contains four polypeptide chains, two heavy and two light chains, that are connected by four disulfide bonds (**Figure 1.3**). Each chain comprises one constant region and one variable region that accommodates antigen-binding specificity[16]. In mammals, the composition difference on the heavy chain serves to classify antibodies into five classes: IgG, IgE, IgD, IgA, and IgM[16]. Each class can be further divided into monoclonal and polyclonal antibodies. A polyclonal antibody is a heterogeneous mix of antibodies and can recognize multiple epitopes on the same antigen, whereas a monoclonal antibody is homogeneous with defined specificity to one epitope. Owing to the key difference, a polyclonal antibody is generally prone to have a higher chance to bind a given antigen but also higher lot-to-lot variability than a monoclonal antibody.

The formation of fluorophore-antibody conjugates is achieved via covalent coupling reactions. One of the most often selected reactions occurs between an antibody's primary amines and n-hydroxysuccinimide (NHS) ester functionalized fluorophores to form stable amide bonds. The reaction is favored due to its simplicity, mild conditions, and high efficiency[17]. There are two common options for the labeling of specimens with fluorophore-antibody conjugates[15] (**Figure 1.3**). For *direct immunofluorescence*, fluorophores are conjugated directly to the antigen-binding antibody. For *indirect immunofluorescence*, an unconjugated primary antibody is used to label an antigen of interest on the specimen in a first step, and then a fluorophore-conjugated secondary antibody is used to label the bonded primary antibody. Although the procedure is slightly more complex, indirect immunofluorescence is more common as it offers a flexible spectral choice of the fluorophore and it enables some signal amplification since more than one secondary antibody can bind a primary antibody. These come at the cost of experimental limitations with immunolabeling of multiple antigens on a specimen in order to avoid channel crosstalk arising from secondary antibodies binding more than one primary antibody.

Taken together, immunofluorescence uses antibodies to specifically bind molecules of interest and fluorophores to read out their locations with high contrast, and it serves as a highly useful tool in life science research. However, immunofluorescence still possesses several challenges such as slow labeling speed due to the antibody's large size (particularly for thick specimens), inconsistent reproducibility due to antibody variability, and strict performance dependence on antigen accessibility[18,19]. A primary focus of this thesis is to partially address these drawbacks (see **Chapter 2** and **Chapter 3**).

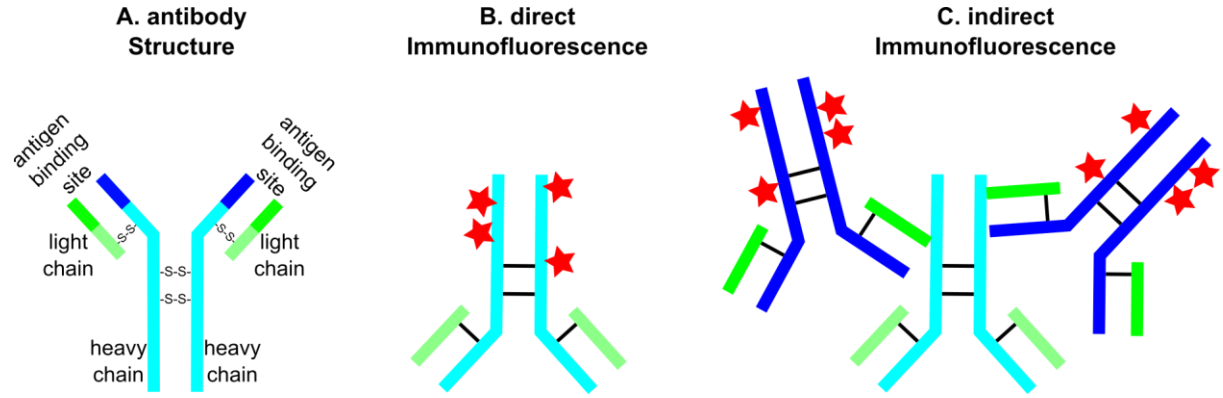

Figure 1.3 | (A) IgG antibodies are Y-shaped molecules that contain four polypeptide chains, two heavy chains, and two light chains, that are connected by four disulfide bonds. (B) Direct immunofluorescence is achieved by using a primary antibody that is itself labeled with a fluorescent dye (red stars). (C) Indirect immunofluorescence is achieved by using a primary antibody that is detected by a fluorophore-conjugated secondary antibody.

1.1.3.2 Small-molecule Probes

Another labeling method is to use key organic molecules that have been designed or discovered to be able to label specific cellular proteins, structures, or organelles. Some molecules are innately fluorescent, whereas others contain distinct binding moieties that are conjugated with fluorophores. Although the selection is not as diverse as antibodies, these organic molecules are smaller in size and their binding properties do not change considerably among different species, making them great alternatives when available. Herein, four examples against actin, lipid membranes, mitochondria, and nuclear DNA are introduced.

Phalloidin belongs to a class of phallotoxin that contains a bicyclic heptapeptide and selectively binds filamentous actin (F-actin) at an interface between monomers, rather than unpolymerized, globular actin (G-actin)[20]. Fluorescent phalloidin conjugates show sensitivity to F-actin at nanomolar concentrations and a similar affinity for both large and small filaments in live and fixed cells. Because of its convenience and reliability, a series of fluorophore-conjugated phalloidin is commercially available, and it has become a preferred choice over antibodies for actin labeling (**Figure 1.4**).

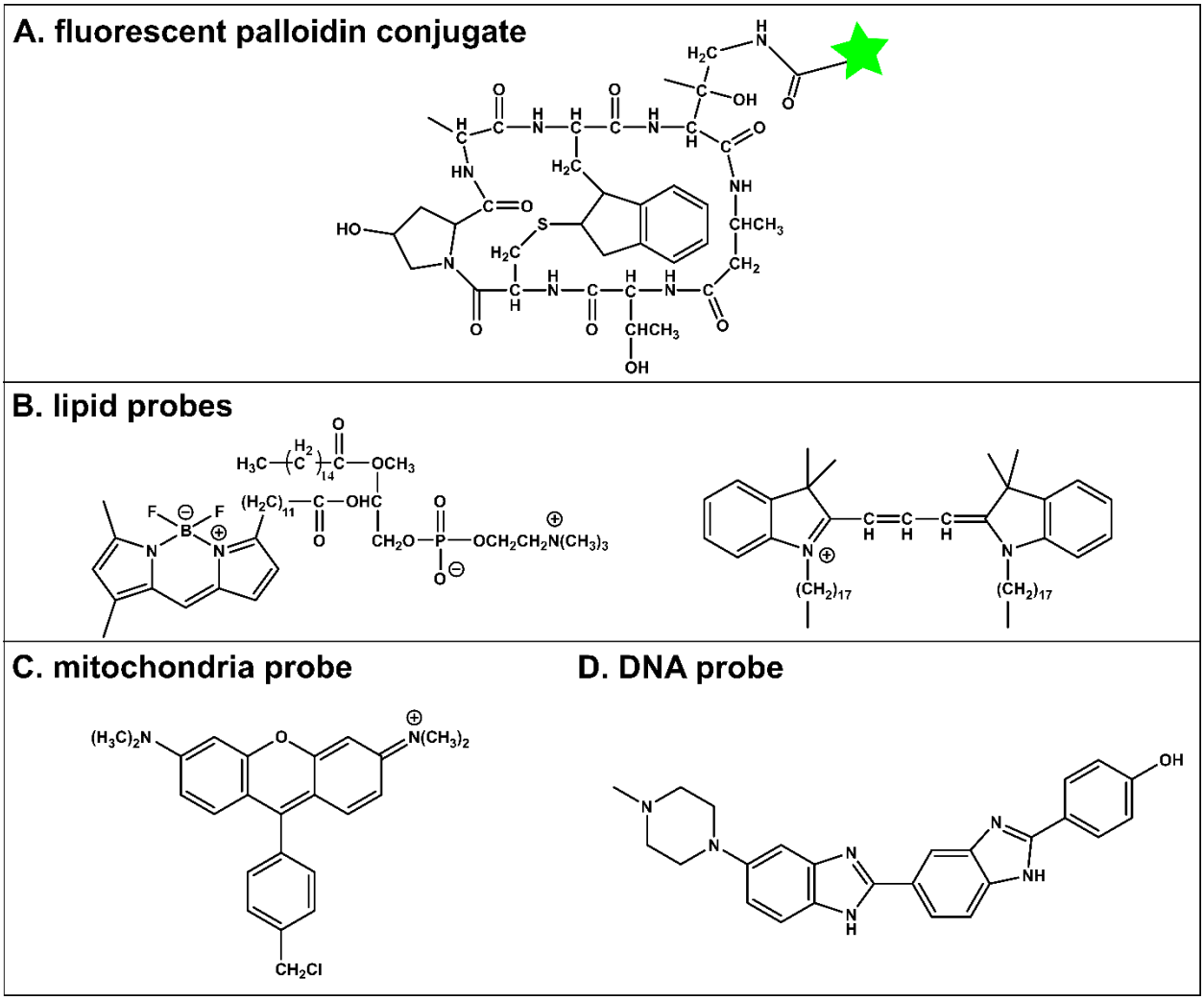

Figure 1.4 | Chemical structures of small-molecule probes for actin, lipid membranes, mitochondria, and nuclear DNA. (A) Phalloidin containing a bicyclic heptapeptide and bearing a fluorophore (green star) at the branch is an example of an actin probe. (B) BODIPY® FL dye-labeled glycerophosphocholine and $DiIC_{18}$ are examples of lipid tags. (C) MitoTracker® Orange is an example of a mitochondria probe. (D) Hoechst is an example of a DNA probe.

As the building block of the cellular membrane and some subcellular organelles, lipids are important in molecular recognition, signal transduction, and trafficking pathways[21]. Commercially available membrane probes can be broadly classified into two groups: fluorescent analogs of natural lipids and lipophilic fluorophores (**Figure 1.4**)[15]. Like fluorescent phalloidin conjugates, a fluorescent analog of a natural lipid uses a natural lipid for targeting and a fluorophore for reporting. Based on the differences in the composition and degree of unsaturation, the natural lipid part can be further divided into phospholipid and sphingolipid. In contrast, when a fluorophore is directly functionalized with a lipophilic tail, this fluorophore belongs to the second class, lipophilic fluorophore. The fluorophore moiety is generally charged and associates with the membrane surface, whereas the lipophilic tail is hydrophobic and inserts in the membrane. Although lipophilic fluorophores possess an intrinsic binding property, their limited water solubility often makes them hard to work with under physiological conditions[22].

In addition to lipid-selective fluorophores, fluorophores that have the intrinsic binding capability for mitochondria and the nucleus have also been investigated. Healthy mitochondria exhibit a difference in electrical potential between the interior and exterior of the inner mitochondrial membrane. Mitochondria-selective dyes, such as MitoTracker® Orange (**Figure 1.4**), take advantage of this and accumulate on the inner mitochondrial membrane[15]. Although the labeling has to be done with live cells, some MitoTracker® probes are fixable meaning the labeling will be retained even after the electric potential gets lost[23]. This is notable for allowing the use of these probes in combination with other assays.

DNA is an abundant and distinct component of the nucleus of cells, and an extensive selection of nucleus probes has been commercially available and studied based on their permeability, specificity, and binding mode. Cell membrane-permeable probes such as the Hoechst family are used in labeling live and fixed cells (**Figure 1.4**). On the other hand, cell membrane-impermeable probes such as the TOTO® family are limited to dead and fixed cells. Some nucleic acid probes have specificity to either DNA or RNA. Nucleic acid probes that bind both DNA and RNA could result in bright nuclear staining as well as cytoplasmic staining, compromising the signal to noise ratio. The TOTO® family is an example that binds RNA and DNA, while the Hoechst family is DNA-selective. For DNA-selective binding, corresponding probes can be further divided based on the binding mode: intercalation, bis-intercalation, minor groove binding, and external binding[24]. Although it is hard to summarize the binding pattern for all DNA-selective dyes, the fluorescent signals of many nucleic acid probes are enhanced after binding to DNA, which improves the contrast and, in some cases, can eliminate a washing step.

1.1.3.3 Fluorescent Proteins

The discovery of green fluorescence protein (GFP) from *Aequorea Victoria* jellyfish in the 1960s led to an invaluable tool that has revolutionized biological imaging. Unlike fluorophore-antibody conjugates and small-molecule probes, fluorescent proteins are used to tag target proteins of the living system via genetic manipulation, enabling researchers with the ability to visualizehe distribution of nearly any protein of interest in fixed or live cells. Therefore, there is no need for exogenous probes, and the technique avoids the problem of probe purification which makes it especially useful in live-cell studies that include tracking proteins of interest, monitoring protein-protein interactions, etc. A broad range of fluorescent proteins whose emission spectra span the visible spectral range has been developed over the past 25 years through mutagenesis or rational protein engineering of green fluorescence protein, or isolation of other fluorescent molecules from other sea organisms, and these probes have been widely adopted by the research community.

Although powerful, fluorescent proteins also face key limitations in their use. Some significant considerations include limited brightness or photostability, oligomerization or other perturbations to live specimens, poor performance in the far-red and near-infrared compared to organic dyes, a general limitation to the labeling of proteins rather than other biological molecules, and the requirement for genetic manipulation that is not typically possible, for instance, with non-model organisms or clinical (human) specimens[25]. Other specialized limitations can also occur for fluorescence proteins such as a limited maturation time or the need for oxygen during maturation, sensitivity to pH or other environmental factors, and low expression efficiency. Overall, fluorescent proteins are extremely powerful tools for the study of complex biological systems, but they are not suitable for many applications.

1.2 Advanced Fluorescence Microscopy Techniques

As discussed before, two key limitations of laser-scanning confocal microscopy are spatial resolution and deep imaging of thick specimens. Here, two advanced fluorescence microscopy techniques are presented to address these limitations. In particular, a recently introduced type of super-resolution microscopy called expansion microscopy focuses on bypassing the spatial resolution by physically enlarging specimens. On the other hand, optical clearing techniques work on homogenizing the components of specimens, so the scattering of light is minimized, making the deep imaging of thick specimens viable. In this section, both techniques are elucidated from introducing their basic principles to summarizing their variants and to discussing their considerations and limitations.

1.2.1 Expansion Microscopy (ExM)

1.2.1.1 Procedures and Mechanisms of ExM

Expansion microscopy (ExM) was first introduced by the Boyden lab at the Massachusetts Institute of Technology in 2015[26]. The key idea behind ExM is to physically expand specimens in three dimensions with extremely low distortion, allowing features closer than the diffraction limit of light to separate apart from each other and thus to become resolvable in the expanded state using conventional microscopy techniques. In the initial version of ExM, the general procedure includes four steps (**Figure 1.5**). First, a sample is immunostained with antibodies. However, unlike indirect immunofluorescence, a DNA oligonucleotide is conjugated with a secondary antibody. Then a complementary DNA oligonucleotide that has a methacryloyl group and a fluorophore on both ends is hybridized to the DNA oligonucleotide of the secondary antibody, making the protein of interest fluorescently labeled. Second, the methacryloyl group is incorporated into acrylamide-based swellable polymer hydrogel that is grown within and around the sample, leading to the formation of covalent linkages between fluorescent oligonucleotides and the polymer hydrogel. Third, proteinase K is applied to digest mechanically rigid structures that could potentially resist expansion. Because of the covalent linkages, fluorophores that have been anchored with the polymer hydrogel are retained during this process. Forth, the polymer hydrogel is soaked in deionized water to expand via dialysis. In detail, sodium acrylate, one of the polymer components, contributes to the high salt concentration inside the polymer at the unexpanded state. When soaked in deionized water, the salt concentration difference between the polymer inside and the outside induces an influx of water into the polymer, stretching the polymer chains and expanding the sample. In this initial version, a four-fold expansion in each dimension is achieved so the spatial resolution is improved to ~ 65 nm laterally.

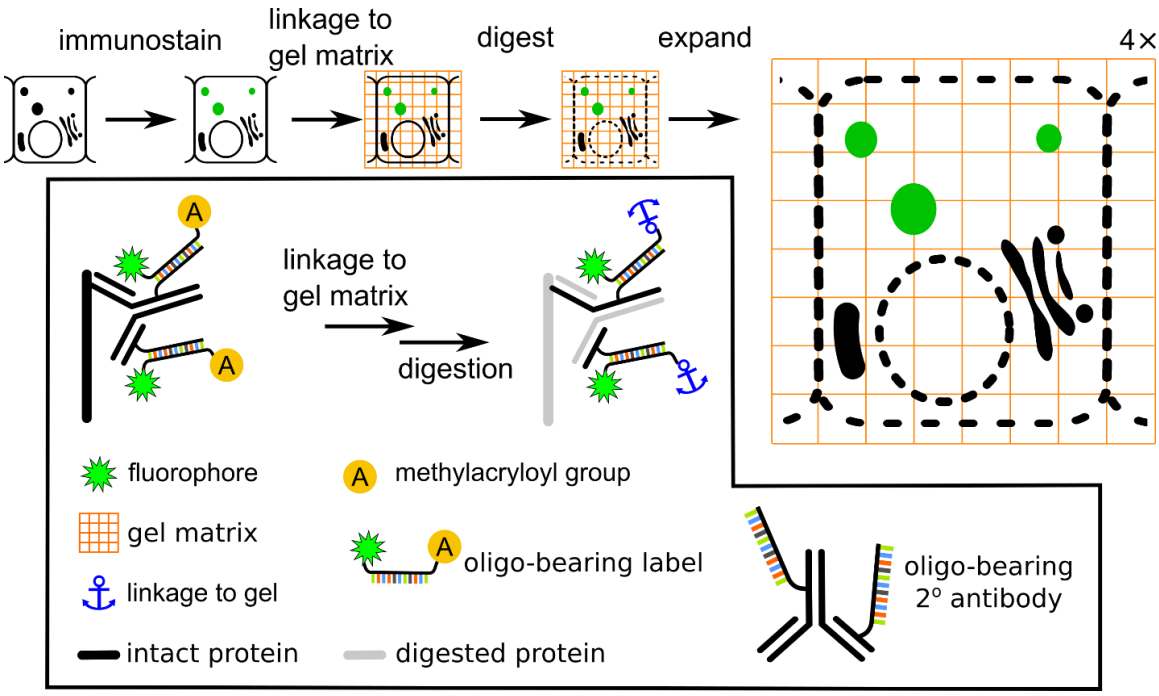

Figure 1.5 | Individual steps of the initial version of ExM are illustrated. The immunostaining step was performed using a custom DNA-conjugated secondary antibody. Then the immunostained sample was embedded in a swellable polymer hydrogel and the oligo-bearing fluorophores were linked to the hydrogel during its polymerization process. The sample was then digested with proteinase K before soaking in deionized water to achieve 4x expansion.

Unlike other super-resolution techniques that require expensive instruments and well-trained operators, ExM is compatible with conventional confocal microscopy which has been broadly accessible at research institutions making it practical for and familiar to most researchers. Additionally, given the expansion mechanism, an expanded sample is filled with water which means the refractive index is uniform throughout the sample, leading to an extremely low scattering and facilitating deep imaging. Because of the power of ExM, extensive studies have been investigated and several variants have been developed since the initial version to further improve its performance.

1.2.1.2 A summary of Existing Variants of ExM

The initial version of ExM uses customized DNA-conjugated antibodies which requires a multistep preparation and expensive reagents. In addition, given the limited modifiable sites on the DNA nucleotide and the intrinsic charge of the DNA nucleotide, it will bear fewer fluorophores than antibody, which leads to a dim signal and eventual problems with photobleaching of fluorophores. This flaw is further exaggerated after expansion since expansion leads to reductions in fluorescence signal intensities (due to dilution) together with a requirement for more exposures to measure the larger volume of the specimen. Our group improved the ExM protocol by the use of an amine-reactive small molecule methacrylic acid N-hydroxysuccinimidyl ester (MA-NHS)[27]. MA-NHS can be applied to a biological specimen already immunolabeled with standard (non-DNA) commercially available fluorescent antibody molecules in order

to form covalent linkages between the antibody and a subsequently grown hydrogel polymer. In addition, this MA-NHS method helps the retention of intrinsic fluorescent protein signal and thus enables direct imaging after expansion. Shortly after, a similar approach that uses another amine-reactive small molecule 6-((Acryloyl)amino) hexanoic acid succinimidyl ester (AcX) was also reported by the Boyden group[28]. This variant called protein retention expansion microscopy (proExM) also allows the use of conventional antibodies and fluorescent proteins and is similar, although AcX is a highly expensive reagent with comparable performance to MA-NHS.

The nanoscopic imaging power of ExM comes from the swellable nature of the polymer hydrogel, therefore, the resolution can be enhanced by increasing the expansion factor of the polymer hydrogel. Iterative expansion microscopy (iExM) was reported to make a sample expand ~20x and enabled ~25 nm axial resolution[29]. To implement iExM, three different polymer hydrogels (two swellable, one not swellable) were sequentially used to achieve two rounds of expansion. During the first gelation, DNA-conjugated antibodies were used as in the initial ExM method. However, unlike the initial method, there was no fluorophore on the DNA oligonucleotide. After digestion and expansion, the expanded sample was embedded in a second polymer. Since this polymer did not contain any charged moieties, the sample was held intact in the expanded state. Then a DNA oligonucleotide that was functionalized with a fluorophore and a methylacryloyl group was applied to hybridize with the oligonucleotide used in the first polymer, and the methylacryloyl group was designed to incorporate with the third polymer. To make sure the first expansion would not interfere with the second expansion, a cleavable crosslinker N,N'-(1,2-dihydroxyethylene) bisacrylamide was used in the first and second polymers so that they could be dissolved before achieving a second expansion.

Another variant of ExM is called Magnified Analysis of the Proteome (MAP)[30]. Different from previous variants, MAP uses heat and detergent in the place of digestion to dissociate mechanically rigid structures. This change allows better preservation of proteome contents thus enabling post-ExM immunolabeling. Additionally, MAP tuned the gel composition by introducing paraformaldehyde and having a high concentration of acrylamide so intra- and inter-protein cross-linking can be minimized. This change helps better preserve the spatial organization of the proteome and allows natural expansion which is another reason making post-ExM immunolabeling successful.

1.2.1.3 Considerations and Limitations of ExM

Since ExM studies a specimen in an expanded state, it is critical to have an isotropic enlargement to achieve a faithful representation of the original state. Among all four steps of ExM, sample homogenization using proteinases or denaturation is the key step dictating the isotropic expansion because incomplete homogenization causes distortion or even breaks within the sample while expanding in deionized water. As a rule of thumb, mechanically tougher specimens require harsher treatments for homogenization than mechanically less tough specimens. For instance, cultured cells and mouse brain tissues expand isotropically simply with proteinase K digestion, but mouse kidney tissues that have more connective components require an additional protease, collagenase, to digest the highly abundant collagen fibers throughout the sample (**Figure 1.6**)[31]. Furthermore, the digestion procedure for mouse kidney tissues has proved to be insufficient for *Drosophila* larvae which have a tough carbohydrate-based chitin cuticle, so proteinase K, collagenase, and chitinase are incorporated together to achieve isotropic expansion[32]. This means individual careful considerations must be followed when encountering a new

sample type. In general, practitioners should take care to assess expansion uniformity quantitatively when establishing protocols new to the lab and/or with new types of samples.

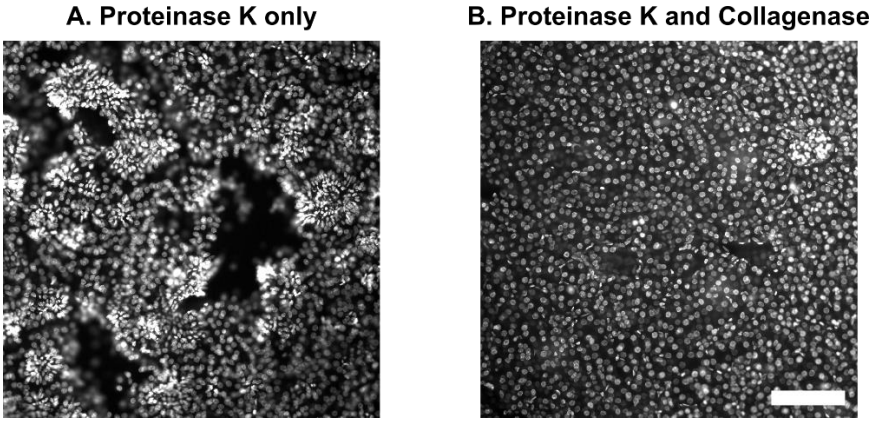

Figure 1.6 | Epifluorescence images of expanded mouse kidney stained for DNA where (A) the digestion performed with proteinase K leads to tissue tearing (empty areas) and uneven distribution of nuclei, but (B) the addition of collagenase leads to uniform sample expansion. Scale bars: 100 µm (pre-expansion units). Images are adapted from Chozinski, Mao et al.[31] with permission.

In addition to developing a robust homogenization strategy for each sample type, quantitatively determining the degree of distortion on the nanoscale helps confirm the faithful representation of the expanded sample to its original state[26,27,31]. The characterization has been commonly achieved by acquiring pre- and post-expansion images from the same region and then quantifying the non-linear warping patterns required to align post-expansion images with pre-expansion images (**Figure 1.7**). To make the comparison more trustworthy, researchers could pick well-studied features, and a super-resolution technique such as structured illumination microscopy (SIM) could be used for pre-expansion images, so their spatial resolution is better matched with that of post-expansion images.

Another general consideration is the reduced brightness after an expansion that could arise from three aspects: 1) fluorophores are photobleached during the gelation step; 2) fluorophores are lost during the homogenization step; 3) fluorophores are diluted during the expansion step. The gelation step used in ExM involves free-radical chemistry that can easily oxidize many fluorophores to a nonfluorescent state. Although the extent of bleaching varies across fluorophores, it has been observed that cyanine dyes that bear diene groups are often completely bleached[26]. Other fluorophores can retain approximately 50% of their brightness. So far, some of the best ExM compatible dyes within different spectral categories are Alexa 405, Alexa 488 or Atto 488, Alexa 546 or Alexa 568 or Atto565, Atto647N, and their close structural relatives[27,33]. However, these top dyes could still be lost during the homogenization step when they were not covalently linked to the hydrogel. Last, the brightness is further reduced through expansion. A very common version of the expansion protocol produces a four-fold expansion along each dimension which equals a sixty-four-fold volumetric expansion, so the number of fluorophores per voxel is dramatically diluted sixty-four times after the expansion.

Although signal dilution is inevitable in ExM, post-expansion labeling that bypasses photobleaching of fluorophores during the gelation step and loss of fluorophores during the homogenization step enables an approach to minimize the brightness dilution. Post-expansion labeling has been demonstrated in MAP variant with improved brightness, but the labeling efficiency depends on the antibody and protein to be labeled because not all epitopes are guaranteed to be preserved after the homogenization step[30]. Therefore, one of the main focuses of this thesis is to develop a robust, bright labeling method for different ExM variants (see **Chapter 2** and **Chapter 3**).

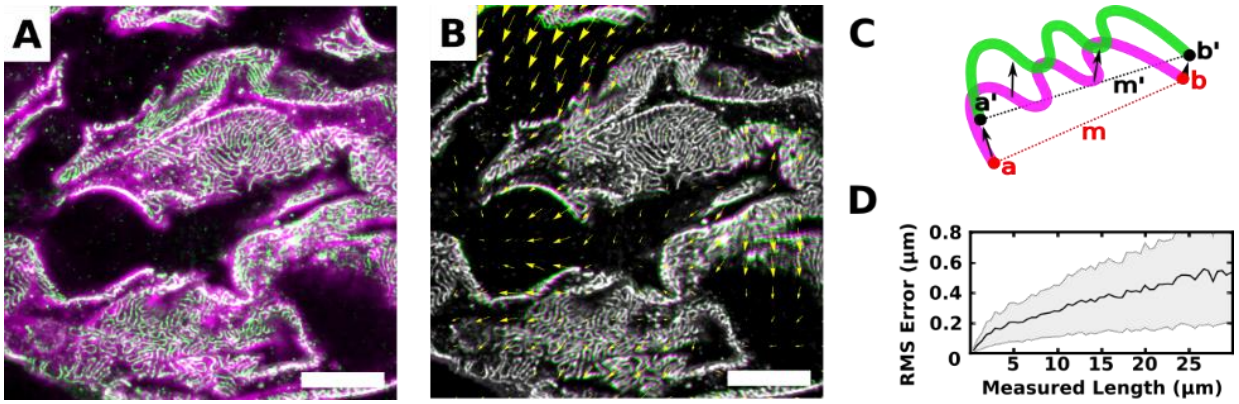

Figure 1.7 | Distortion analysis. (A) Confocal images of pre-expanded (magenta) and post-expanded (green) mouse kidney tissue stained for podocin were registered by similarity transform. (B) Post-expansion images before (magenta) and after (green) the application of a B-Spline registration were merged, where yellow arrows indicated the direction and relative magnitude for the alignment. (C) A further illustration of the correlation analysis corresponding to panel B. Green and magenta lines represent post-expansion images before and after B-spline registration, respectively. Black arrows represent the direction and relative magnitude of the alignment. The value *m* represents the distance between points a and b while *m*' is the distance between a' and b'. (D) A root-mean-square (RMS) error plot that quantifies the distortion is generated by calculating the difference between *m* and *m*' as a function of distance *m* for multiple points throughout the chosen image. Scale bars: 5 µm (pre-expansion units). Images are adapted from Chozinski, Mao et al.[31] with permission.

Since the initial publication, ExM has undergone a rapid development that extends its applicability towards nanoscale imaging of proteins using antibodies or genetically encoded fluorophores, and nucleic acids using fluorescence in situ hybridization probes. However, other commercially available probes for small biomolecules have remained to be incompatible with ExM. Lipid probes are the main example of such a class. Due to a scarcity of amine and other easily anchorable groups, commercially available lipid probes are unable to be covalently linked with a hydrogel and conjugated with fluorophores at the same time, leading to a failure of lipid imaging. Wen et al. designed a trifunctional linker that consists of 1,2-distearoyl-sn-glycero-3-phosphoethanolamine (DSPE) for targeting phospholipid bilayers, a fluorescent reporter unit, and an acryloyl group for covalently grafting hydrogel[34]. This DSPE-functionalized linker enabled clear visualization of the plasma membrane and other organelles' membranes on expanded cells. A similar anchoring strategy was also presented by Karagiannis et al.[35] and Sun et al.[36] Although overcoming the aforementioned incompatibility, this strategy requires custom synthesis which is

complicated and hard to be implemented in typical biology laboratories. Overall, ExM is still in its early stages compared with more established super-resolution modalities.

1.2.2 Optical Clearing Methods

Although biological systems are intrinsically complicated with an enormous number of components that arrange in the context of three dimensions, inquiring three-dimension information of each component at a high spatial resolution has remained to be one of the fundamental challenges for microscopists. Indeed, when imaging intact biological systems, there are three major obstacles. First, out-of-focus fluorescence from regions above and below the focal plane degrades contrast. Second, components have various refractive indices and are non-homogeneously distributed in biological systems, making them appear opaque. Third, some biological systems contain pigments that absorb excitation light and consequently limit light penetration depth. Advances in optical-sectioning techniques that can filter out-of-focus information have successfully resolved the first obstacle. Additionally, recent innovations of optical clearing methods have demonstrated the capability to resolve the other two obstacles by making biological systems transparent[10,12–14,37]. Herein, the basic concepts and mechanisms of three major groups of the optical clearing method are discussed.

1.2.2.1 Organic Solvent-based Approaches

The organic solvent-based approach generally contains two steps: 1) dehydration and delipidation and 2) refractive index matching. The dehydration and delipidation step is performed using water-miscible organic solvents such as methanol or tetrahydrofuran (THF)[5]. Since water and lipids are the two most abundant components, their removal improves the system's homogeneity and leaves components with a high refractive index within the system. Therefore, the second step must be performed using organic solvents with high a refractive index. The transparency could be further improved if the selected organic solvent is able to remove the remaining lipids. To date, the most commonly used organic solvents are benzyl alcohol, benzyl benzoate, benzyl ether.

3D Imaging Solvent Cleared Organs (3DISCO) and its variants (iDISCO, FDISCO, uDISCO) are representatives that have been widely used in many different types of samples[38–41]. 3DISCO presents the utilization of THF during the dehydration and delipidation step and offers a reduced background signal and enhanced fluorescence signal than the utilization of other water-miscible solvents[13]. iDISCO added a pre-treatment step that uses DMSO and triton X-100 to improve penetration of antibodies to the 3DISCO protocol and enhanced immunolabeling of intact samples[39]. FDISCO achieved longer and more effective preservation of endogenous fluorescence than the 3DISCO method by tuning the pH and temperature conditions[40]. uDISCO, on the other, focused on substantially shrinking samples, so neuronal connections and vascular networks throughout an entire mouse body were visualized unbiasedly and to fit the entire specimen within the finite working distance of the microscope[41]. Despite the broad and robust capabilities offered by the organic solvent-based approach, the utilization of toxic organic solvents is a remaining pitfall.

1.2.2.2 Aqueous Solution-based Approaches

The aqueous solution-based approach achieves tissue clearing via delipidation, hyperhydration, and RI matching[5]. Although the aqueous solution-based approach and the organic solvent-based approach share the same delipidation as the first step, unlike water-miscible solvents in the organic solvent-based approach, detergents (such as Triton X-100) are used in the aqueous solution-based approach. The major advantage of the aqueous solution-based approach comes from the hyperhydration step where a hydrophilic substance, urea, is used to hydrate the hydrophobic regions of proteins and thus reduces the refractive index of the sample. Eventually, the homogenized overall RI closes to water's RI (~1.33), enabling compatible imaging with water-immersion objective lenses. The first reported technique that took advantage of this mechanism was called Sca*l*e[42]. Although powerful, it required a high concentration of urea, which created an osmotic gradient that induced water diffusion into the sample and resulted in sample enlargement. Sca*l*eS is a variant of Sca*l*e that uses the addition of sorbitol to reduce the sample expansion caused by urea in Sca*l*e[43].

Another main class sharing this mechanism is called CUBIC (Clear, Unobstructed Brain/Body Imaging Cocktails and Computational Analysis)[10]. CUBIC uses two subsequent mixtures of chemicals to clear a sample. The first chemical mixture contains N,N,N',N'-tetrakis(2-hydroxypropyl) ethylenediamine, urea, and triton X-100. The second chemical mixture contains sucrose, urea, triethanolamine, and triton X-100. The major advantage of CUBIC comes from the introduction of these two amino alcohols that decolorize hemes making the intact systems more transparent. In addition, the existence of sucrose compensates for urea-induced sample swelling, making the samples' integrity better preserved. Despite the given high clearing capacity, the aqueous solution-based approach generally requires a long processing period (up to months) and it has mainly been applied to the clearing of lipid-rich organs or organisms.

1.2.2.3 Hydrogel Embedding-based Approaches

The hydrogel embedding-based approach is a completely new method that was first introduced by Chung et al. in 2013 as CLARITY[14]. It involves three major steps. First, a sample is embedded in a polyacrylamide-based hydrogel. If the sample was an intact organ, the perfusion of the sample with monomers of the hydrogel helps facilitate the penetration of monomers into the sample using the organ's vasculature. Second, an ionic detergent such as sodium dodecyl sulfate is used to remove lipid bilayers passively. Because of the formation of the polyacrylamide hydrogel, the integrity of the sample is maintained throughout the second step. Additionally, the hydrogel forms covalent linkages with proteins, nucleic acids, and other macromolecules within the sample, making fluorescent proteins well preserved and downstream processing possible. Third, the sample is subjected to a RI-matching solution to render its transparency.

The removal of lipids can be assisted via electrophoresis, which also shortens the waiting period. However, this active CLARITY can change the molecular and structural integrity of the sample and cause more protein loss than passive CLARITY. Therefore, newer methods have emerged to overcome this challenge. For example, Passive Clarity Techniques (PACT) optimized the hydrogel composition to achieve larger porous sizes that increase the passive delivery of sodium dodecyl sulfate, extracted lipids at a higher concentration of sodium dodecyl sulfate, and developed another RI-matching solution whose RI value can

vary based on the sample type[44]. Although diverse samples have been successfully cleared with the hydrogel embedding-based approach, this method requires more complicated handling skills than the previous two methods and the clearing time is usually long.

1.3 Advanced Fluorescence Microscopy Techniques Applied to Kidney

Light microscopy, immunohistochemistry, and electron microscopy have enabled fundamental kidney research and diagnosis of kidney diseases for decades. Despite the considerable successes that have been achieved with these techniques, each technique still cannot fully capture the kidney's structural complexity. For instance, light microscopy is not sufficient to investigate fine structures that are below the diffraction of light; immunohistochemistry requires epitopes' antigenicity to be well-preserved; electron microscopy is typically only performed using very thin specimens and is absent of molecular details. As discussed previously, expansion microscopy can bypass spatial resolution limitations by physically enlarging specimens and optical clearing methods can make the deep imaging of thick specimens viable, so these techniques would enable detailed volumetric assessment of kidney structures and provide insights into understanding kidney functions. In this section, the kidney's structural complexity is briefly introduced followed by a discussion of how expansion microscopy and optical clearing methods have been contributed to improving kidney imaging with all the advantages of light microscopy, immunohistochemistry, and electron microscopy.

1.3.1 An Anatomic Introduction of The Kidney

The kidneys are responsible for removing waste from the bloodstream, maintaining water/electrolyte homeostasis in the body, and regulating blood pressure[45]. The functional and structural unit of the kidney is called the nephron (**Figure 1.8**). Each adult human kidney contains about one million nephrons[45]. A nephron consists of a glomerulus, a proximal tubule, a loop of Henle, a distal convoluted tubule, and a collecting duct, and all structures collaborate to fulfill the kidney's responsibilities. When unfiltered blood flows into the kidney through the afferent arteriole, a glomerulus is the initial filtering site. The filtered blood leaves the kidney through the efferent arteriole and returns toward the heart. The filtrates, including water, electrolytes, and other small molecules are collected by a Bowman's capsule of glomerulus and enter the proximal tubule. Here, most filtrates are reabsorbed either passively or actively. Brush borders are fine structures inside the proximal tubule that help increase the area of reabsorption greatly. Then the filtrate is concentrated by the concentration gradient along the loop of Henle. Thereafter, the distal convoluted tubule regulates the pH of the filtrate by either absorbing bicarbonate and secreting protons or absorbing protons and secreting bicarbonate into the filtrate. Finally, the filtrate passes through a collecting duct and is ready to be secreted into a bladder. In addition to this sophisticated mechanism regarding the creation and processing of filtrates, each component is multidimensionally positioned and connected with others. Therefore, being able to achieve 3D visualization of these components opens the door for answering more questions in the study of the kidney.

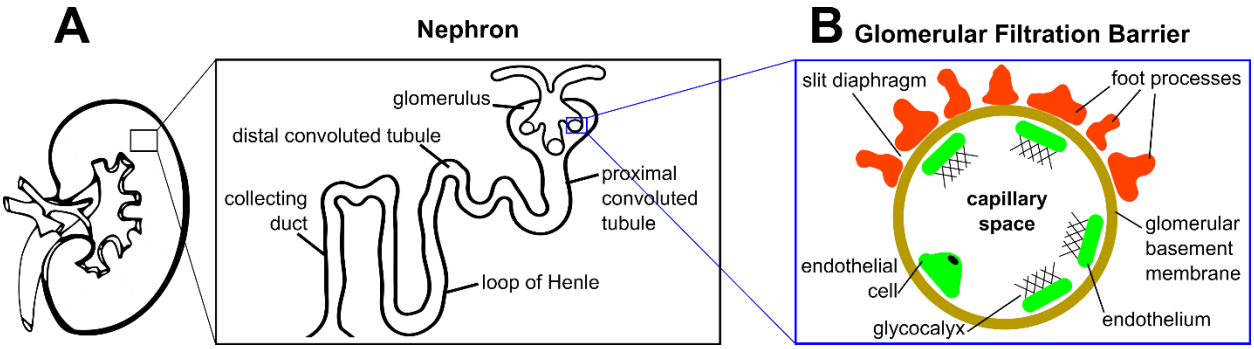

Figure 1.8 | (A) The structural unit of the kidney, nephron, is comprised of a glomerulus, proximal convoluted tubule, the loop of Henle, distal convoluted tubule, and collecting duct. (B) The glomerular filtration barrier within a glomerulus is made of diverse elements that form three layers. The endothelium layer (green) contains endothelial cells and glycocalyx. The glomerular basement membrane is the middle layer (brown). Foot processes (red) extending from podocyte cells are situated on the glomerular basement membrane as the third layer. The gap between two foot processes is called the slit diaphragm.

The glomerulus is not simply a mechanical filter, but a highly compact network that comprises multiple elements[46]. An afferent arteriole branches into capillaries that are surrounded by three layers: endothelial cells, the glomerular basement membrane (GBM), and epithelial podocytes (**Figure 1.8**). The endothelial layer is coated with a highly negatively charged glycoprotein layer called a glycocalyx layer which contributes to the selection of filtrates in terms of charge. Additionally, there are holes between endothelial cells called fenestrae that allow diffusion of small molecules but prevent loss of proteins. The GBM is known for being rich in extracellular matrix proteins which form porous meshes to selectively remove substances. Podocytes locate at the outer layer where podocytes extend their "foot processes" to attach onto GBM but their cell bodies sit on the top. Furthermore, foot processes of neighboring podocytes interdigitate, and their narrow gaps are called slit diaphragms. Taken together, these three layers are called the glomerular filtration barrier, and any disturbance of their structures could lead to one or more kidney diseases. Another important element inside a glomerulus is the mesangium, or the core of the glomerulus. The mesangium contains mesangial cells and mesangial matrix and fills the space between capillaries. Mesangial cells secrete mesangial matrix that can regulate the filtration rate, but abnormal mesangial matrix deposits cause renal sclerosis. Collectively, advanced imaging techniques that permit high resolution 3D morphological analysis of each glomerular structure across a range of length scales will provide key insights in basic research and in the diagnosis of kidney diseases.

1.3.2 Expansion Microscopy (ExM) Imaging of Ultra-structures of Kidney

In its early stages of development, ExM mainly focused on cultured cells and mouse brain sections that were relatively "soft" biological specimens[26–29]. Given the nature of a relatively high amount of connective tissue, an improved protocol of ExM is required to implement ExM to study kidney's ultrastructures. Zhao et al. optimized the initial ExM protocol and applied the new version to clinical tissue samples including human kidney sections[47]. Using the optimized protocol, Zhao et al. isotropically expanded human kidney samples, visualized podocyte foot processes, and demonstrated the structural alteration between normal human kidney and minimal-change diseased kidney samples. However, the

clinical tissue samples in the study were restricted to 4-5 µm thickness, which made the collecting of volumetric information still challenging. In parallel, Unnersjö-Jess et al. amended the MAP-based protocol and achieved an expansion of rat and mouse kidney tissues[48]. Although this protocol works for thicker samples that made foot processes volumetrically visualized with standard confocal microscopy, simultaneous visualizations of other fine elements of the filtration barrier were absent. Shortly after these two publications, our group reported another optimization of the initial ExM protocol for thicker mouse kidney tissues (~ 100 µm). We performed a careful validation of the optimized protocol in 3-dimensions to make sure the distortions are minimal, tested various antibodies against glomerular details with a special focus on the volumetric artitecture of the glomerular filtration barrier, and extracted quantitative information of the filtration barrier that is of clinical use[31]. Furthermore, we easily tuned our protocol to enable an expansion of human kidney tissues (~ 50 µm) with minimal distortion and demosntrated the first ExM-based volumetric imaging of glomerulus.

1.3.3 Volumetric, Large-Scale Imaging of Optically Cleared Kidney

As discussed previously, all structures of the nephron collaborate to fulfill the kidney's responsibilities. Therefore, visualizing and understanding each structure is as important as that of the glomerular filtration barrier. Since these structures are larger than the diffraction limit of light but multidimensionally positioned and connected with others, the optical clearing method is more suitable as a processing tool than ExM. In 2014, Renier et al.[39] and Yang et al.[44] demonstrated whole-mouse-kidney clearing using iDISCO and PACT methods, respectively. Combining with immunolabeling and advanced microscopes, the volumetric distributions of glomeruli, collecting ducts, and other structures were mapped within the intact whole kidney. Building on the power of the optical clearing methods, later, Klingberg et al.[49] integrated an automated quantification analysis with a clearing method to enable the total glomerular count and the measurement of glomerular tufts' volumes in a whole kidney. In addition, this analysis pipeline helped investigate the difference between healthy and nephritic kidneys leading to benefit studies of the effect of kidney diseases on whole-organ physiology. Similar to the evaluation of total glomerular numbers, Puelles et al. demonstrated a method for counting and sizing podocytes in an intact glomerulus using a transgenic mouse model[50]. This analysis could be an efficient tool for the assessment of podocyte depletion which is one of the roots of glomerular diseases.

Beyond glomeruli, the study of nephron tubules could be aided by optical clearing methods as well. The proximal convoluted tubule (PCT) is in charge of the reabsorption via endocytosis. With the help of the CLARITY-based clearing method, Schuh et al. were able to reveal the ligand uptake along with the PCT segments, and found early PCT segments showed a higher uptake rate than the late PCT segments, and this heterogeneity correlated with the expression of endolysosomal proteins along with the PCT segments[51]. On the other hand, Saritas et al. focused on tubule remodeling under the mediation of potassium[52]. After clearing the whole kidney using either the CLARITY-based method or the DISCO-based method, it turned out low/depleted potassium diet caused a significant shortening of distal convoluted tubules and a great increase of proliferation in tubule segments[52]. The clearing method CUBIC was also applied to kidney research. For instance, Hasegawa et al. visualized the distribution of sympathetic nerves within a whole kidney and studied their denervation after the ischemia/reperfusion injury[53].

1.4 Summary

Advances in expansion microscopy and optical clearing methods have permitted the possibility of comprehensive 3-dimensional analysis of biological specimens on a wide range of length scales and thus make one of the main limitations now to be the success of fluorescently labeling the specimens. In the following chapters, this thesis specifically introduces novel covalent stains that address some pitfalls associated with two current dominant labeling methods, immunofluorescence using fluorophore-antibody conjugates and genetic manipulation using fluorescent proteins. In chapter 2, the inspiration of the novel covalent stains from classic histology stains will be discussed and their great utility in both expansion microscopy and optical clearing methods will be demonstrated. In chapter 3, a detailed step-by-step protocol of this new labeling method along with a troubleshooting guide, its further applications in fundamental biological research and clinical pathology, and its extensive combination with other labeling modalities will be presented to disseminate this new labeling method.

1.5 References

1. Marqués, G., Pengo, T. & Sanders, M. A. Imaging methods are vastly underreported in biomedical research. *eLife* **9**, e55133 (2020).
2. *Basic Confocal Microscopy*. (Springer International Publishing, 2018). doi:10.1007/978-3-319-97454-5.
3. Minsky, M. Memoir on inventing the confocal scanning microscope. *Scanning* **10**, 128–138 (1988).
4. Sahl, S. J., Hell, S. W. & Jakobs, S. Fluorescence nanoscopy in cell biology. *Nature Reviews Molecular Cell Biology* **18**, 685–701 (2017).
5. Richardson, D. S. & Lichtman, J. W. Clarifying Tissue Clearing. *Cell* **162**, 246–257 (2015).
6. Abbe, E. Beiträge zur Theorie des Mikroskops und der mikroskopischen Wahrnehmung: I. Die Construction von Mikroskopen auf Grund der Theorie. *Archiv für Mikroskopische Anatomie* **9**, 413–418 (1873).
7. *Handbook of biological confocal microscopy*. (Springer, 2006).
8. Saitoh, Y. *et al.* Three-dimensional reconstruction of living mouse liver tissues using cryotechniques with confocal laser scanning microscopy. *Journal of Electron Microscopy* **59**, 513–525 (2010).
9. Berlanga, M. L. *et al.* Three-Dimensional Reconstruction of Serial Mouse Brain Sections: Solution for Flattening High-Resolution Large-Scale Mosaics. *Front. Neuroanat.* **5**, (2011).
10. Susaki, E. A. *et al.* Whole-Brain Imaging with Single-Cell Resolution Using Chemical Cocktails and Computational Analysis. *Cell* **157**, 726–739 (2014).
11. Tainaka, K., Kuno, A., Kubota, S. I., Murakami, T. & Ueda, H. R. Chemical Principles in Tissue Clearing and Staining Protocols for Whole-Body Cell Profiling. *Annual Review of Cell and Developmental Biology* **32**, 713–741 (2016).
12. Becker, K., Jährling, N., Saghafi, S., Weiler, R. & Dodt, H.-U. Chemical Clearing and Dehydration of GFP Expressing Mouse Brains. *PLoS ONE* **7**, e33916 (2012).
13. Ertürk, A. *et al.* Three-dimensional imaging of solvent-cleared organs using 3DISCO. *Nat Protoc* **7**, 1983–1995 (2012).
14. Chung, K. *et al.* Structural and molecular interrogation of intact biological systems. *Nature* **497**, 332–337 (2013).
15. *The molecular probes handbook: a guide to fluorescent probes and labeling technologies*. (Life Technologies, 2010).
16. *Immunobiology: the immune system in health and disease*. (Garland Science, 2005).
17. Hermanson, Greg. *Bioconjugate Techniques, 2nd Edition*.
18. Schnell, U., Dijk, F., Sjollema, K. A. & Giepmans, B. N. G. Immunolabeling artifacts and the need for live-cell imaging. *Nature Methods* **9**, 152–158 (2012).
19. Bradbury, A. & Plückthun, A. Reproducibility: Standardize antibodies used in research. *Nature* **518**, 27–29 (2015).
20. Wulf, E., Deboben, A., Bautz, F. A., Faulstich, H. & Wieland, T. Fluorescent phallotoxin, a tool for the visualization of cellular actin. *Proceedings of the National Academy of Sciences* **76**, 4498–4502 (1979).
21. van Meer, G., Voelker, D. R. & Feigenson, G. W. Membrane lipids: where they are and how they behave. *Nat Rev Mol Cell Biol* **9**, 112–124 (2008).
22. Hughes, L. D., Rawle, R. J. & Boxer, S. G. Choose Your Label Wisely: Water-Soluble Fluorophores Often Interact with Lipid Bilayers. *PLoS ONE* **9**, e87649 (2014).
23. Presley, A. D., Fuller, K. M. & Arriaga, E. A. MitoTracker Green labeling of mitochondrial proteins and their subsequent analysis by capillary electrophoresis with laser-induced fluorescence detection. *Journal of Chromatography B* **793**, 141–150 (2003).

24. Wang, Y., Schellenberg, H., Walhorn, V., Toensing, K. & Anselmetti, D. Binding Mechanism of Fluorescent Dyes to DNA Characterized by Magnetic Tweezers. *Materials Today: Proceedings* **4**, S218–S225 (2017).
25. Shaner, N. C., Steinbach, P. A. & Tsien, R. Y. A guide to choosing fluorescent proteins. *Nature Methods* **2**, 905–909 (2005).
26. Chen, F., Tillberg, P. W. & Boyden, E. S. Expansion microscopy. *Science* **347**, 543–548 (2015).
27. Chozinski, T. J. *et al.* Expansion microscopy with conventional antibodies and fluorescent proteins. *Nature Methods* **13**, 485–488 (2016).
28. Tillberg, P. W. *et al.* Protein-retention expansion microscopy of cells and tissues labeled using standard fluorescent proteins and antibodies. *Nature Biotechnology* **34**, 987–992 (2016).
29. Chang, J.-B. *et al.* Iterative expansion microscopy. *Nat. Methods* **14**, 593–599 (2017).
30. Ku, T. *et al.* Multiplexed and scalable super-resolution imaging of three-dimensional protein localization in size-adjustable tissues. *Nature Biotechnology* **34**, 973–981 (2016).
31. Chozinski, T. J. *et al.* Volumetric, Nanoscale Optical Imaging of Mouse and Human Kidney via Expansion Microscopy. *Scientific Reports* **8**, (2018).
32. Jiang, N. *et al.* Superresolution imaging of *Drosophila* tissues using expansion microscopy. *Molecular Biology of the Cell* **29**, 1413–1421 (2018).
33. Min, K., Cho, I., Choi, M. & Chang, J.-B. Multiplexed expansion microscopy of the brain through fluorophore screening. *Methods* **174**, 3–10 (2020).
34. Wen, G. *et al.* Evaluation of Direct Grafting Strategies *via* Trivalent Anchoring for Enabling Lipid Membrane and Cytoskeleton Staining in Expansion Microscopy. *ACS Nano* **14**, 7860–7867 (2020).
35. Karagiannis, E. D. *et al. Expansion Microscopy of Lipid Membranes*. http://biorxiv.org/lookup/doi/10.1101/829903 (2019) doi:10.1101/829903.
36. Sun, D. *et al. Click-ExM enables expansion microscopy for all biomolecules*. http://biorxiv.org/lookup/doi/10.1101/2020.03.19.998039 (2020) doi:10.1101/2020.03.19.998039.
37. Tainaka, K. *et al.* Chemical Landscape for Tissue Clearing Based on Hydrophilic Reagents. *Cell Reports* **24**, 2196-2210.e9 (2018).
38. Dodt, H.-U. *et al.* Ultramicroscopy: three-dimensional visualization of neuronal networks in the whole mouse brain. *Nat Methods* **4**, 331–336 (2007).
39. Renier, N. *et al.* iDISCO: A Simple, Rapid Method to Immunolabel Large Tissue Samples for Volume Imaging. *Cell* **159**, 896–910 (2014).
40. Qi, Y. *et al.* FDISCO: Advanced solvent-based clearing method for imaging whole organs. *Sci. Adv.* **5**, eaau8355 (2019).
41. Pan, C. *et al.* Shrinkage-mediated imaging of entire organs and organisms using uDISCO. *Nature Methods* **13**, 859–867 (2016).
42. Hama, H. *et al.* Scale: a chemical approach for fluorescence imaging and reconstruction of transparent mouse brain. *Nat Neurosci* **14**, 1481–1488 (2011).
43. Hama, H. *et al.* ScaleS: an optical clearing palette for biological imaging. *Nat Neurosci* **18**, 1518–1529 (2015).
44. Yang, B. *et al.* Single-Cell Phenotyping within Transparent Intact Tissue through Whole-Body Clearing. *Cell* **158**, 945–958 (2014).
45. Amerman, E. C. *Human anatomy & physiology*. (2019).
46. *Renal physiology*. (Published for the American Physiological Society by Oxford University Press, 1992).
47. Zhao, Y. *et al.* Nanoscale imaging of clinical specimens using pathology-optimized expansion microscopy. *Nature Biotechnology* (2017) doi:10.1038/nbt.3892.

48. Unnersjö-Jess, D. *et al.* Confocal super-resolution imaging of the glomeruluar filtration barrier enables by tissue expansion. *Kidney International* (2017) doi:https://doi.org/10.1016/j.kint.2017.09.019.
49. Klingberg, A. *et al.* Fully Automated Evaluation of Total Glomerular Number and Capillary Tuft Size in Nephritic Kidneys Using Lightsheet Microscopy. *Journal of the American Society of Nephrology* **28**, 452–459 (2017).
50. Puelles, V. G. *et al.* Validation of a Three-Dimensional Method for Counting and Sizing Podocytes in Whole Glomeruli. *JASN* **27**, 3093–3104 (2016).
51. Schuh, C. D. *et al.* Combined Structural and Functional Imaging of the Kidney Reveals Major Axial Differences in Proximal Tubule Endocytosis. *JASN* **29**, 2696–2712 (2018).
52. Saritas, T. *et al.* Optical Clearing in the Kidney Reveals Potassium-Mediated Tubule Remodeling. *Cell Reports* **25**, 2668-2675.e3 (2018).
53. Hasegawa, S. *et al.* Comprehensive three-dimensional analysis (CUBIC-kidney) visualizes abnormal renal sympathetic nerves after ischemia/reperfusion injury. *Kidney International* (2019) doi:10.1016/j.kint.2019.02.011.

Chapter 2

Feature-Rich Covalent Stains for Super-Resolution and Cleared-Tissue Fluorescence Microscopy

2.1 Preface

As discussed in **Chapter 1**, expansion microscopy (ExM) and optical clearing method are two advanced fluorescence microscopy techniques that enable imaging nanoscale features beneath the diffraction limit of resolution of traditional light microscopy, and deep imaging of intact samples without concerning light scattering that typically limits the imaging depth to 100 μm, respectively. Although powerful, the success of using these two methods relies on fluorescently labeling the sample for measuring the distribution of biological molecules or structures of interest. Currently, immunofluorescence and fluorescent protein tagging are two dominant approaches. However, they still possess significant challenges. For instance, due to their relatively large size, it can take days of incubation to deliver antibody conjugates through a thick specimen. Additionally, the antibody's variability among lots and/or vendors can cause inconsistent reproducibility. Furthermore, genetic manipulation is complicated, and the success rate is not always high. Finally, labeling efficiency is challenging for both approaches because antibody labeling suffers from binding heavily fixed or processed specimens, and fluorescent proteins can dimerize and are likely denatured and/or dissociated during sample processing which involves harsh conditions.

With these limitations in mind, we are interested in developing alternative methods that are simple, robust, and easily accessible. In this chapter, I will present two fluorescent analogs of classic histology stains that we established using commercially available small-molecule probes. When combining with expansion microscopy and optical clearing methods, we are able to reveal key general features in a variety of specimens (from cultured cells to mouse and human organs) and easily adapt them to a range of biological applications.

I was heavily involved in this project at all stages. My main contributions were the adaptation of the protein-retention variation of ExM termed MAP, the application of these probes to MAP-processed mouse kidney tissues, and the demonstration of the compatibility of these probes with other labeling modalities. Another co-first author, Dr. Min Yen Lee contributed to the cultured cell- and thick tissue-related portions of the project. In addition, this work was also in collaboration with members from the laboratories of Dr. Jonathan T.C. Liu and Dr. Stuart J. Shankland who contributed to using open-top light-sheet microscopy to image thick tissues and providing FFPE mouse kidney tissues, respectively. All authors edited the manuscript. Supplementary figures are provided in addition to the main text.

The following material in this chapter is reproduced with permission from:

Chenyi Mao,† Min Yen Lee,† Jing-Ru Jhan, Aaron R. Halpern, Marcus A. Woodworth, Adam K. Glaser, Tyler J. Chozinski, Leonard Shin, Jeffrey W. Pippin, Stuart J. Shankland, Jonathan T.C. Liu, Joshua C. Vaughan; "Feature-Rich Covalent Stains for Super-Resolution and Cleared-Tissue Fluorescence Microscopy", *Science Advances*, Vol. 6, no. 22, 2020.

† indicated equal contributions.

All material in this chapter has been reformatted to conform to the style of this thesis.

2.2 Abstract

Fluorescence microscopy is a workhorse tool in biomedical imaging but often poses significant challenges to practitioners in achieving bright or uniform labeling. In addition, while antibodies are effective specific labels, their reproducibility is often inconsistent, and they are difficult to use when staining thick specimens. We report the use of conventional, commercially available fluorescent dyes for rapid and intense covalent labeling of proteins and carbohydrates in super-resolution (expansion) microscopy and cleared-tissue microscopy. This approach, which we refer to as Fluorescent Labeling of Abundant Reactive Entities (FLARE), produces simple and robust stains that are modern equivalents of classic small-molecule histology stains. It efficiently reveals a wealth of key landmarks in cells and tissues under different fixation or sample processing conditions and is compatible with immunolabeling of proteins and in situ hybridization labeling of nucleic acids.

2.3 Introduction

Two of the most important developments in fluorescence microscopy over the past 1-2 decades are super-resolution microscopy, for imaging small features beneath the ~250 nm diffraction limit of visible light, and cleared-tissue microscopy, for deep imaging of intact specimens[1–5]. Researchers are now able to routinely measure nanoscale molecule distributions, protein oligomerization or protein-protein interactions, and to determine the large-scale organization of biological specimens. Central to these efforts are a wide range of probes to fluorescently label the sample, with one of the most important classes being fluorescently labeled antibodies. While antibodies are powerful in their ability to specifically label specimens without need for genetic manipulation, they often suffer slow penetration in thick tissues, poor binding in specimens that have been heavily fixed or processed (e.g., formalin-fixed paraffin-embedded tissue), high cost, and inconsistent lot-to-lot reproducibility or commercial availability[6, 7].

Small-molecule histology stains such as H&E (hematoxylin and eosin)[8] are attractive potential alternative labels for super-resolution and cleared-tissue microscopy but they pose several challenges[9]. First, many histology stains are affinity-based, rather than covalent, and produce uneven staining particularly for relatively thick specimens, whereas covalent labeling renders the labels compatible with a wider range of sample processing or clearing techniques. Second, nonfluorescent histology stains are poorly suited to volumetric imaging and fluorescence-based super-resolution microscopy methods. Third, classic histology stains have limited flexibility in their spectral properties whereas modern fluorescent dyes are available in many forms across the visible and near infrared with high quantum yields and good resistance to photobleaching.

To partly address the limitations of antibodies and small-molecule histology stains, we developed simple procedures for using commercially available small-molecule fluorophores to brightly label a wide variety of major organelles and landmark structures in cells and tissues for super-resolution microscopy and cleared-tissue microscopy. The idea is to use small molecules to covalently label abundant chemical functional groups on biological samples, instead of specific biomolecules, in order to reveal the general physiology of the sample. These include the use of amine-reactive fluorophores for measuring distributions of proteins and aldehyde-reactive fluorophores for measuring distributions of oxidized carbohydrates, although other abundant reactive groups (thiols, carboxylates, etc.) may also be suitable. We termed this approach Fluorescent Labeling of Abundant Reactive Entities (FLARE). While the

underlying chemical reactions are well known[10–16], for instance when labeling purified proteins[12], specimen surfaces[17], or isolated live cells for subsequent tracking[18], the great utility of this simple labeling approach in super-resolution and cleared-tissue microscopy has not been previously recognized. For super-resolution microscopy, we utilized expansion microscopy, a recently developed technique that physically expands biological specimens embedded in a swellable polymer[19–21]. The physical expansion enables features closer than the ~250 nm diffraction limit of traditional light microscopy to be resolved in the expanded state on a conventional microscope. For cleared-tissue microscopy with unexpanded specimens, we utilized a variant of the solvent-based tissue clearing method DISCO[22] that uses ethyl cinnamate for index matching[23].

2.4 Results

2.4.1 FLARE reveals key landmarks in hydrogel-expanded specimens

We first tested the ability of FLARE to stain cultured human retinal pigment epithelium cells (RPE) that had been expanded five-fold using ExM. Using the labeling schematic in **Figure 2.1**, we stained oxidized carbohydrates on the specimen with ATTO 565 hydrazide, amines with ATTO 647N NHS (N-hydroxysuccinimidyl) ester, and DNA (non-covalently) with SYBR Green (**Figure 2.2, Supplementary Figure 2.1**). Mitochondria were densely labeled by the amine stain, while lysosomes and the plasma membrane were densely labeled by the carbohydrate stain, and perinuclear structures including portions of the Golgi were labeled by both amine and carbohydrate stains (**Figure 2.2a-c, Supplementary Figure 2.1, Supplementary Figure 2.2**). The nucleus and nuclear envelope of interphase cells were clearly evident as were nuclear pores in both the amine and carbohydrate channels (**Figure 2.2c, Supplementary Figure 2.2i-l**). In dividing cells (**Figure 2.2d-f, Supplementary Figure 2.1**), kinetochores and centrosomes were also labeled well. Thus, the chemical stains efficiently report on many major landmark structures and components of the cell.

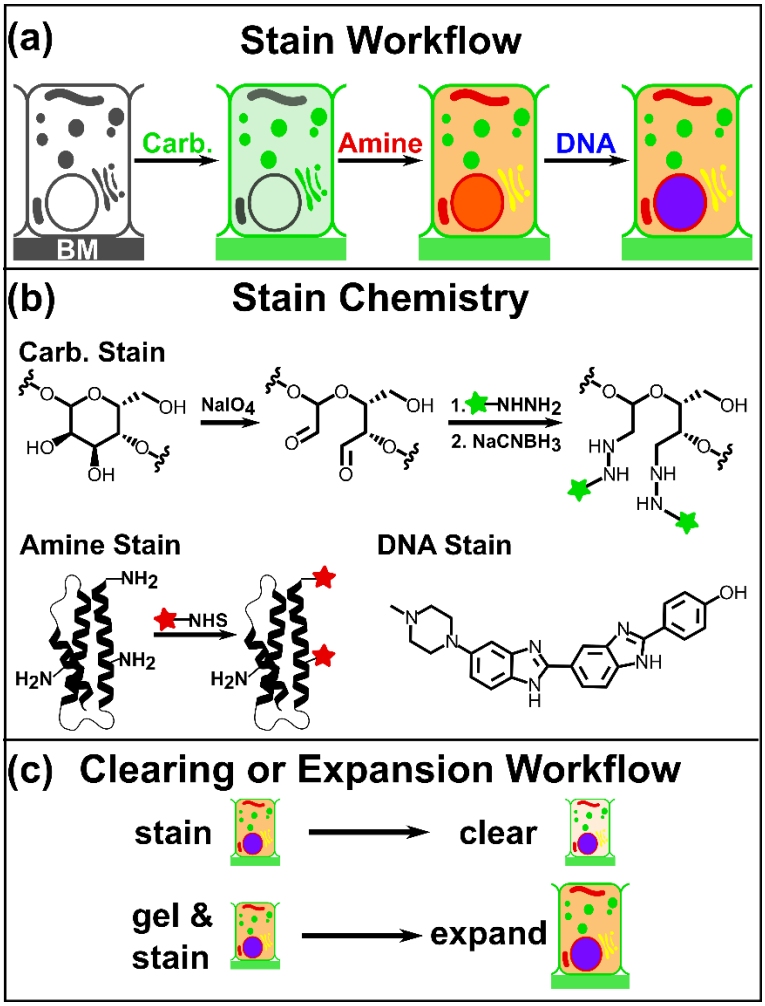

Fig. 2.1 | Schematic illustration of FLARE staining of amines and carbohydrates, together with DNA staining, for super-resolution and cleared-tissue microscopy. (a) Carbohydrates, amines, and DNA on cells or tissues are stained as the order shown. (b) Vicinal diols on carbohydrates are oxidized to aldehydes using sodium periodate, coupled to hydrazide-functionalized fluorophores (green), and then stabilized by reduction with sodium cyanoborohydride. Amines are labeled by reaction with an NHS-functionalized fluorophore (red). DNA is labeled non-covalently by incubation with a conventional DNA stain such as Hoechst or SYBR Green (blue). (c) Specimen processing workflow with respect to clearing and expansion.

FLARE can be straightforwardly combined with antibody labeling, which we used here to confirm the identities of some sub-cellular organelles or structures such as mitochondria, lysosomes, and the golgi apparatus (**Supplementary Figure 2.2**). However, we also realized that some features observed in the images are not easily identified, and some known structural features are difficult to detect in the images. For instance, in dividing RPE cells, we frequently observed a swirling tuft of unknown amine-rich cytoskeletal filaments toward one end of the cell while at the same time we were surprised that microtubules of the mitotic spindle were unlabeled (**Figure 2.2d**). Nonetheless, results with cultured cells indicate that these relatively non-specific covalent stains together with the improved spatial resolution

(~65 nm) attained using specimen expansion with confocal microscopy[19–21] can reveal a wealth of details but that more work will be required to better understand and possibly tune the specificity of labeling.

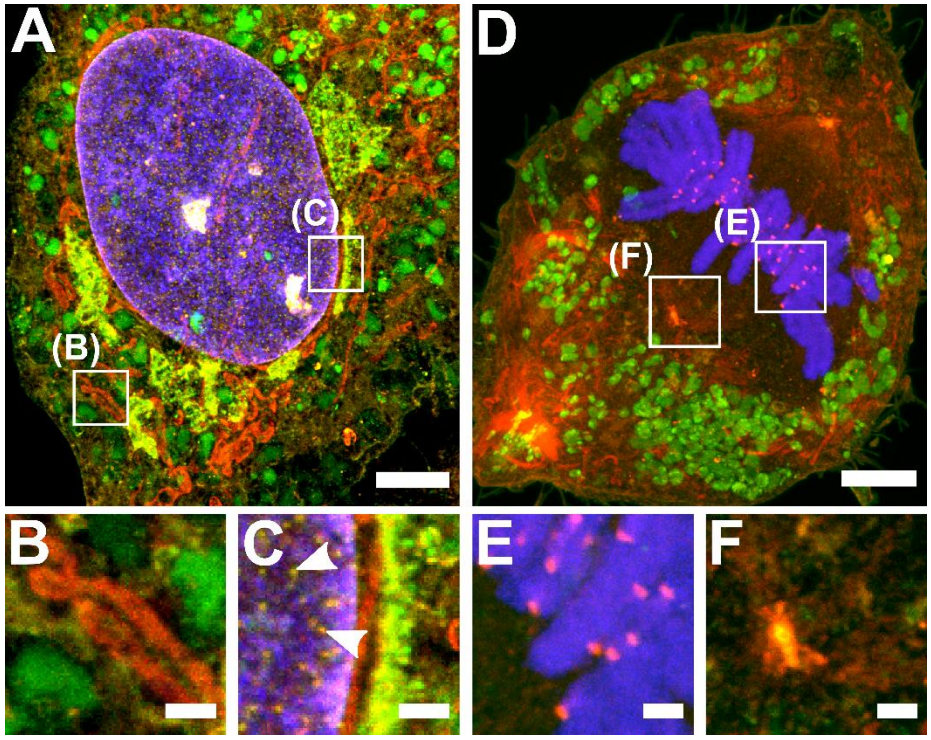

Fig. 2.2 | FLARE staining of hydrogel-expanded cultured cells. Confocal microscopy images of hydrogel-expanded RPE cells that have been covalently stained for amine (red) and carbohydrate (green) using FLARE along with a conventional noncovalent stain for DNA (blue). (a) Interphase cell showing various subcellular organelles including mitochondria (red), lysosomes (green), and perinuclear structures (yellow). (b-c) Zoomed-in views of boxed regions in a). Arrowheads in c) indicate nuclear pores. (d) Dividing cell showing various subcellular organelles. (e-f) Zoomed-in views of boxed region in d) showing kinetochores and centrosomes, respectively. All scale bars are in pre-expansion units. Scale bars are 3 µm (a,d), 500 nm (b-c, e-f).

Beyond cultured cells, we found that FLARE also works well in hydrogel-expanded tissues, as we demonstrate using mouse kidney, a model specimen containing a diverse range of structures and cell types (**Figure 2.3**). Within glomeruli, the filtration units of the kidney, the carbohydrate stain brightly labeled the basement membranes of the capillary loops and the mesangial matrix, while the amine stain efficiently outlined cell boundaries and other structures, including the intricate details of interdigitated podocyte epithelial cells that form a major component of the glomerular filtration barrier (**Figure 2.3a-c, Supplementary Video 2**). In proximal convoluted tubules of the kidney, the basement membrane was also labeled by the carbohydrate stain, and the amine stain revealed mitochondria, the nuclear envelope, and brush border microvilli (**Figure 2.3d**). While we focus in this paper on a variation of ExM termed MAP (magnified analysis of the proteome)[20] that utilizes heat and detergent to dissociate tissue-hydrogel hybrids, rather than enzymatic digestion as in the original ExM method[21], we found that enzymatically digested mouse kidney tissue could also be covalently stained (**Supplementary Figure 2.3a-d**), indicating

that the possible loss of material due to digestion was not prohibitive. Additionally, we found that FLARE is compatible with in-situ hybridization for detection of nucleic acids (**Supplementary Figure 2.3e-h**).

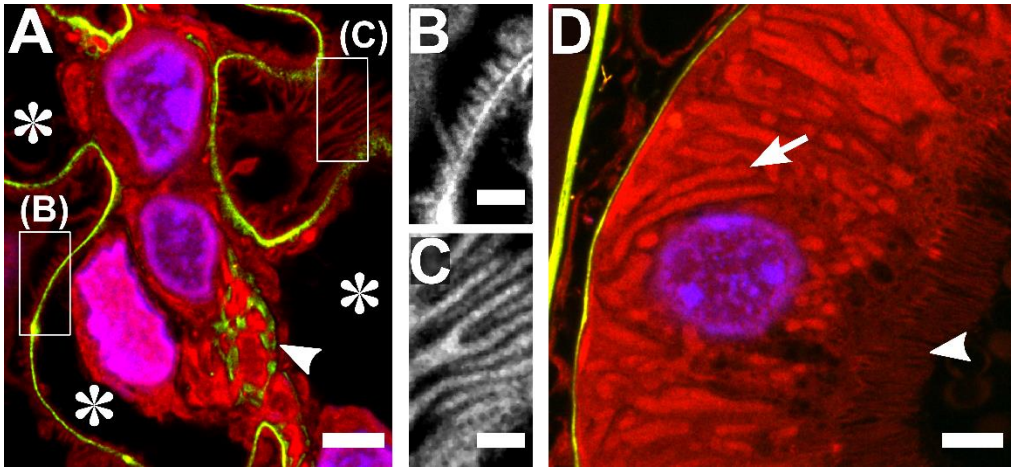

Fig. 2.3 | FLARE staining of hydrogel-expanded mouse kidney tissue. Confocal microscopy images of hydrogel-expanded mouse kidney that have been covalently stained for amines (red) and carbohydrates (green) using FLARE along with a conventional noncovalent stain for DNA (blue). (a) A region of a mouse kidney glomerulus in which carbohydrates are intensely labeled along the basement membrane of the capillary loops (stars) and within the mesangial matrix (arrowhead). (b-c) Zoomed-in views of amine channel for boxed regions in panel (a) showing interdigitated podocyte foot processes. (d) A region of a proximal convoluted tubule in which carbohydrates highlight tubular basement membrane and amines intensely label mitochondria (arrow) and microvilli (arrowhead). All scale bars are in pre-expansion units. Scale bars are 3 µm (a,d), 500 nm (b-c).

2.4.2 FLARE labels thick tissue sample rapidly and uniformly

We next tested FLARE in various unexpanded specimens that were subsequently optically cleared using dehydration in a graded series of tetrahydrofuran (THF) followed by immersion in ethyl cinnamate, a variant of the iDISCO clearing method[22, 23]. The labeling protocol was approximately the same as for the labeling of tissue-hydrogel specimens with two important adjustments in order to help enhance the uniformity of the stains throughout the depth of the tissue. First, during both covalent labeling reactions, we dissolved dyes in a co-solvent mixture consisting of a 1:1 ratio of aqueous buffer to THF in order to increase the rate of diffusion through the specimen (**Figure 2.4a-e, Supplementary Figure 2.4**). Second, for the amine-labeling reaction, we adjusted the pH to 6.0 in order to reduce the rate of the coupling reaction while also reducing the rate of hydrolysis of the ester that would render the dye unreactive[24, 25]. These measures greatly improved the uniformity (**Figure 2.4a-e**). For example, approximately uniform covalent amine-labeling of a ~500 µm thick section of mouse kidney could be achieved in ~2 hr, whereas the same tissue section when labeled with antibodies for 6 days was only stained at a depth of <50 µm at each surface of the tissue section (**Figure 2.4e**). We then used this procedure to stain and clear a relatively large volume of mouse kidney (~4 mm × ~3.5 mm × ~1 mm) and imaged it using a recently published open-top light sheet microscope[26] at a resolution of ~2 µm (**Figure 2.4f-h, Supplementary Figure 2.5a-d**). We were able to observe renal tubules over long distances with characteristic segment-specific stain distributions for proximal tubules, distal tubules, loop of Henle, etc., that provide bearing on the location

of the tubule within the nephron. We validated the identities of these key features in mouse kidney using covalent amine and carbohydrate labeling concurrent with a triple immunostain against cytokeratin (CK8+18, enriched on collecting ducts), aquaporin (AQP-1, enriched on proximal tubules) and podocalyxin (PODXL, enriched on glomeruli) (**Supplementary Figure 2.6**).

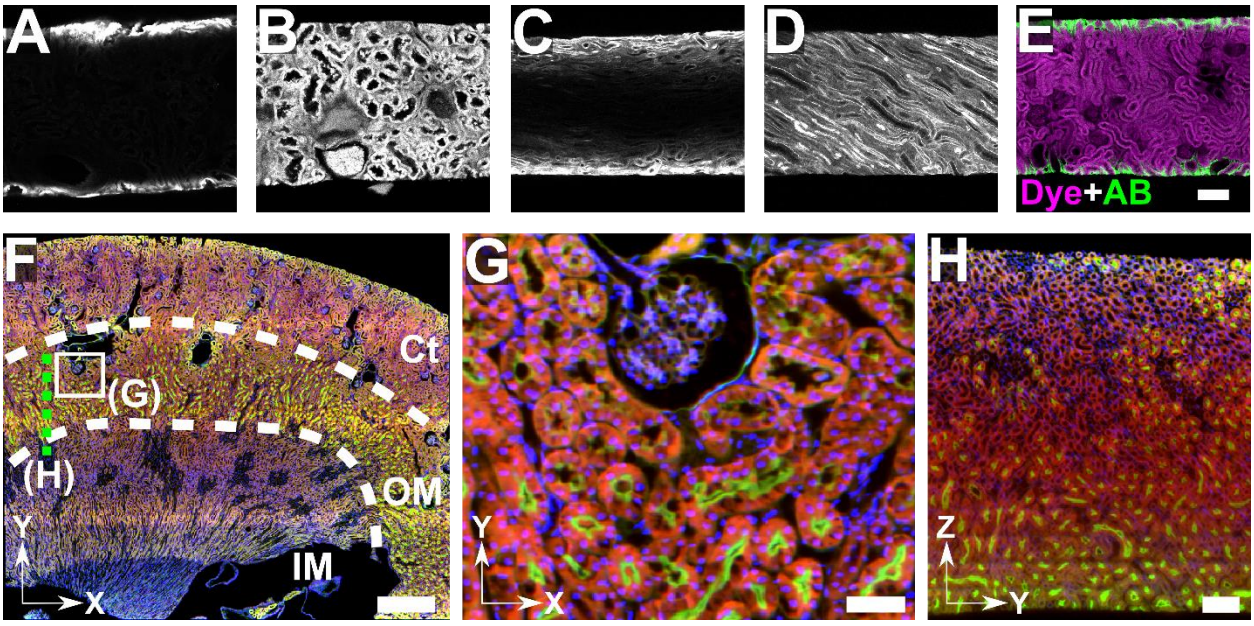

Fig. 2.4 | FLARE staining of thick, cleared tissue specimens. (a-e) 500 µm thick kidney sections were covalently stained, cut perpendicular to the section face, and imaged to measure stain intensity as a function of depth. Staining using an aqueous buffered solution produced uneven surface stains for (a) ATTO 647N-NHS and (c) ATTO 565-hydrazide, but labelling with an aqueous/THF co-solvent mixture greatly improved the uniformity, as shown in (b) and (d), respectively. (e) Comparison of stain uniformity for immunolabeling of collagen (AB, green) for 6 days and amine labelling (Dye, magenta) with ATTO 647N-NHS for 2 hours. (f) Open-top light sheet microscopy images of ~1 mm thick mouse kidney sections in which amines (red) and carbohydrates (green) show distinct distributions among the cortex (C), outer medulla (OM), and inner medulla (IM) regions. (g) Zoom-in view of panel (f) taken from outer medullar region which contains various tubular architectures. (h) Cross-sectional view of the optically cleared mouse kidney sections along the dashed green line in panel (f). Scale bars are 100 µm (a-e, h), 50 µm (g), 0.5 mm (f).

2.4.3 FLARE is applicable to a wide range of tissues

Besides kidney tissue, FLARE also revealed an abundance of physiological details in a diverse range of other specimens (**Figure 2.5, Supplementary Figure 2.5e-x**). For instance: mouse intestine exhibited clear staining of intestinal villi, crypts, sub-epithelial cells, specialized cells (goblet cells, Paneth cells), lymphatic vessels, muscle cell boundaries; mouse liver revealed glycogen-rich hepatocytes with a strongly anticorrelated sub-cellular distribution of amine-reactive and carbohydrate-reactive domains; mouse sperm exhibited distinct developmental patterns of carbohydrates within seminiferous tubules of the testis; and human prostate gland and connective tissue from stroma are distinctly labeled and well distinguished from each other. Even formalin-fixed paraffin-embedded (FFPE) human kidney tissue was

straightforwardly labeled using FLARE, a notable capability because FFPE tissue processing often leads to loss of antigenicity for immunolabeling, whereas primary amines and carbohydrates remain quite reactive. We further compared FLARE with traditional histological staining by treating consecutive 10 µm thick mouse kidney FFPE sections to either H&E or FLARE (**Supplementary Figure 2.7**). By converting the DNA and amine channels of the FLARE-stained sections to a simulated H&E image using the procedure of Giacomelli et al.[27] we found that the FLARE and H&E tissues are qualitatively quite similar, although the standard fluorescence display of the DNA, amine, and carbohydrate signals of the FLARE data provided much greater detail (**Supplementary Figure 2.7**).

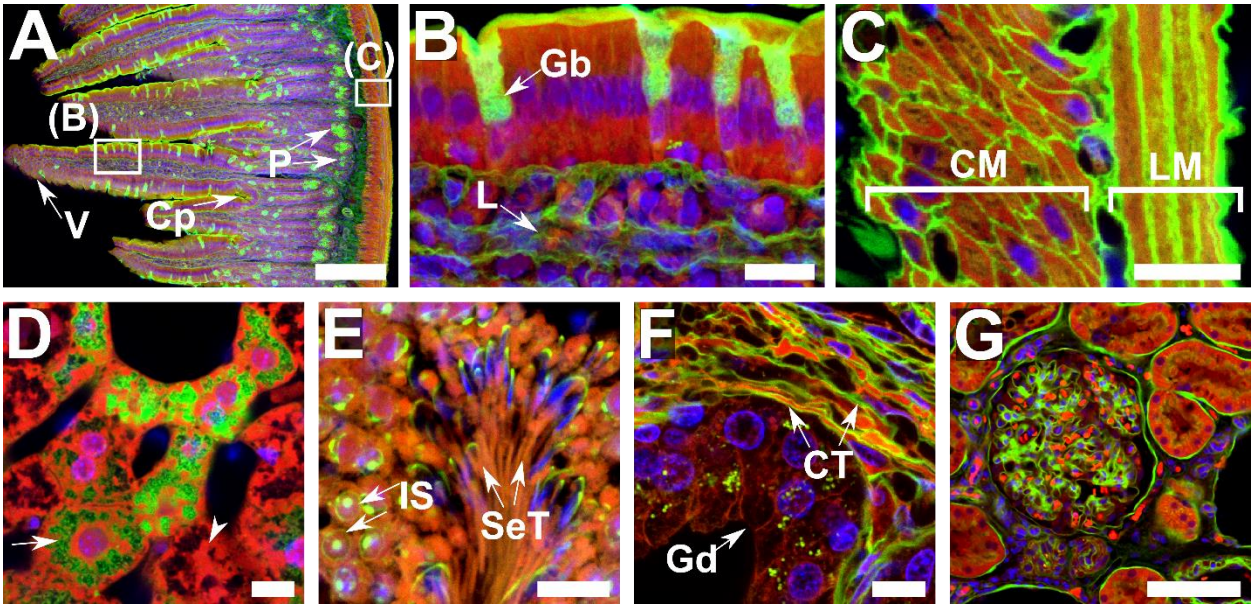

Fig. 2.5 | FLARE staining of a variety of cleared tissue specimens. Fluorescence microscopy images of optically cleared tissue specimens that were covalently stained for amines (red) and oxidized carbohydrates (green) along with a conventional noncovalent stain for DNA (blue). (a-c) mouse intestine, in which villi (V), crypt (Cp), Paneth cells (P), goblet cells (G), lymphatic vessels (L), circular muscle (CM), and longitudinal muscle (LM) layers are evident in the carbohydrate channel. (d) mouse liver where carbohydrate-rich and amine-rich regions are indicated with arrow and arrowhead, respectively. (e) mouse testis, in which immature spermatocytes (IS) and mature spermatocytes (MS) are evident and contain distinct carbohydrate distributions in the carbohydrate channel. (f) human prostate, where gland (Gd) and connective tissue (CT) from stroma are distinctly labeled. (g) formalin-fixed, paraffin-embedded human kidney. Scale bars are 100 µm (a, g), 10 µm (b-f).

2.4.4 Order of processing for FLARE is flexible

While there is considerable flexibility in the order of processing for FLARE in both expanded and non-expanded samples, some care is required (see Methods and **Supplementary Table 2.1**). First, the sodium periodate oxidation reaction used in carbohydrate labeling bleaches fluorophores already on the sample and tended to produce cracks in the expanded kidney tissue specimen if the oxidation step was done before sample gelation. As a result, we performed carbohydrate labeling before amine labeling, in general, and after expansion for kidney specimens (**Figure 2.3, Figure 2.4f-h, Supplementary Figure 2.1,**

Supplementary Figure 2.5a-d, Supplementary Figure 2.6 and Supplementary Figure 2.7e-f). Second, although covalent modification of the sample via FLARE has the potential to perturb epitope antigenicity necessary for antibody binding, we found that antibody labeling generally works quite well after FLARE. Out of a panel of 16 antibodies, 14 antibodies were able to effectively stain mouse kidney tissue (**Supplementary Figure 2.8**) or RPE cells (**Supplementary Figure 2.9**) after covalent labeling of carbohydrates and amines. Among the two impacted antibody stains, we found that the carbohydrate staining step partially blocked antibody staining of agrin on mouse kidney and fully blocked the antibody staining GM130 on RPE cells, but that both of these antibodies bound their targets well after covalent labeling of amines. This may indicate that we only labeled a small fraction of available amines, such that most amines on epitopes are unmodified, but that carbohydrate oxidation and/or fluorophore labeling may be more complete. We found that it was straightforward to change the order of labeling in cases like anti-GM130 (**Supplementary Figure 2.2m-q**) in order to immunolabel prior to covalent staining, although it is possible that a milder oxidation step may help better preserve antigenicity.

2.5 Discussion

One might initially expect that the indiscriminate labeling of primary amines and carbohydrates in cells and tissues would yield little contrast because of the high abundance of these species. However, the resulting feature-rich labeling we obtained likely results from an interplay between the uneven distribution of these groups throughout the specimen[28, 29], the reactivity of those groups (which can vary depending on the amine pKa[30] or other local factors), and earlier reactions with the specimen, such as may have occurred during aldehyde fixation and would consume some available reactive groups. Some known structures that were difficult to detect in expanded RPE cells, such as the endoplasmic reticulum or kinetochore fibers of the mitotic spindle, likely result from the above considerations and from the possibility that relatively weak labeling of these structures may be difficult to detect clearly due to the presence of many other brightly labeled structures within the specimen.

Here we have shown that simple amine-reactive and carbohydrate-reactive covalent stains, together with established DNA-stains, are versatile tools in super-resolution fluorescence microscopy and cleared-tissue fluorescence microscopy. Although we recently published a preliminary application of the use of amine-reactive fluorophores for rapid (<5 min) surface labeling of unexpanded and uncleared clinical specimens for rapid diagnosis[31, 32], the versatility of FLARE for super-resolution microscopy and cleared-tissue microscopy was not explored. In addition, FLARE can be easily combined with different staining modalities (e.g., fluorescence in situ hybridization labeling of nucleic acids and immunolabeling of proteins (**Supplementary** Figure 2.3e-h, **Supplementary** Figure 2.8-9)), is compatible with a large selection of excellent fluorophores across the visible and near infrared, and reveals abundant details in a wide range of samples and sample processing methods. While the contrast provided by these non-specific stains allows researchers to identify a range of features and key landmarks, the highlighted features vary between types of specimens and the utility of the stains are therefore somewhat dependent on the specific application. In the future, we look toward expanding the palette of covalent probes for FLARE by developing stains that target a wider range of chemical groups and by developing probes that target more specific subsets of proteins or carbohydrates. FLARE, together with newly developed custom probes against lipids[33] or other groups, will provide a versatile toolset that complements molecule specific probes such as antibodies and FISH probes.

2.6 Materials and Methods

2.6.1 Chemicals and reagents

Primary antibodies were purchased as follows: goat anti-podocalyxin (R&D Systems, Inc., AF1556), rabbit anti-collagen IV (Abcam, ab6586), mouse anti-alpha smooth muscle actin (BioLegend, Inc., 904601), rabbit anti-aquaporin 1 (Abcam, ab15080), guinea pig anti-cytokeratin 8+18 (Abcam, ab194130), mouse anti-agrin (DSHB, Inc., 6D2), rabbit anti-podocin (Sigma Aldrich, P0372), rabbit anti-TOMM20 (Santa Cruz Biotechnology, sc-11415), rabbit anti-LAMP-1 (Abcam, 24170), anti-GM130 (BD Biosciences, 610822), rabbit anti-GFP conjugated with Alexa Fluor 488 (Thermo Fisher Scientific, A-21311), rabbit anti-GFP conjugated with Alexa Fluor 647 (Thermo Fisher Scientific, A-31852), rabbit anti-H3K27ac (Active Motif, 39133), rabbit anti-H3K4me3 (Active Motif, 39159), rat anti-alpha tubulin (Invitrogen, MA1-80017), goat anti-nogo N-18 (Santa Cruz Biotechnology, sc-11027), rabbit anti-PMP70 (Thermo Fisher Scientific, PA1-650), anti-vimentin V9 (Invitrogen, 18-0052). Unconjugated secondary antibodies were purchased as follows: donkey anti-goat (Jackson Immunoresearch, 705-005-151), donkey anti-rabbit (Jackson Immunoresearch, 712-545-150), donkey anti-mouse (Jackson Immunoresearch, 715-005-151), donkey anti-guinea pig (Jackson Immunoresearch, 706-001-003), donkey anti-rat (Jackson Immunoresearch, 712-005-153). Donkey anti-rabbit conjugated with Alexa Fluor 488 (711-545-152) and donkey anti-mouse conjugated with Alexa Fluor 488 (715-545-150) was purchased from Jackson Immunoresearch. Fluorescent dyes were purchased as follows: Alexcea Fluor 750 NHS ester (Thermo Fisher Scientific, A20011), Alexa Fluor 546 NHS ester (Thermo Fisher Scientific, A2002), ATTO 647N NHS ester (Sigma-Aldrich, 18373-1MG-F), ATTO 565 NHS ester (Sigma-Aldrich, 72464-1MG-F), ATTO 565 hydrazide (ATTO-TEC GmbH, AD 565-121), AFdye 405 NHS ester (Fluoroprobes, 1061-1). Hoechst 33258 (Sigma-Aldrich, B2883-25MG), SYBR Green I (Invitrogen, S7563). 50% glutaraldehyde (GA, 16320) was purchased from Electron Microscopy Sciences. Reagents for polymerization were purchased as follows: 32% paraformaldehyde (PFA) aqueous solution (Electron Microscopy Sciences, RT15714), 40% acrylamide (AA) aqueous solution (Bio-Rad Laboratories, 1610140), 2% Bis-acrylamide (BA) aqueous solution (Bio-Rad Laboratories, 14101420), 97% sodium acrylate (SA) powder (Sigma-Aldrich, 408220), VA-044 initiator (Thermo Fisher Scientific, NC0471397), ammonium persulfate (APS, Thermo Fisher Scientific, 17874), Tetramethylethylenediamine (TEMED, Thermo Fisher Scientific, 17919), 97% 4-hydroxy-2,2,6,6-tetramethylpiperadin-1-oxyl (TEMPO, Sigma-Aldrich, 176141). Reagents for enzymatic digestion were purchased as follows: proteinase K (Thermo Fisher Scientific, EO0491), 10× Tris-acetate-EDTA (TAE buffer, Fisher Bioreagents, BP2434-4), 10× Phosphate Buffered Saline (PBS buffer, Fisher Bioreagents, BP399-1), guanidine hydrochloride (Sigma-Aldrich, G3272), collagenase (F type blend, Sigma Aldrich, C7926), Hank's Balanced Salt Solution (HBSS, 1×, Corning). Tris Base (BP-152), calcium chloride ($CaCl_2$, S25223), sodium chloride (NaCl, S271500), d-glucose (D16-1) and sodium acetate (NaOAc, BP333-500) powders were purchased from Thermo Fisher Scientific. Sodium dodecyl sulfate (SDS, L3771), sodium periodate (NaIO4, 311448), sodium cyanoborohydride ($NaCNBH_3$, 156159), ethyl cinnamate (EC, 112372), methacrylic acid NHS (MA-NHS, 730300), 4-(1,1,3,3-tetramethylbutyl)phenyl-polyethylene glycol (Triton X-100, X100), 4-morpholineethanesulfonic acid (MES, M3ti671), Piperazine-1,4-bis(2-ethanesulfonic acid) disodium salt (PIPES disodium salt, P3768), ethylene glycol-bis(2-aminoethylether)-N,N,N',N'-tetraacetic acid (EGTA, E4378), magnesium chloride ($MgCl_2$, M8266), sodium borohydride ($NaBH_4$, 213462), sodium azide (NaN_3, S2002) and poly-L-lysine (P8920), trolox (238813), glucose oxidase (G2133-50KU), catalase (C100) were

purchased from Sigma-Aldrich. Sodium bicarbonate ($NaHCO_3$, 470302) was purchased from VWR Scientific. Bovine serum albumin (BSA, BAS-50) was purchased from Rockland Immunochemicals Inc. Reagents for DNA fluorescence in situ hybridization (FISH) were purchased as follows: Formamide (Fisher Chemical, F84-1), 20× Saline Sodium Citrate (SSC Buffer, Sigma-Aldrich, S6639), 50% OmniPur Dextran Sulfate (EMD Millipore, 3730), Tween 20 (Sigma-Aldrich, P9416). Major Satellite and ATTO 647N conjugated reporter oligonucleotides were obtained from IDT.

2.6.2 Cell culture

H-tert Retinal Pigment Epithelium Cells (RPE) were obtained and authenticated from ATCC and were used without further authentication. RPE cells were tested negative for mycoplasma with 4',6-diaminodino-2-phenylindole dihydrochloride. RPE cells were cultured in Dulbecco's Modified Eagle Medium (DMEM, Gibco, 11995-065) supplemented with 100 Units/mL Penicillin Streptomycin (Gibco, 15140-122), 5% non-essential amino acids (NEAA, Gibco, 11140-050) and 10% fetal bovine serum (FBS, Gibco, 25200-056), and grown to ~70-90% confluency. The cells were then trypsinized with 0.25% Trypsin-EDTA (Gibco, 25200056) and seeded (~50,000 cells/well) on #1.5 round coverslip (~12 mm) in 24-well culture plates. 24 hours later, the cells were fixed with either 3.2% PFA and 0.1% GA or 4% PFA in PEM buffer (100 mM aqueous PIPES, 1 mM EGTA, 1 mM $MgCl_2$, pH 7) for 10 minutes at room temperature. In some cases, cells were extracted with 0.5% Triton X-100 in PEM buffer for 30 secs before fixation with 3.2% PFA and 0.1% GA in PEM buffer (**see Supplementary Table 2.1** for details). Fixed cells were stored in 1× Phosphate Buffer Saline with 3mM sodium azide (1× PBS azide) at 4°C prior to use.

2.6.3 Transfection of cultured cells

Trypsinized RPE cultured cells (~1- 2 x 106 cells) were pelleted down by centrifugation (150 g for 5 min) and resuspended in nucleofection solution (Lonza Kit V, VACA-1003) with 2 µg plasmid mEmerald-Golgi-7, and electroporated following manufacturer's (Lonza Amaxa Nucleofector I/II) X-001 pulse program. mEmerald-Golgi-7 was a gift from Michael Davidson's Lab (Addgene plasmid #54108; http://n2t.net/addgene:54108; RRID:Addgene_54108). pAc-GFPC1-Sec61β was a gift from Tom Rapoport (Addgene plasmid #15108; http://n2t.net/addgene:15108; RRID:Addgene_15108). Transformed cells (transfection efficiency ~70%) were then seeded (~80,000 cells/well) on #1.5 round coverslips (~12 mm) in 24-well culture plates and allowed to recover for 24 hours before fixation with 3.2% PFA and 0.1% GA in PEM buffer for 10 minutes at room temperature. Fixed cells were stored at 4 °C in 1× PBS azide until use.

2.6.4 Preparation of fluorophore-labeled secondary antibodies

NHS ester functionalized dyes were used to conjugate with secondary antibodies. In brief, 40 µL of secondary antibody, 5 µL of 1M $NaHCO_3$, and 1-2 µg of fluorophore were mixed. The reaction mixture was protected from light and was completed in 30 minutes. The fluorophore-conjugated secondary antibody was purified and collected from the crude reaction mixture via a disposable NAP-5 column (GE Healthcare Life Sciences, 17085301), and further characterized by UV/Vis absorption spectroscopy.

2.6.5 Mouse organ dissection and preparation

All protocols and methods involving animals in this work were approved by the Institutional Animal Care and Use Committee (IACUC) at University of Washington.

Two-month-old C57BL/6 male mice were anesthetized by isoflurane/oxygen mixture followed by cardiovascular perfusion with 1× PBS for 3 minutes followed by 4% PFA solution in 1× PBS for 5 minutes. Kidneys were then collected, and the renal capsules were removed. Other organs such as intestine and testis were also collected. Organs were fixed for 1-6 hours in 4% PFA solution in 1× PBS (see **Supplementary Table 2.1** for details). Then they were washed by 1× PBS solution three times and sliced by a vibratome to 100 µm thick. Due to the softness of testis and intestine, agarose gel was used to embed them while slicing. All slices were stored in 1× PBS azide at 4 °C until use.

For the comparison of H&E and FLARE stains (**Supplementary Figure 2.7**), mouse kidney tissue was collected from healthy Balb/c male mice at 12 weeks of age. Kidneys were perfused with PBS to remove blood cells, fixed in 10% buffered formalin and then embedded in paraffin. FFPE kidney tissue was sliced into sections of ~10 µm, deparaffinized and stained with haematoxylin and eosin (H&E) by Pathology Research Services Laboratory at University of Washington. The stained tissue sections were then imaged with an Aperio ScanScope AT2 digital whole slide scanner at the Harborview Medical Center (HMC) Digital Pathology Facility.

2.6.6 Human kidney and prostate preparation

A deidentified formalin-fixed and paraffin-embedded (FFPE) human kidney tissue block was obtained from NW BioTrust under approval from University of Washington Institutional Review Board with de-identification. Sections of ~60 µm thickness were prepared using a microtome. In order to deparaffinize the section, the section was soaked in xylene solution for 10 min. Then, the section was rehydrated by incubation in a series of ethanol/water mixtures with descending ethanol concentration (100%, 95%, 85%, 70%, 50%, 0%). Eventually, rehydrated slices were stored in 1× PBS at 4 °C until further use. Deidentified, freshly fixed human prostate samples were received from the University of Washington Genitourinary Biorepository with patient consent and, stored at 4 °C, and 100 µm sections were prepared with a vibratome. Approval was obtained from the University of Washington Institutional Review Board.

2.6.7 Cell gelation, denaturation, and expansion

The MAP (magnified analysis of the proteome) sample preparation used here for cells was adapted from Ku et al.[20]. Fixed cells on 12 mm round coverslips were treated with 10 mM aqueous $NaBH_4$ solution for 10 min, washed with 1× PBS, and then incubated in monomer solution (20% (wt/wt) AA, 10% (wt/v) SA, 0.05% (wt/wt) BA, 4% (v/v) PFA, 0.67% (v/v) TEMED) overnight at room temperature before gelation with 0.2% (wt/v) APS at room temperature for at least 30 min. After polymerization, the cell-embedded hydrogel on the coverslip was cleared in denaturing solution (200 mM SDS, 200 mM NaCl, 50 mM Tris Base, pH 9.3) for 1 hr at 90 °C. The denatured cell-embedded hydrogel was then sequentially washed by PBST (1× PBS, 0.1% (wt/v) Triton X-100, and 0.02% (wt/v) NaN_3) and 1× PBS before placing into DI water for sample expansion.

2.6.8 Tissue gelation, denaturation/digestion, and expansion

The MAP sample preparation used here for expanded mouse kidney tissues was adapted from Unnersjö et al.[34]. Fixed kidney sections were soaked in monomer solution (20% (wt/wt) AA, 10% (wt/v) SA, 0.05% (wt/wt) BA, 4% (v/v) PFA, 0.1% (wt/v) VA-44) overnight at 4 °C. Gelation was done at 45 °C for 2 hr. The polymerized gel was carefully peeled off, trimmed, and then transferred into denaturing solution (200 mM SDS, 200 mM NaCl, 50 mM Tris, pH 9.3). The expanded mouse kidney tissue was processed in a similar way but with denaturation at 70 °C for 24 hours followed by 90 °C for another 24 hours. The sample was then thoroughly washed by PBST before placing into DI water to expand.

The ExM sample preparation for **Supplementary Figure 2.3** was adapted from Chozinski et al.[21]. Immunostained fixed mouse kidney sections were first incubated in 1 mM MA-NHS in 1× PBS at room temperature, followed by incubation in monomer solution (1× PBS, 2 M NaCl, 2.5% (wt/wt) AA, 0.15% (wt/wt) BA, 8.625% (wt/wt) SA) for at least an hour in 4 °C. Gelation of the kidney section was then done at 37 °C for 1.5-2.5 hr with monomer solution containing 0.2% (wt/wt) APS, 0.2% (wt/wt) TEMED and 0.01% (wt/wt) TEMPO. The hydrogel-embedded kidney sample was digested overnight with 8 units/mL proteinase K in proteinase digestion buffer (1× TAE buffer, 0.5% Triton X-100, 0.8 M guanidine hydrochloride) at 37 °C. The sample was then further digested with 5 mg/mL collagenase in collagenase digestion buffer (1× HBSS with 0.7 mM $CaCl_2$) overnight at 37 °C.

2.6.9 General covalent staining procedure for hydrogel samples and cleared tissues

All samples were stained in the same sequence: carbohydrates, amines, and lastly, DNA. For carbohydrate staining, the samples were first oxidized with $NaIO_4$, then incubated with fluorescent dye ATTO 565-hydrazide after washing off excess $NaIO_4$. $NaCNBH_3$ was then used to reduce the hydrazone bond formed for better stability. The samples were then incubated with fluorescent dye ATTO 647N-NHS for the staining of amines in proteins after washing off excess NaCNBH3. Lastly, fluorescent DNA dye (Hoechst 33258 or SYBR Green I) was added for nuclei staining. Samples were either expanded (for hydrogel samples) or refractive index matched with EC (for organic cleared samples) before imaging. A summary of the various reagents, buffers, quantities and conditions for all data in this paper is listed in **Supplementary Table 2.1.**

2.6.10 Immunostaining procedures

All non-transfected samples covalently stained prior to gelation were processed in this sequence: carbohydrates, amines, antibodies, gelation and lastly, DNA. For carbohydrate, amine and DNA staining, see above section on General Covalent Staining Procedure. For general immunostaining of cell samples prior to gelation, the sample was incubated first in block and permeabilization solution (BP, 0.3% (wt/v) BSA, 0.5% (wt/v) Triton X-100, 1× PBS) for 30 min, followed by primary antibodies in BP for 90 min, and lastly, secondary antibodies in BP for 45 min. Samples were post-fixed with 0.25% GA in 1× PBS for 5 min. For general immunostaining of tissue samples, the same procedure was followed but with different incubation conditions (see **Supplementary Table 2.1** for details). After immunolabeling, samples for hydrogel expansion were treated for 1 hr with freshly prepared 1 mM MA-NHS in 1× PBS.

All non-transfected cell samples covalently stained post-gelation were proceeded in this sequence: antibodies, gelation, carbohydrates, and lastly, amine. For post-gelation carbohydrate and amine staining, in order to immunostain prior to gelation, the procedure requires the use of secondary antibodies conjugated to biotin instead of a fluorescent dye because the mild oxidation used in carbohydrate staining step later may chemically bleach fluorophores on the secondary antibodies.

For the transfected cell sample in **Supplementary Figure 2.2r-v**, immunostaining with anti-GFP Alexa Fluor 488 was performed after the post-gelation covalent stains. The immunostain on the hydrogel sample was performed in BP for 15 hr at room temperature. Samples were either expanded (for hydrogel samples) or refractive index matched with EC (for organic cleared samples) before imaging. A summary of the various reagents, buffers, quantities, and conditions for all data in this paper is listed in **Supplementary Table 2.1**.

2.6.11 DNA fluorescence in situ hybridization

The DNA-FISH procedure was adapted from Beliveau et al.[35] FLARE-stained and MAP-expanded mouse kidney samples were first incubated in 0.5% Triton X-100 in 1× PBS for 2 hr. Samples were washed once in 1× PBS, then in 2× SSCT (0.1% Tween 20 in 2× SSC), and last in hybridization buffer (50% formamide, 0.1% Tween 20 in 2× SSC) for 10 minutes each time. Samples were incubated in fresh hybridization buffer for 30 min at 60 °C. The hybridization mixture (50% formamide, 10% dextran sulfate, 0.1% Tween 20, 3 mM sodium azide, 100 nM MaSat oligo probe, 100nM oligo reporter in 2× SSC) was pre-heated to 92.5 °C for 5 minutes, then added to each sample at an approximate 2:1 volume ratio. Samples were denatured at 92.5 °C for 10 minutes and hybridized at 37 °C overnight. Samples were washed three times in 2× SSCT, first at 60 °C, second at 37 °C and finally at room temperature, 15 minutes each time. Samples were stored in 0.2× SSCT at 4 °C for at least 1 hour or until needed for imaging (within a week). Before imaging, samples were fully expanded by replacing the sample buffer at least twice with water every ten minutes at 4 °C.

The MaSat oligo probe (5'-GGAATATGGC GAGAAAACTG AAAATCACGG AATGATACGG CGACCACCGA ACTGCTACAG-3') contains 30 nucleotides of the mouse Major satellite repeat DNA sequence (obtained from Lehnertz et al.[36]) and 30 nucleotides complimentary to the fluorophore conjugated oligo reporter (5'-/5ATTO647NN/ CTGTAGCAGT TCGGTGGTCG CCGTATCATT-3').

2.6.12 Organic solvent clearing

Stained tissue specimens were dehydrated using solutions of THF/H_2O with ascending THF (v/v) concentrations (50%, 80%, 100%) as follows. Stained 100 µm thick tissue specimens were first incubated in 50% THF for 10 min, then in 80% THF twice for at least 15 min each, and lastly, in 100% THF twice for at least 15 min each. Stained 500-800 µm thick tissue specimens were first incubated in 50% THF for 30 min, then in 80% THF twice for at least 1 hr each and lastly in 100% THF twice for at least 1 hr each. After THF dehydration, 100% dichloromethane (DCM) was then added and incubated until the specimen sank. DCM was removed and 100% ethyl cinnamate oil (EC) was added to the sample followed by incubation for 2 hours or more. For thicker specimens, EC was exchanged a few times to ensure good index-matching.

2.6.13 Sample mounting

EC-cleared samples were transferred onto a rectangular #1.5 coverslip (Fisher Scientific, #12544E, 24 x 50 mm) using a paintbrush. A piece of double-sided tape was attached to the surface of the coverslip along the each of the short edges of the coverslip, then a drop of EC was added on sample surface to prevent it from drying, and a second coverslip was pressed onto the first to form a sandwich structure held together by the double-sided tape. For the fully expanded hydrogel-embedded samples, the gel was adhered to a poly-L-lysine coated coverslip and imaged immediately.

2.6.14 Fluorescence microscopy and imaging

All data, except for 1 mm EC cleared mouse kidney and **Supplementary Figure 2.6-2.9**, were acquired using a Leica SP5 inverted confocal point scanning microscope at the University of Washington Biology Imaging Facility. The objective lenses used on the confocal microscope were a HC Plan Apo CS 63× 1.2 NA water-immersion objective, a HC Plan APO CS 63× 1.4 NA oil-immersion objective, a HC Plan Apo CS 20× 0.7 NA air objective, and a HC Plan Apo CS 10× 0.4 NA air objective. A summary of the various imaging conditions used for each data set can be found in **Supplementary Table 2.1**.

Supplementary Figures 2.7-2.9 were acquired with a conventional wide-field epifluorescence inverted Nikon Ti-S microscope. The objective lenses used on the wide-field microscope were CFI Plan Apo VC 60× 1.2 NA (Nikon, Melville, NY, USA) water-immersion objective, CFI S Plan Fluor 20× 0.45 NA (Nikon) air objective, and CFI Plan Apo λ 4× 0.2 NA (Nikon) air objective. The illumination source was a four-channel light emitting diode (LED4D251, Thorlabs, Newton, NJ, USA) that used a quad-band filter set (Chroma 89402). The detection unit used to capture the images was a ZWO-AS174MM-COOL CMOS camera (ZWO, Suzhou, China). When applicable, for single-channel observations, single-band emission filters (Chroma ET 525/50, ET 605/70, or ET700/75) were used.

Supplementary Figure 2.6 was acquired with a homebuilt spinning disk confocal microscope using a Nikon CFI S Plan Fluor 20× 0.45 NA (Nikon) air objective lens. This microscope will be the subject of a future publication.

3D volumetric imaging of the 1 mm EC cleared mouse kidney was acquired using a recently published open-top light sheet microscope[26]. Briefly, illumination light is coupled into the system by a single-mode fiber from a four-channel (405, 488, 561, and 638 nm) laser package (Skyra, Cobolt Lasers). The light is scanned using a galvanometer, GM (6210H, Cambridge Technology) to create a digital light sheet with a numerical aperture of ~0.06. Fluorescence is collected by a multi-immersion objective (#54-10-12, Special Optics, distributed by Applied Scientific Instrumentation). This objective provides <1 µm in-plane resolution for clearing media with a usable refractive index range of 1.33 – 1.56. The collected fluorescence is focused onto a 2048×2048 pixel sCMOS camera (ORCA-Flash4.0 V2, Hamamatsu) by a tube lens, TL2 (TTL165, Thorlabs, f = 165 mm) which provides a sampling of ~0.45 µm/pixel at n = 1.56 which satisfies the Nyquist criterion. This results in a horizontal field of view of ~0.9 mm over the 2048 pixels of the camera. The vertical field of view is reduced to 256 pixels (113 µm) to closely match the depth of focus of the illumination light sheet (~110 µm). The 256 pixels are oriented parallel to the rolling shutter readout direction of the camera, which provides an exposure time of 1.25 ms and a frame rate of 800 Hz. 3D

imaging is achieved using a combination of stage-scanning and lateral/vertical tiling with a motorized XY stage and Z actuators (FTP-2050-XYZ, Applied Scientific Instrumentation).

2.7 Acknowledgements

The authors would like to thank the Biology Imaging Facility at the University of Washington for imaging assistance, R.D. Palmiter and H.Y. Kueh (University of Washington, Seattle, WA) for generously providing mice for this study, Michael Davidson for generously providing mEmerald-Golgi-7 plasmids (Addgene, Watertown, MA), Tom Rapoport for generously providing pAc-GFPC1-Sec61β plasmids (Addgene, Watertown, MA), and C.E. Alpers and R.O.L. Wong (University of Washington, Seattle, WA) for access to tissue-sectioning instruments.

This work was supported by the University of Washington, NIDDK Diabetic Complications Consortium grants DK076169 and DK115255 (J.C.V.), NIH grant numbers R01 MH115767 (J.C.V.), R01 CA175391 (J.T.C.L.), RO1 DK097598 (S.J.S.), UH2 DK107343 (S.J.S.), R01 AG046231 (S.J.S.), K99 CA240681 (A.K.G.), DoD PCRP PC170176 (J.T.C.L.) and by an NSF Graduate Research Fellowship DGE-1256082 (T.J.C.). NW BioTrust, a core service for patient consenting, and NWBioSpecimen, a core service for procurement and annotation of research biospecimens, are supported by National Cancer Institute grant P30 CA015704 (G. Gilliland, principal investigator [PI]), Institute of Translational Health Sciences grant UL1 TR000423 (M. Disis, PI), the University of Washington School of Medicine and Department of Pathology, and Fred Hutchinson Cancer Research Center.

2.8 Supporting Information

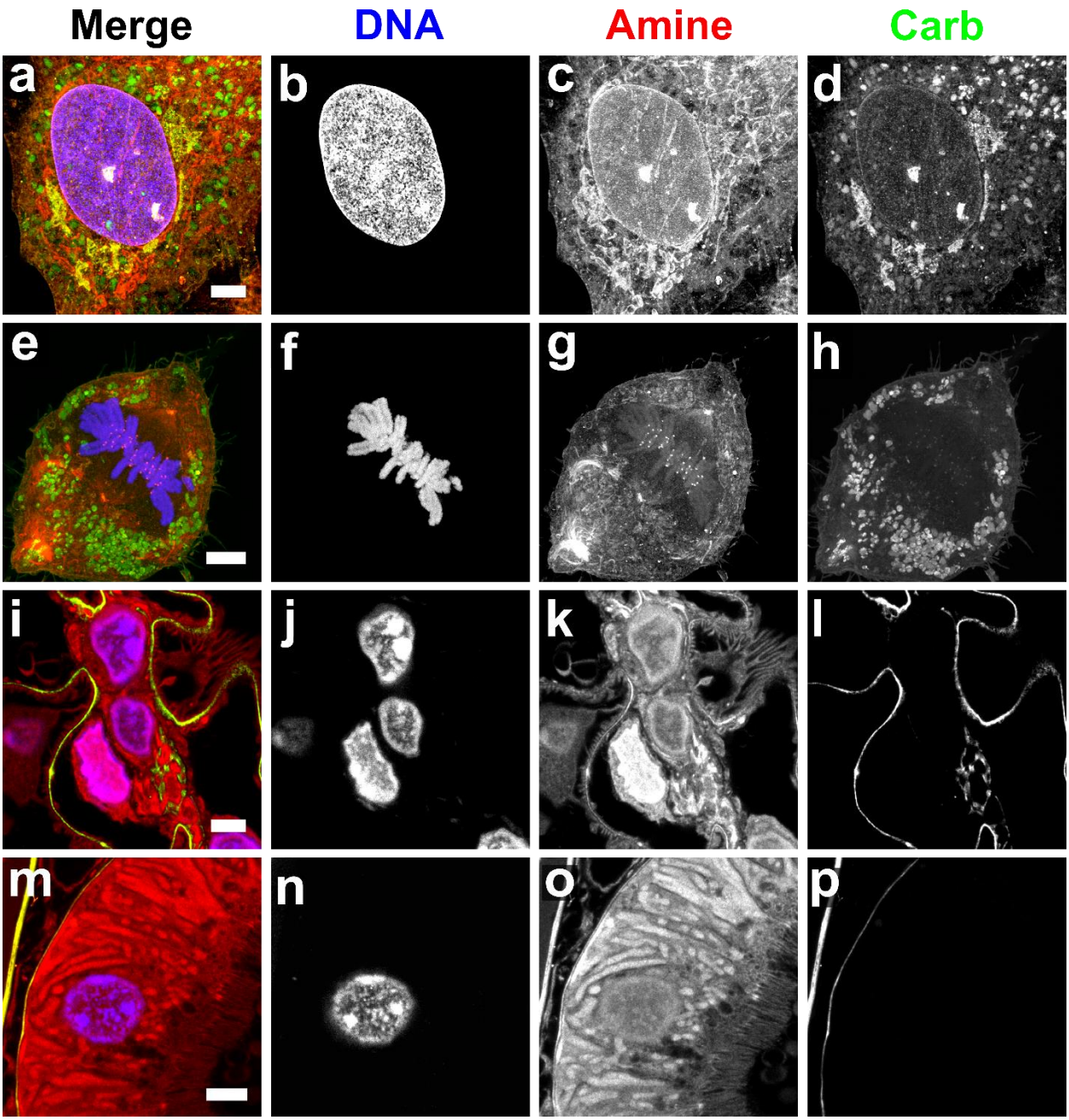

Supplementary Fig. 2.1 | Single-channel images from the multichannel data in **Fig. 2.2 and 2.3.** Confocal microscopy images of expanded specimens stained for carbohydrates, amines, and DNA (see also Fig. 2.2 and Fig. 2.3), together with their respective individual channels. These include (a-d) a single interphase RPE cell, (e-h) a single dividing RPE cell, (i-l) a region of a mouse kidney glomerulus, and (m-p) a region of a mouse kidney proximal convoluted tubule. Scale bars are 3 µm and are in pre-expansion units.

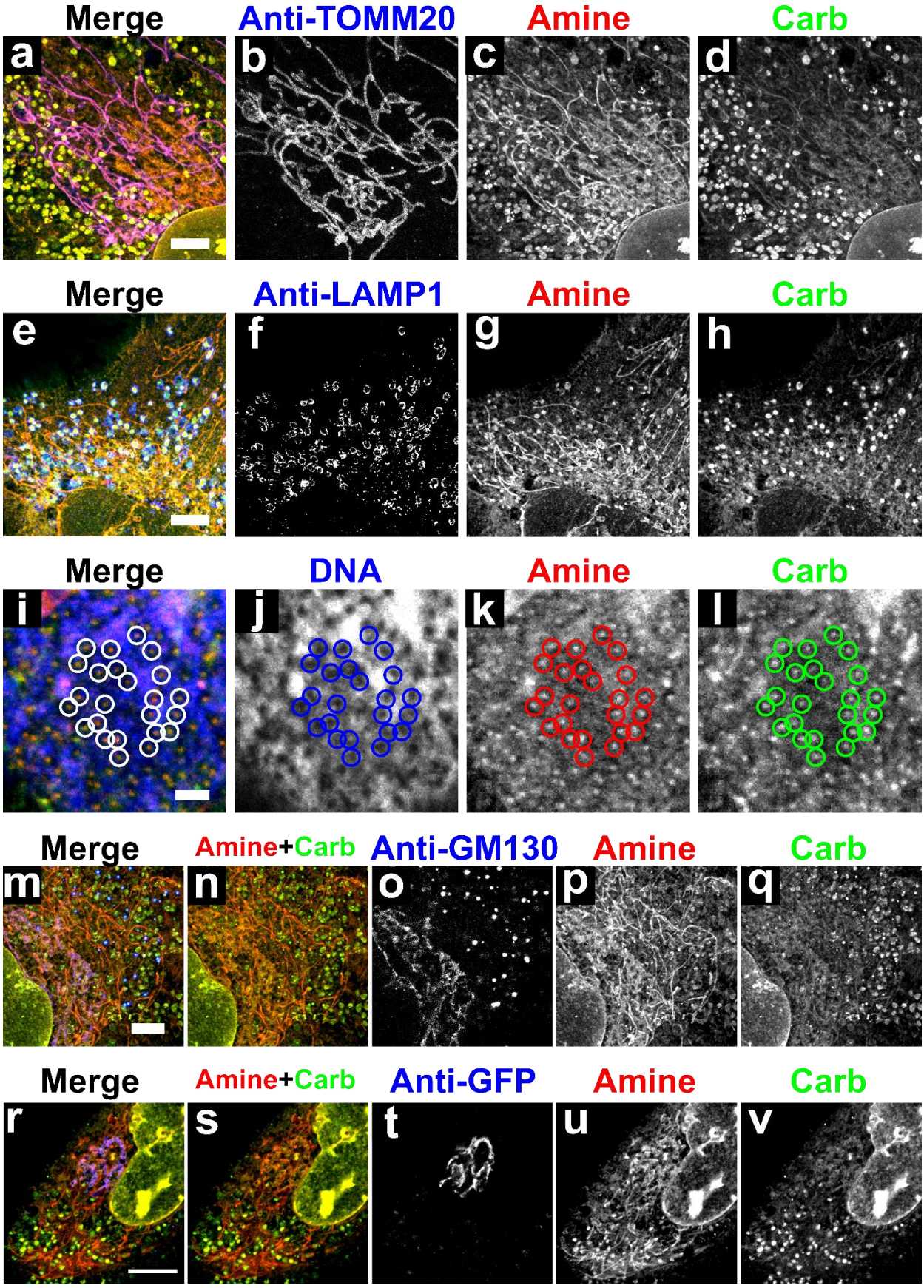
Merge
Anti-TOMM20
Amine
Carb
a
b
c
d
Merge
Anti-LAMP1
Amine
Carb
e
f
g
h
Merge
DNA
Amine
Carb
i
j
k
l
Merge
Amine+Carb
Anti-GM130
Amine
Carb
m
n
o
p
q
Merge
Amine+Carb
Anti-GFP
Amine
Carb
r
s
t
u
v

Supplementary Fig. 2.2 | Validation of sub-cellular features identified by FLARE staining in expanded RPE cells. Confocal microscopy images of expanded RPE cells showing that mitochondria, lysosomes, nuclear pores, and parts of the Golgi apparatus are readily identifiable from covalent stains of amines and carbohydrates. (a-d) An immunostain against the mitochondrial protein TOMM20 colocalizes extensively with the filamentous structures in the amine channel. (e-h) An immunostain against the lysosomal protein LAMP1 colocalizes extensively with bright punctae in the carbohydrate channel. (i-l) In this zoom-in view of a region of a nucleus, heterochromatin voids in the DNA channel colocalize with punctae in the amine and carbohydrate channels and are indicative of nuclear pores (same cell as in **Fig. 2.2a**, but here a projection of a thin volume near the bottom of the nucleus). (m-q) An immunostain against cis-Golgi matrix protein GM-130 partially colocalizes with a distinct perinuclear signal coming from amine and carbohydrate channels. (r) Multichannel, maximum intensity projection of an expanded transfected RPE cell that was labeled with anti-GFP, (s) corresponding combined amine and carbohydrate channels, and (t-v) corresponding single-channel images. All scale bars are in pre-expansion units. Scale bars, 3 µm (a, e, m, r), 500 nm (i).

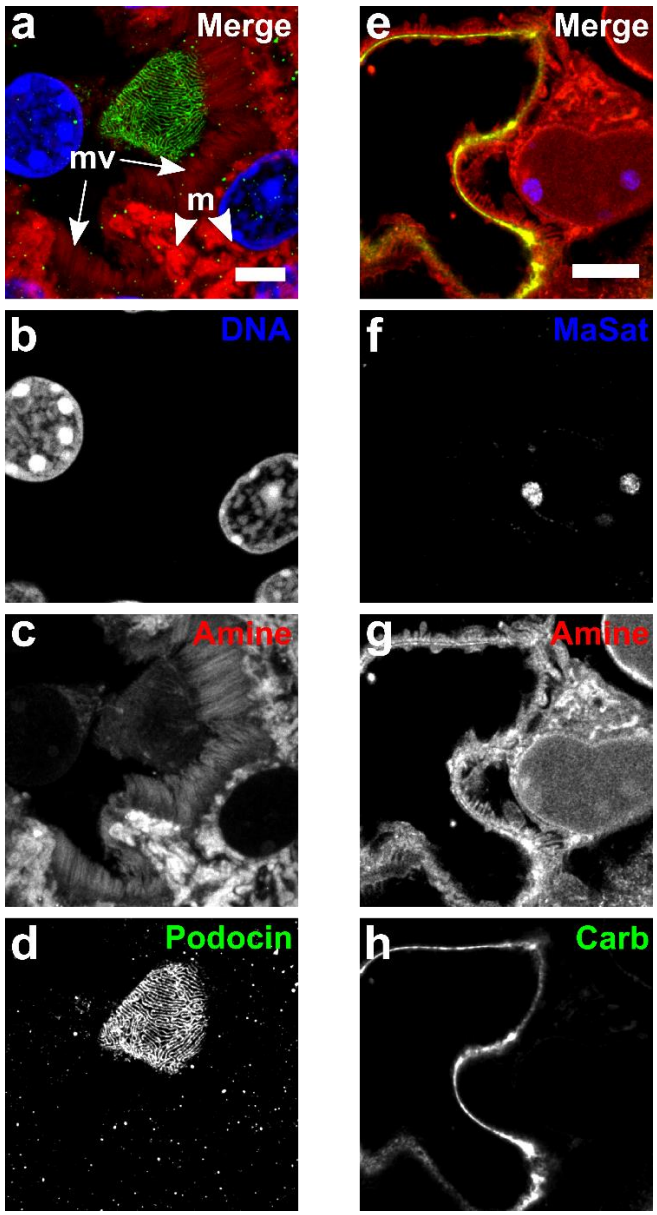

Supplementary Fig. 2.3 | Use of FLARE staining with enzymatic digestion expansion protocol or DNA FISH protocol mouse kidney tissue. (a-d) Confocal microscopy images of expanded mouse kidney. Prior to covalent labeling, tissue was processed with an expansion microscopy[21] (ExM) procedure that uses enzymatic digestion, rather than a magnified analysis of the proteome[20] (MAP) procedure that uses heat and detergent to dissociate tissues as was done for all other expansion data in this paper (see Materials and Methods and **Supplementary Table 2.1**). Prior to gelation, the sample was immunolabeled against podocin and covalently stained for amines. After gelation, the sample was homogenized using enzymatic digestion, expanded, and stained with the DNA-binding dye Hoechst (see Materials and Methods and **Supplementary Table 2.1**). (a) Maximum intensity projection of a region showing interdigitated podocytes (green, podocin) on a glomerulus as well as a proximal convoluted tubule lined with microvilli ('mv') and containing abundant mitochondria ('m'). (b-d) corresponding single-channel images. (e-h) Confocal microscopy images of an expanded mouse kidney tissue that was stained for carbohydrates, amine, and then DNA FISH against pericentromeric major satellite (MaSat) DNA. (e) Multichannel, maximum intensity projection and (f-h) corresponding single channel images. Scale bars are 3 µm and are in pre-expansion units.

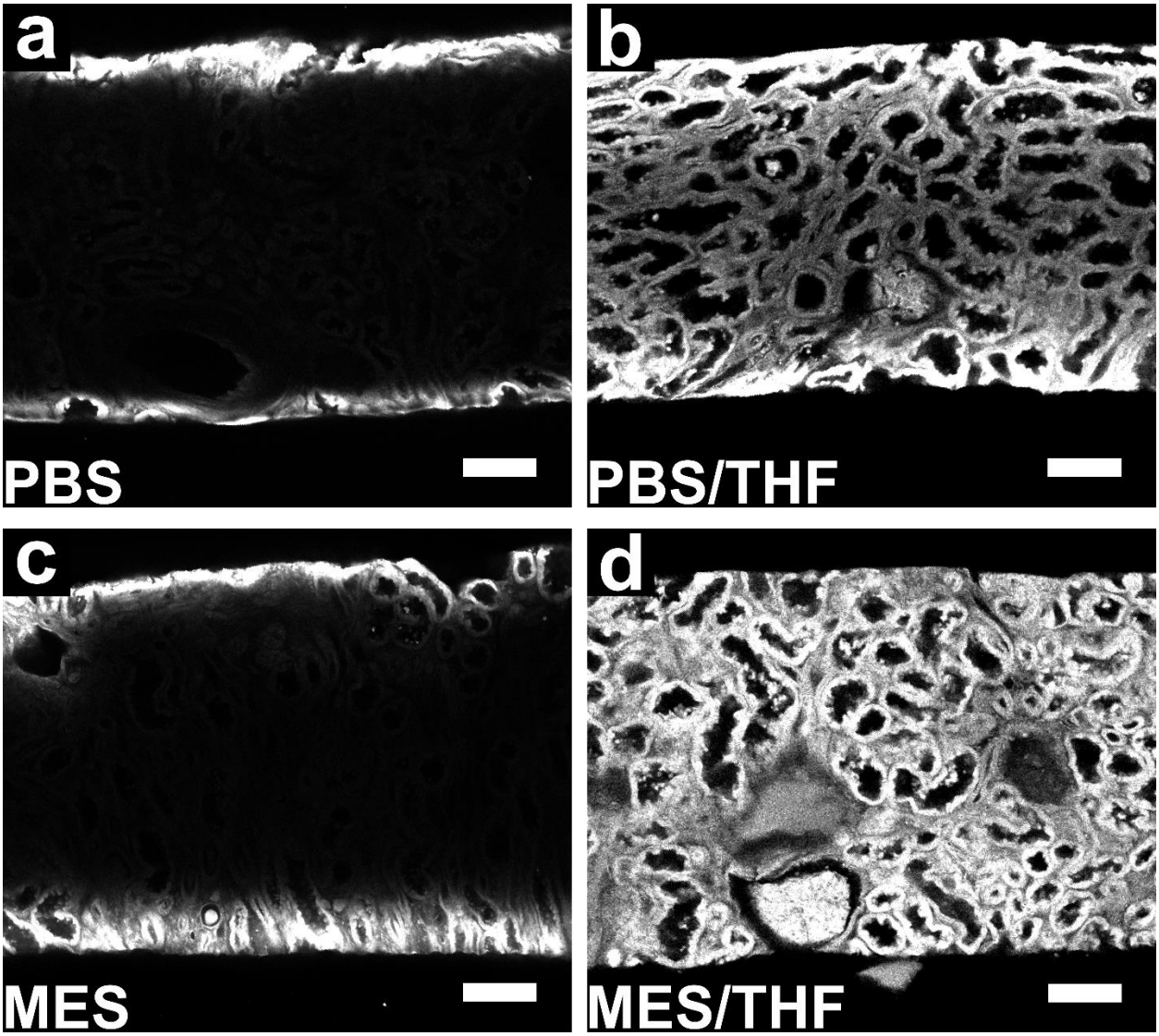

Supplementary Fig. 2.4 | Enhancement of FLARE stain uniformity in unexpanded thick tissue. Comparison of stain uniformity for amine labeling of ~500 μm thick human kidney sections stained for 15 hours with 1 μg/mL ATTO 647N-NHS (see also **Fig. 2.4** for panel c and d). Sections were stained, cut perpendicular to the section face, and imaged on a confocal microscope to measure the stain intensity at different depths for (a) a pH 7.4 1×PBS solution, (b) a pH 7.4 1×PBS:THF (1:1) mixture, (c) a pH 6.0 MES buffer solution, and (d) a pH 6.0 MES:THF (1:1) mixture. Scale bars are 100 μm.

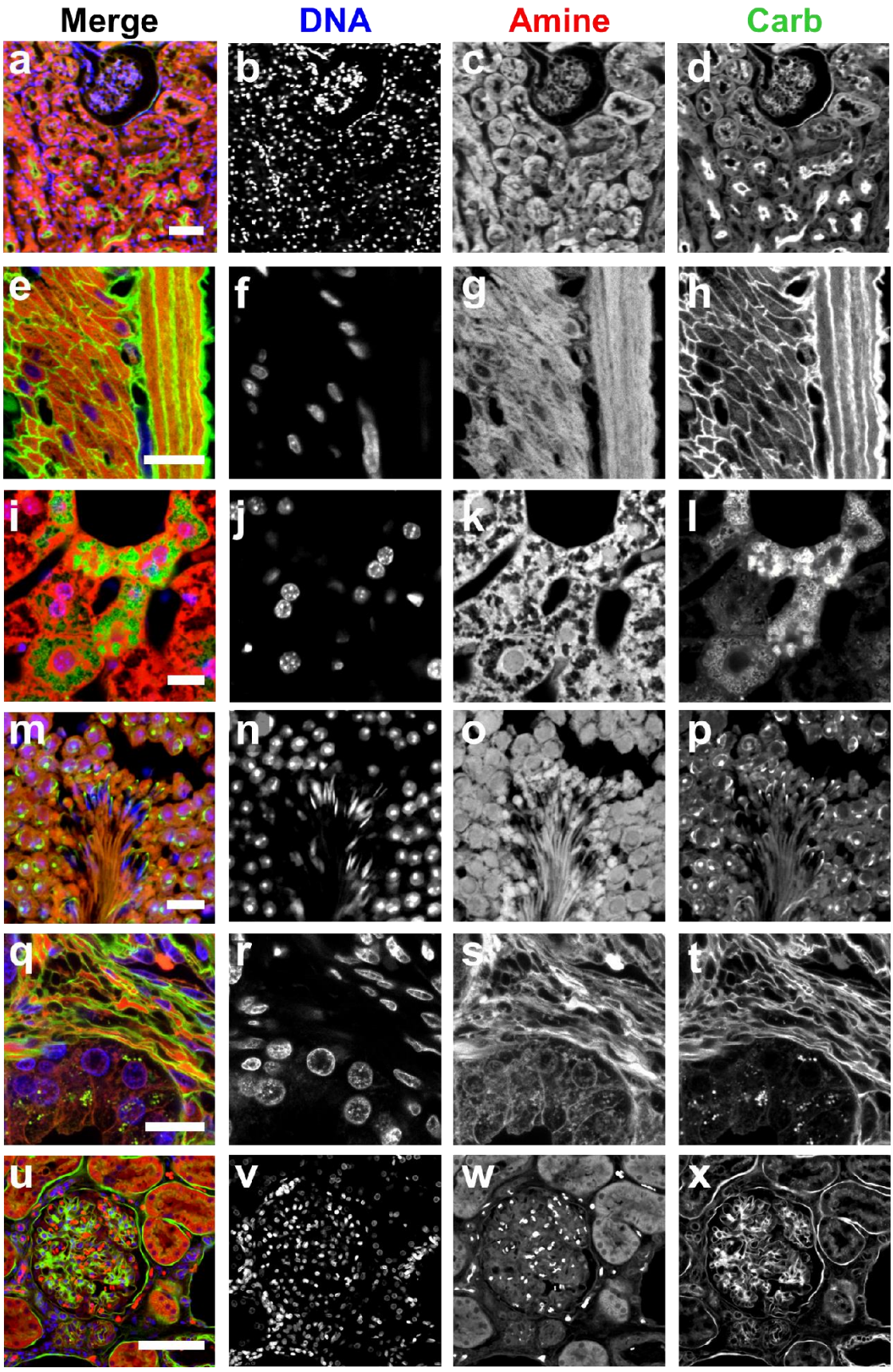
Merge
DNA
Amine
Carb
a
b
c
d
e
f
g
h
i
j
k
l
m
n
o
p
q
r
s
t
u
v
w
x

Supplementary Fig. 2.5 | Single-channel images from the multichannel data in **Fig. 2.4 and 2.5.** Confocal microscopy images of unexpanded, optically cleared tissue specimens that were FLARE-stained for carbohydrates, amines, and DNA (see also **Fig. 2.4** and **Fig. 2.5**), together with their respective individual channels, including (a-d) a region of mouse half kidney tissue, (e-h) circular and longitudinal muscle from mouse intestine, (i-l) mouse liver, (m-p) mouse testis, (q-t) human prostate, and (u-x) a formalin-fixed, paraffin-embedded (FFPE) human kidney. All images are maximum intensity projections as described in **Supplementary Table 2.1**. Scale bars are 50 µm (a), 10 µm (e, i, m, q), and 100 µm (u).

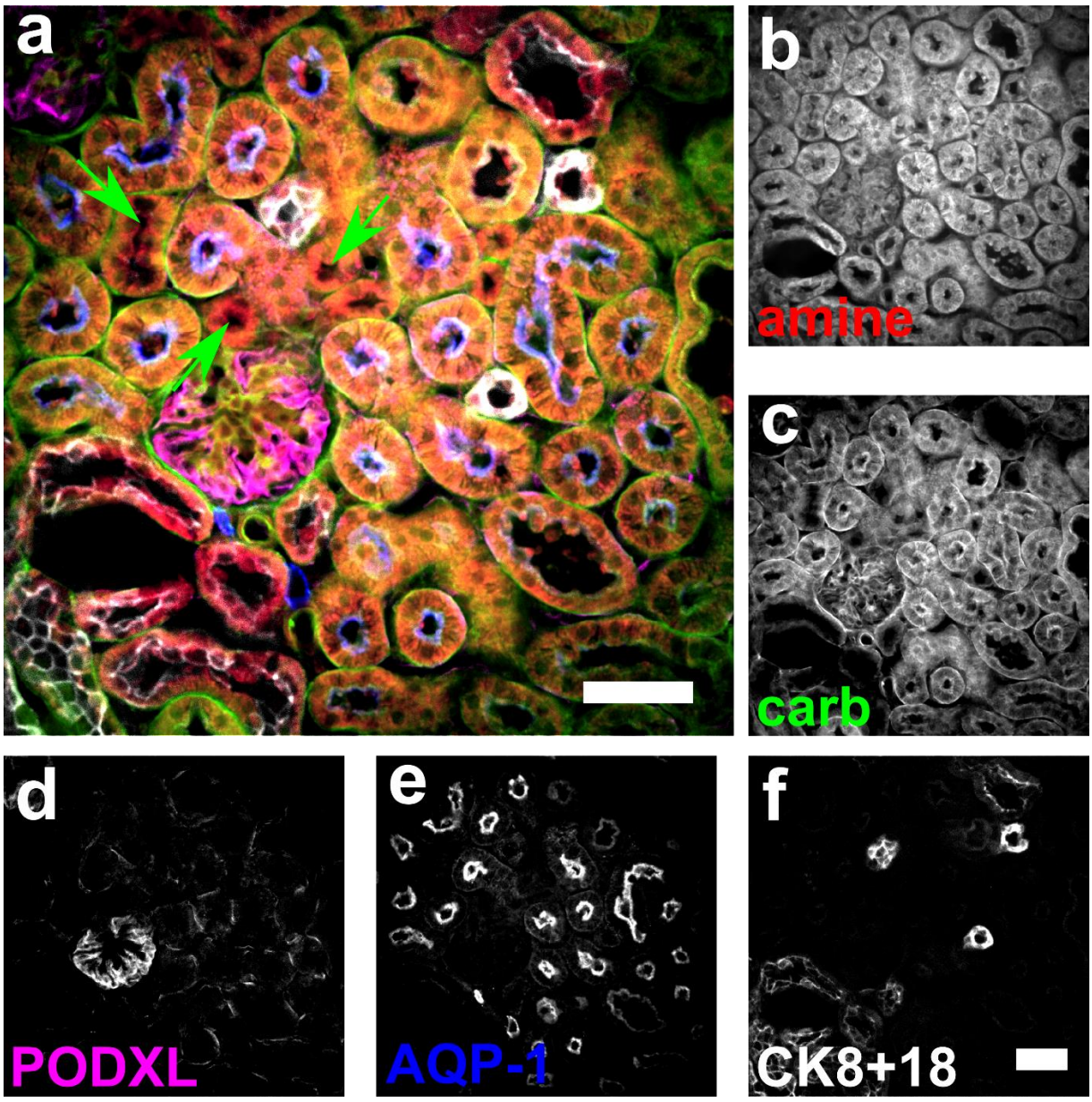

Supplementary Fig. 2.6 | Concurrent use of FLARE staining with immunostaining to identify general features in mouse kidney. (a) Confocal microscopy image of a mouse kidney tissue section that was stained for carbohydrates and amines, and then immunostained for podocalyxin (PODXL, labels glomeruli), aquaporin-1 (AQP-1, labels proximal tubules), and cytokeratin 8+18 (CK8+18, labels collecting ducts). Renal tubules that lack antibody signals here are most likely distal convoluted tubules and are indicated by green arrows. (b-f) Corresponding single-channel images of the specific channels indicated. Scale bars are 50 µm.

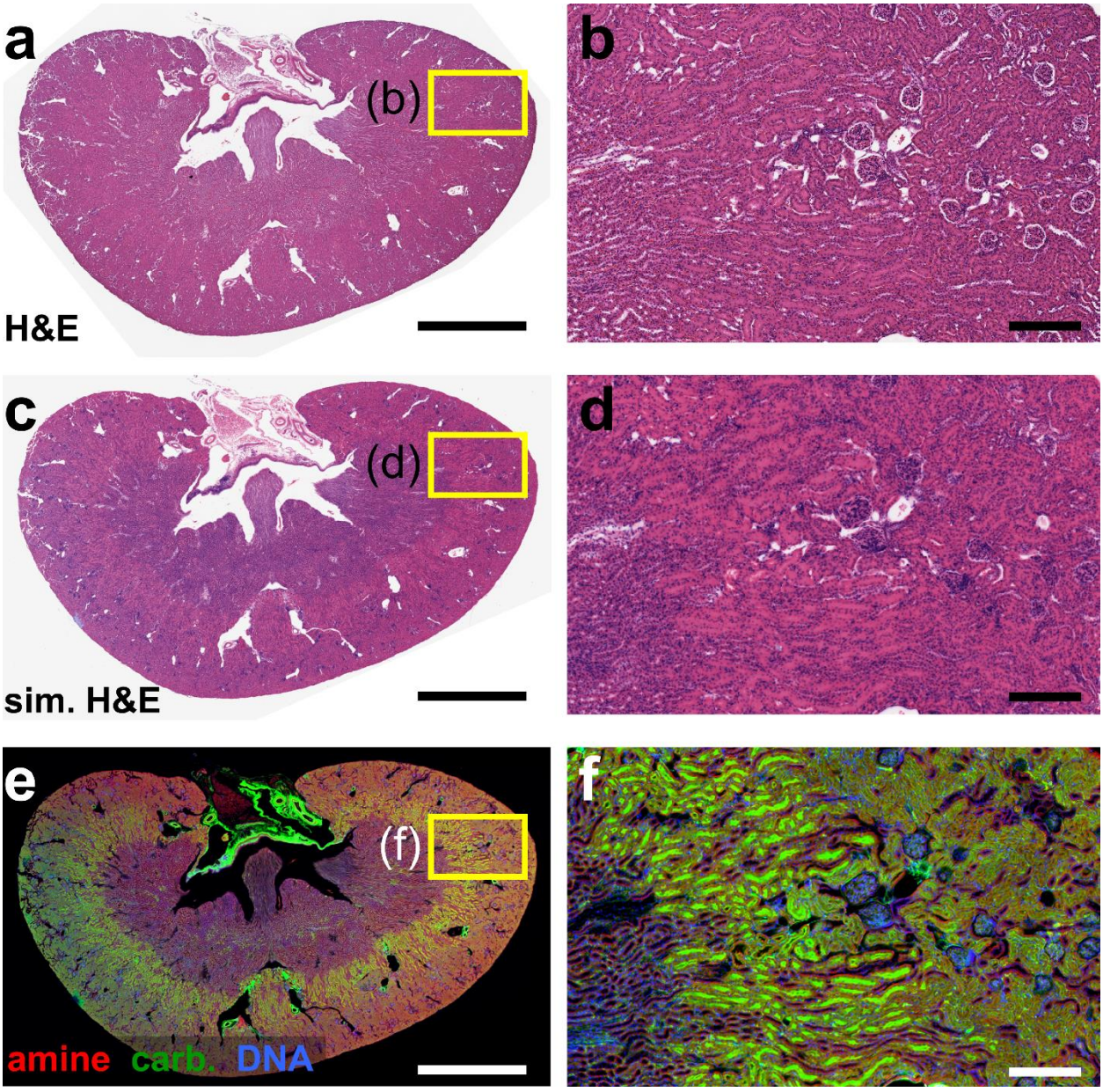

Supplementary Fig. 2.7 | Side-by-side comparison of H&E and FLARE stains on FFPE mouse kidney sections. Two consecutive 10 µm thick mouse kidney FFPE sections were used for (a-b) H&E and (c-f) FLARE stains, respectively. The FLARE stain DNA and amine channels were converted to a simulated (sim.) H&E image (c-d), showing a similar pattern as for H&E. However, the molecular distribution and general features are substantially more informative in (e-f) the standard fluorescence display. Scale bars are 2 mm (a, c, e), 200 µm (b, d, f).

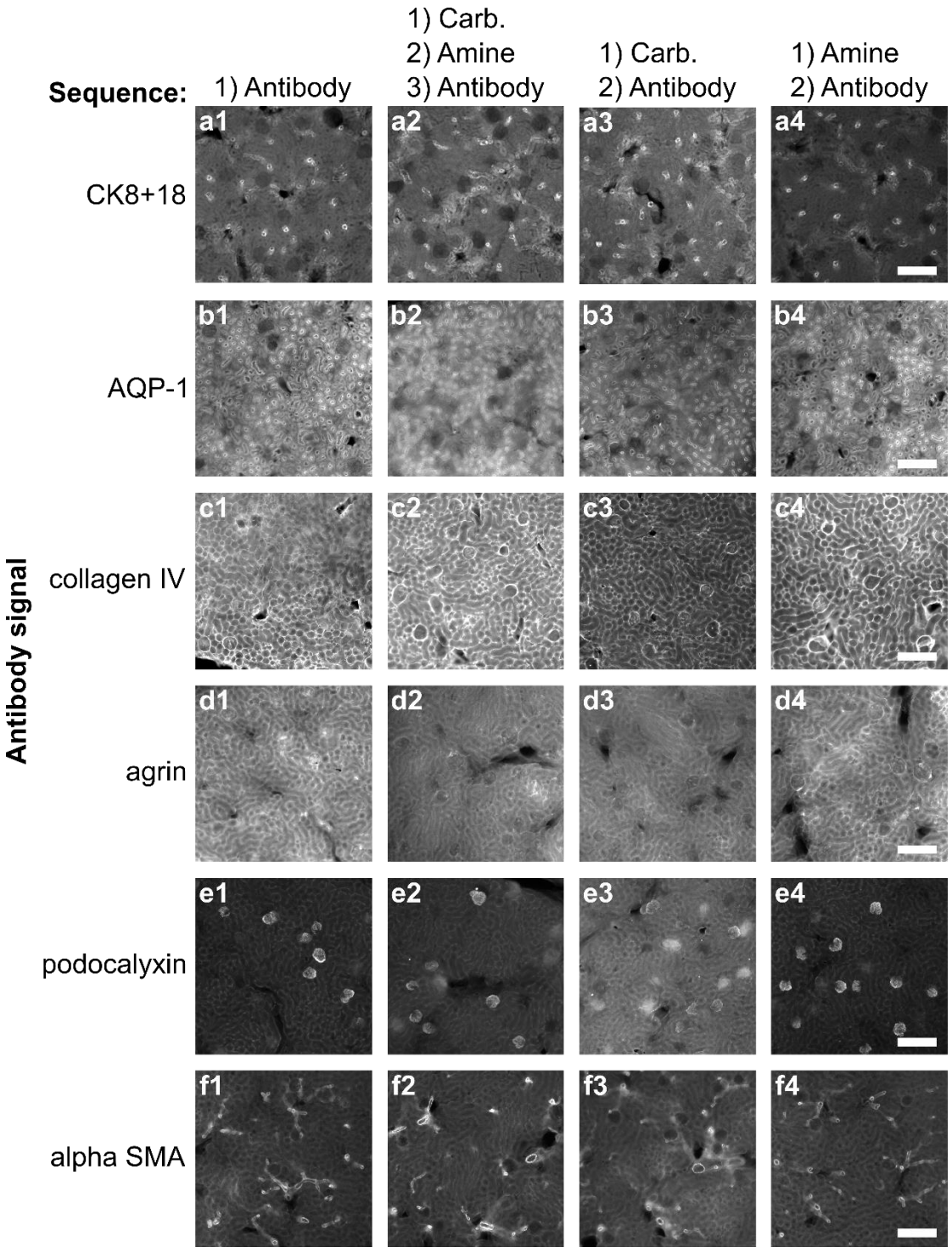

Supplementary Fig. 2.8 | Effect of FLARE staining on antibody binding for unexpanded mouse kidney tissue. Unexpanded mouse kidney tissue was labeled with various covalent reactions (or none) as indicated in the column headings, immunostained against the protein indicated in each row, and then imaged by widefield fluorescence microscopy. None of the six immunostains were perturbed by the covalent labeling of amines (compare columns 1 and 4) but agrin immunostaining was partially perturbed by covalent labeling of carbohydrates (compare columns 1 and 3). Scale bars are 200 µm.

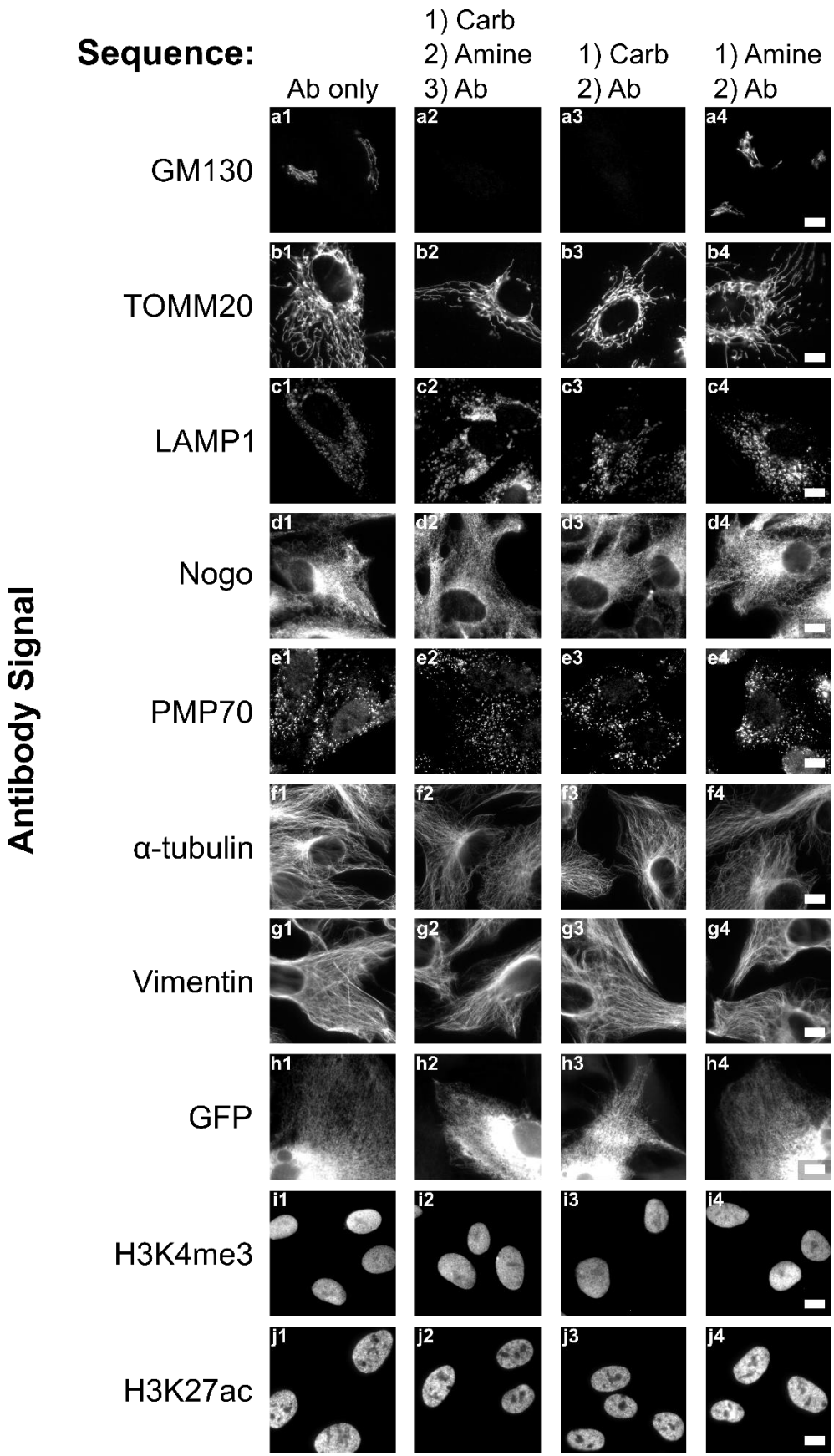
Sequence:
Ab only
1) Carb
2) Amine
3) Ab
1) Carb
2) Ab
1) Amine
2) Ab
Antibody Signal
GM130
TOMM20
LAMP1
Nogo
PMP70
α-tubulin
Vimentin
GFP
H3K4me3
H3K27ac
a1
a2
a3
a4
b1
b2
b3
b4
c1
c2
c3
c4
d1
d2
d3
d4
e1
e2
e3
e4
f1
f2
f3
f4
g1
g2
g3
g4
h1
h2
h3
h4
i1
i2
i3
i4
j1
j2
j3
j4

Supplementary Fig. 2.9 | Effect of FLARE staining on antibody binding for unexpanded RPE cells. Unexpanded RPE cells were labeled with various covalent reactions (or none) as indicated in the column headings, immunostained against the protein indicated in each row, and then imaged by widefield fluorescence microscopy. None of the ten immunostains were perturbed by the covalent labeling of amines (compare columns 1 and 4) but GM130 immunostaining was disrupted by covalent labeling of carbohydrates (compare columns 1 and 3). Scale bars are 10 μm. Ab = antibody; Carb = carbohydrate covalent stain; Amine = amine covalent stain.

Supplementary Table 2.1 Summary of sample preparation and imaging conditions.

Fig.	Sample	Fixation	Tissue Sectioning	Carbohydrate Stain	Amine Stain	Other Stain(s) and Stain Order	Expansion or Clearing	Imaging
2	RPE cell	PFA/GA 10min	---	1hr, 20mM $NaIO_4$ in 100mM NaOAc with 1M NaCl, pH5; then 3hr, 6.65μM hydrazide-AT565 in 100mM NaOAc, pH5; then 30 min, 50mM $NaBH_3CN$ in 100mM NaOAc, pH5.	1hr, 3.0μM NHS-AT647N in PBS.	DNA: 30min, 1.96μM SYBR Green in DI water Order: gel, covalent stains, expand, DNA.	Expansion	Confocal, 63× 1.2NA water lens. Image thickness: a) 738nm, b) 462nm, c) 738nm, d) 1.85μm, e) 1.57μm, f) 462nm. Filter: none.
3	Mouse kidney	PFA 1hr	100μm vibratome sections	Same as **Fig. 2**.	6hr, 5.9μM NHS-AT647N in 100mM MES, pH6.	DNA: 30min, 1.87μM Hoechst 33258 in PBS, pH7.4. Order: gel, covalent stains, DNA, expand.	Expansion	Confocal, 63× 1.2NA water lens. Image thickness: 92.3nm. Filter: 2.
4a-b	Human kidney	PFA 1hr	500μm vibratome sections (resliced after labeling)	---	1.2μM NHS-AT647N, 15hr in a) MES, b) MES:THF (1:1).	---	Clearing	Confocal, 10× 0.4NA air lens. Image thickness: 1.52μm. Filter: none.
4c-d	Mouse kidney	PFA 1hr	500μm vibratome sections (resliced after labeling)	4hr, 100mM $NaIO_4$ in 100mM NaOAc, pH5; then 15hr, 1.2μM hydrazide-AT565 in c) NaOAc and d) THF:NaOAc (1:1); then 30min, 50 mM $NaBH_3CN$ in THF:NaOAc (1:1).	---	---	Clearing	Confocal, 10× 0.4NA air lens. Image thickness: 1.52μm. Filter: none.
4e	Mouse kidney	PFA 1hr	500μm vibratome sections	---	2 hr, 17.7μM NHS-AT647N in THF: MES (1:1).	Immuno: Rb×Collagen 5 μg/mL 72hr; D×Rb AT488 10μg/mL, 72hr; at 4°C. Order: immuno, covalent stain, clear.	Clearing	Confocal, 10× 0.4NA air lens. Image thickness: 1.52μm. Filter: none.
4f-h	Mouse kidney block	PFA 1hr	1mm vibratome section	5hr, 100mM $NaIO_4$ in 100mM NaOAc, pH5; then 6hr, 3.33μM hydrazide-AT565 in THF:NaOAc (1:1); then 1hr, 100mM $NaBH_3CN$ in THF:NaOAc (1:1).	8hr, 5.9μM NHS-AT647N in THF: MES (1:1).	DNA: 15hr, 20μM SYBR green in H_2O: PBS (1:1). Order: covalent stains, DNA, clear.	Clearing	Light sheet microscope, 20× 0.43NA oil lens. Image thickness: f-h) 446nm. Filter: none.
5a-f	Mouse intestine, liver, testis, human prostate	PFA 1hr, intestine, testis; PFA 6hr, liver; formalin 20hr, prostate	100μm vibratome sections	30min, 100mM $NaIO_4$ in 100mM NaOAc, pH 5; then 2hr, 3.33μM hydrazide-AT565 in THF:NaOAc (1:1); then 30min, 100mM $NaBH_3CN$ in THF:NaOAc (1:1).	2hr, 5.9μM NHS-AT647N in THF: MES (1:1).	DNA: 30min, 1.87μM Hoechst 33258 in THF: PBS (1:1). Order: covalent stains, DNA, clear.	Clearing	Confocal, a) 20× 0.7NA air lens, b-f) 63× 1.4NA oil lens. Image thickness: a) 8.06μm, b) 2.26μm, c) 377nm, d) 377nm, e) 1.89μm, f) 377nm. Filter: a-e) none, f) 2.
5g	Human FFPE kidney	Formalin 24hr	60μm microtome sections	Same as **Fig. 5a-f.**	Same as **Fig. 5a-f.**	Same as **Fig. 5a-f.**	Clearing	Confocal, g) 20× 0.7NA air lens. Image thickness: 1 μm. Filter: 2.
S1a-h	RPE cell	Same as **Fig. 2**	---	Same as **Fig. 2.**	Same as **Fig. 2.**	Same as **Fig. 2.**	Expansion	Same as **Fig. 2.**
S1i-p	Ms. kidney	Same as **Fig. 3**	---	Same as **Fig. 3.**	Same as **Fig. 3.**	Same as **Fig. 3.**	Expansion	Same as **Fig. 3.**
S2a-d	RPE cell	Same as **Fig. 2**	---	Same as **Fig. 2.**	Same as **Fig. 2.**	Immuno: Rb×TOMM20 2μg/mL 90min; D×Rb biotin 3μg/mL 45min; streptavidin AF488 5μg/mL in PBS 15hr; at ~20°C. Order: immuno, gel, covalent stains, streptavidin, expand.	Expansion	Confocal, 63× 1.2NA water lens. Image thickness: a-d) 646nm. Filter: none.
S2e-h	RPE cell	Same as **Fig. 2**	---	30min, 20mM $NaIO_4$ in 100mM NaOAc with 1M NaCl, pH5; then 1.5hr, 2.66μM hydrazide-AT565 in 100mM NaOAc, pH5; then 15min, 50mM $NaBH_3CN$ in 100mM NaOAc, pH5.	1hr, 1.2μM NHS-AT647N in PBS.	Immuno: Rb×LAMP1 4μg/mL 90min; D×Rb AF488 5μg/mL 45min; at ~20°C. Order: covalent stains, immuno, gel, expand.	Expansion	Confocal, 63× 1.2NA water lens. Image thickness: e-h) 923nm. Filter: none.
S2i-l	RPE cell	Same as **Fig. 2**	---	Same as **Fig. 2.**	Same as **Fig. 2.**	DNA: Same as **Fig. 2.** Order: Same as **Fig. 2.**	Expansion	Confocal, 63× 1.2NA water lens. Image thickness: i-l) 277nm. Filter: none
S2m-q	RPE cell	Same as **Fig. 2**	---	Same as **Fig. 2.**	Same as **Fig. 2.**	Immuno: Ms×GM130 2μg/mL 90min; D×Ms biotin 3 μg/mL 45min; streptavidin AF488 5μg/mL in PBS 15hr; at ~20°C. Order: immuno, gel, covalent stains, streptavidin, expand.	Expansion	Confocal, 63× 1.2NA water lens. Image thickness: m-q) 1.15μm. Filter: none.
S2r-v	RPE cell transfected	Same as **Fig. 2**	---	Same as **Fig. 2.**	Same as **Fig. 2.**	Immuno: Rb×GFP-AF488 4μg/mL 15hr; at ~20°C. Order: gel, covalent stains, immuno, expand.	Expansion	Confocal, 63× 1.2NA water lens. Image thickness: f-j) 185nm. Filter: none.
S3a-d	Mouse kidney	PFA 1hr	100μm vibratome sections	---	1hr, 3.0μM NHS-AF546 in PBS.	DNA: Same as **Fig. 3a-d**. Immuno: Rb×Podocin 5μg/mL 18hr; D×Rb AT488 5μg/mL 18hr; at 4°C. Order: immuno, covalent stain, gel, expand, then DNA.	Expansion	Confocal, 63× 1.2NA water lens. Image thickness: 1.04μm. Filter: none.
S3e-h	Mouse kidney	PFA 1hr	100μm vibratome sections	Same as **Fig. 3.**	Same as **Fig. 3.**	DNA FISH: denature 10min at 92.5°C; hybridize 18hr at 37°C with 100nM MaSat oligo + 100nM AT647N oligo. Order: gel, covalent stains, DNA FISH, then expand	Expansion	Confocal, 63× 1.2NA water lens. Image thickness: 92nm. Filter: 2.
S4	Human kidney	PFA 1hr	500μm vibratome sections	---	1.2μM NHS-AT647N, 15hr in: a) PBS, b) PBS:THF (1:1), c) MES, d) MES:THF (1:1).	---	Clearing	Confocal, 10× 0.4NA air lens. Image thickness: 1.52μm. Filter: none.
S5a-d	Mouse kidney	PFA 1hr	1mm vibratome section	Same as **Fig. 4g**	Same as **Fig. 4g**	Same as **Fig. 4g**	Clearing	Same as **Fig. 4g**
S5e-x	Same as for **Fig. 5a-g**	Same as **Fig. 5a-g**	Same as **Fig. 5a-g**	Same as **Fig. 5a-g**	Same as **Fig. 5a-g**	Same as **Fig. 5a-g**	Clearing	Confocal, e-t) 63× 1.4NA oil lens, u-x) 20× 0.7NA air lens. Image thickness: Same as **Fig. 5a-g** Filter: e-l) none, m-t) 2, u-x) none.
S6	Mouse kidney	PFA 1hr	100μm vibratome sections	30min, 100mM $NaIO_4$ in 100mM NaOAc, pH 5; then 1hr, 3.33μM hydrazide-Al568 in NaOAc; then 30min, 100mM $NaBH_3CN$ in NaOAc.	1hr, 3.0μM NHS-AT647N in 1× PBS	Immuno: 2μg/mL G×PODXL, Rb×AQP-1, Gp×CK8+18 18h; 2μg/mL D×G-AFdye405, D×Rb-AF488, D×Gp-AF750 18h; at ~4°C. Order: covalent stains, immuno	Neither	Homebuilt spinning-disk confocal, 20× 0.45NA air lens; imaging cocktail was tris 200mM pH8.0, 10% glucose, 1mM Trolox, 0.4mg/mL glucose oxidase, 0.2% catalase. Image thickness: single plane Filter: none
S7a-b	Mouse kidney	Formalin 24hr	10μm microtome sections	---	---	---	Neither	Aperio ScanScope AT2 digital whole slide scanner for H&E.
S7c-f	Mouse kidney	Formalin 24hr	10μm microtome sections	Same as **Fig. S6**	Same as **Fig. S6**	Immuno: 2μg/mL primary ab. 18h; 2μg/mL secondary ab. (AF 488 conjugates) 18h; at ~4°C. Order: covalent stains, immuno	Neither	Widefield, 20× 0.45NA air lens. Image thickness: single plane. Filter: none.
S8	Mouse kidney	Same as **Fig. 3**	100μm vibratome sections	Same as **Fig. S6**	Same as **Fig. S6**	Immuno: 2μg/mL primary ab. 18h; 2μg/mL secondary ab. (AF488 conjugates) 18h; at ~4°C. Order: covalent stains, immuno	Neither	Widefield, 4× 0.2NA air lens. Image thickness: single plane. Filter: none.
S9 a-e	RPE cell	PFA/GA 10min	---	30min, 20mM $NaIO_4$ in 100mM NaOAc with 1M NaCl, pH5; then 1.5hr, 2.66μM hydrazide-AT565 in 100mM NaOAc, pH 5; then 15min, 50mM $NaBH_3CN$ in 100mM NaOAc, pH5.	1hr, 1.2μM NHS-AT647N in PBS.	Immuno: 2μg/mL primary ab. 90min; 2μg/mL secondary ab. (AF488 conjugates) 45min; at ~20°C. Order: covalent stains, immuno	Neither	Widefield, 60× 1.2NA water lens. Image thickness: Single plane. Filter: none.
S9 h	RPE cell	PFA/GA 10min	---	Same as **Fig. S9 a-e**	1hr, 1.2μM NHS-AT565 in PBS.	Immuno: 2μg/mL of Rb×GFP-AF647 90min; at ~20°C. Order: covalent stains, immuno	Neither	Same as **Fig. S9 a-e**
S9 f-g	RPE cell	0.5% Triton-x100 extraction 30sec, PFA/GA 10min	---	Same as **Fig. S9 a-e**	Same as **Fig. S9 a-e**	Same as **Fig. S9 a-e**	Neither	Same as **Fig. S9 a-e**
S9 i-j	RPE cell	4% PFA 10min	---	Same as **Fig. S9 a-e**	Same as **Fig. S9 a-e**	Immuno: permeabilize 10min with 0.1% Triton-x100 in PBS; 2μg/mL primary ab. 18h at ~4°C; 2μg/mL secondary ab. (AF488 conjugtaes) 2hr at ~20°C. Ab. incubations in 10% (w/v) BSA in PBS. Order: covalent stains, immuno	Neither	Same as **Fig. S9 a-e**

Acronyms: Ab=antibody; AF=Alexa Fluor; AT=ATTO-TEC; DI=deionized; FFPE=formalin-fixed, paraffin-embedded; NA=numerical aperture; RPE=retinal pigment epithelium cell line.

Additional notes: median filter indicates number of pixels used for application of 3D median filter if used on confocal data sets. Image thickness refers to the thickness of the data displayed in terms of the pixel sizes of the data set, where distances are in pre-expansion units for expanded tissues.

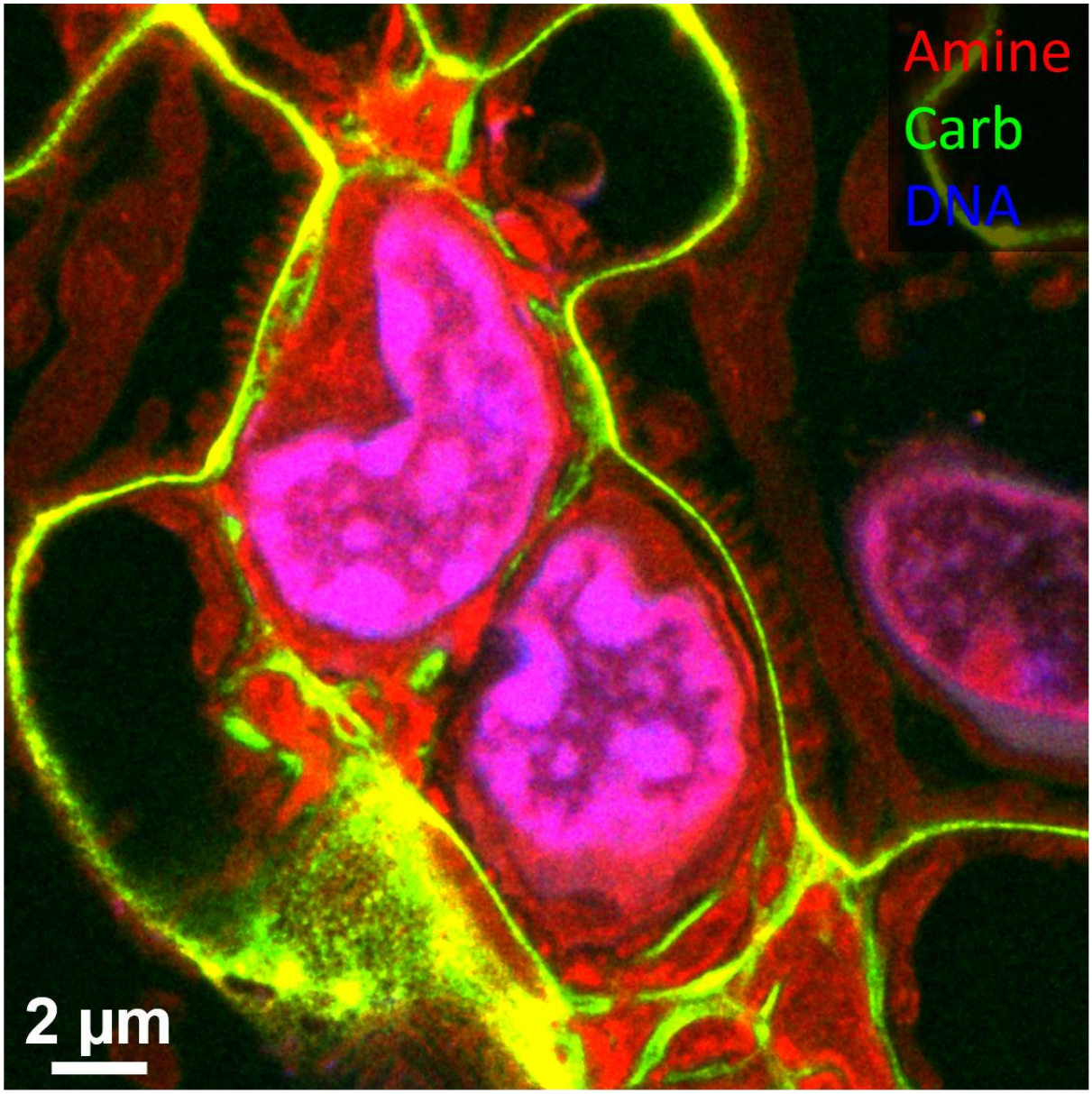

Supplementary Movie 2.1 | Animation of FLARE-stained expanded mouse kidney. Shown is the first frame from an animation of an expanded mouse kidney section that focuses on a small volume of a glomerulus. The animation shows successive z-slices of the confocal stacks and highlights the basement membrane of capillary loops and mesangial matrix (green) as well as the fine details of the interdigitated podocyte epithelial cells (red). The same data set was used to create **Fig. 2.3a-c**. The animation covers a depth of 12.1 µm. All distances are in pre-expansion units.

2.9 References

1. D. S. Richardson, J. W. Lichtman, Clarifying Tissue Clearing. Cell. 162, 246–257 (2015).
2. S. J. Sahl, S. W. Hell, S. Jakobs, Fluorescence nanoscopy in cell biology. Nature Reviews Molecular Cell Biology. 18, 685–701 (2017).
3. Y. M. Sigal, R. Zhou, X. Zhuang, Visualizing and discovering cellular structures with super-resolution microscopy. Science. 361, 880–887 (2018).
4. K. Tainaka, A. Kuno, S. I. Kubota, T. Murakami, H. R. Ueda, Chemical Principles in Tissue Clearing and Staining Protocols for Whole-Body Cell Profiling. Annual Review of Cell and Developmental Biology. 32, 713–741 (2016).
5. L. Schermelleh, A. Ferrand, T. Huser, C. Eggeling, M. Sauer, O. Biehlmaier, G. P. C. Drummen, Super-resolution microscopy demystified. Nature Cell Biology. 21, 72–84 (2019).
6. U. Schnell, F. Dijk, K. A. Sjollema, B. N. G. Giepmans, Immunolabeling artifacts and the need for live-cell imaging. Nature Methods. 9, 152–158 (2012).
7. A. Bradbury, A. Plückthun, Reproducibility: Standardize antibodies used in research. Nature. 518, 27–29 (2015).
8. K. S. Suvarna, C. Layton, J. D. Bancroft, Eds., Theory and practice of histological techniques (Elsevier Churchill Livingston, Edinburgh, 7. ed., 2013).
9. K. N. Elfer, A. B. Sholl, M. Wang, D. B. Tulman, S. H. Mandava, B. R. Lee, J. Q. Brown, DRAQ5 and Eosin ('D&E') as an Analog to Hematoxylin and Eosin for Rapid Fluorescence Histology of Fresh Tissues. PLOS ONE. 11, e0165530 (2016).
10. L. Ornstein, W. Mautner, B. Davis, new horizons in fluorescence microscopy. J. Mount. Sinai. Hosp. 24, 1066.
11. F. M. Weinblatt, W. A. Shannon, A. M. Seligman, A new fluorescent method for the demonstration of macromolecular aldehydes. Histochemistry. 41, 353–359 (1975).
12. Hermanson, Greg, Bioconjugate Techniques, 2nd Edition.
13. A. J. Lomant, G. Fairbanks, Chemical probes of extended biological structures: synthesis and properties of the cleavable protein cross-linking reagent [35S]dithiobis(succinimidyl propionate). J. Mol. Biol. 104, 243–261 (1976).
14. P. D. Bragg, C. Hou, Subunit composition, function, and spatial arrangement in the Ca2+- and Mg2+-activated adenosine triphosphatases of Escherichia coli and Salmonella typhimurium. Archives of Biochemistry and Biophysics. 167, 311–321 (1975).
15. J. M. Baskin, K. W. Dehnert, S. T. Laughlin, S. L. Amacher, C. R. Bertozzi, Visualizing enveloping layer glycans during zebrafish early embryogenesis. Proceedings of the National Academy of Sciences. 107, 10360–10365 (2010).
16. Y. Saitoh, N. Terada, S. Saitoh, N. Ohno, Y. Fujii, S. Ohno, Three-dimensional reconstruction of living mouse liver tissues using cryotechniques with confocal laser scanning microscopy. Journal of Electron Microscopy. 59, 513–525 (2010).
17. D. E. Hill, R. H. Fetterer, J. F. Urban, Biotin as a probe of the surface of Ascaris suum developmental stages. Molecular and Biochemical Parasitology. 41, 45–52 (1990).
18. F. K. Swirski, C. R. Berger, J.-L. Figueiredo, T. R. Mempel, U. H. von Andrian, M. J. Pittet, R. Weissleder, A Near-Infrared Cell Tracker Reagent for Multiscopic In Vivo Imaging and Quantification of Leukocyte Immune Responses. PLoS ONE. 2, e1075 (2007).
19. F. Chen, P. W. Tillberg, E. S. Boyden, Expansion microscopy. Science. 347, 543–548 (2015).
20. T. Ku, J. Swaney, J.-Y. Park, A. Albanese, E. Murray, J. H. Cho, Y.-G. Park, V. Mangena, J. Chen, K. Chung, Multiplexed and scalable super-resolution imaging of three-dimensional protein localization in size-adjustable tissues. Nature Biotechnology. 34, 973–981 (2016).

21. T. J. Chozinski, A. R. Halpern, H. Okawa, H.-J. Kim, G. J. Tremel, R. O. L. Wong, J. C. Vaughan, Expansion microscopy with conventional antibodies and fluorescent proteins. Nature Methods. 13, 485–488 (2016).
22. N. Renier, Z. Wu, D. J. Simon, J. Yang, P. Ariel, M. Tessier-Lavigne, iDISCO: A Simple, Rapid Method to Immunolabel Large Tissue Samples for Volume Imaging. Cell. 159, 896–910 (2014).
23. A. Klingberg, A. Hasenberg, I. Ludwig-Portugall, A. Medyukhina, L. Männ, A. Brenzel, D. R. Engel, M. T. Figge, C. Kurts, M. Gunzer, Fully Automated Evaluation of Total Glomerular Number and Capillary Tuft Size in Nephritic Kidneys Using Lightsheet Microscopy. Journal of the American Society of Nephrology. 28, 452–459 (2017).
24. R. B. Mujumdar, L. A. Ernst, S. R. Mujumdar, C. J. Lewis, A. S. Waggoner, Cyanine dye labeling reagents: sulfoindocyanine succinimidyl esters. Bioconjugate chemistry. 4, 105–111 (1993).
25. E. Murray, J. H. Cho, D. Goodwin, T. Ku, J. Swaney, S.-Y. Kim, H. Choi, Y.-G. Park, J.-Y. Park, A. Hubbert, M. McCue, S. Vassallo, N. Bakh, M. P. Frosch, V. J. Wedeen, H. S. Seung, K. Chung, Simple, Scalable Proteomic Imaging for High-Dimensional Profiling of Intact Systems. Cell. 163, 1500–1514 (2015).
26. A. K. Glaser, N. P. Reder, Y. Chen, C. Yin, L. Wei, S. Kang, L. A. Barner, W. Xie, E. F. McCarty, C. Mao, A. R. Halpern, C. R. Stoltzfus, J. S. Daniels, M. Y. Gerner, P. R. Nicovich, J. C. Vaughan, L. D. True, J. T. C. Liu, Multi-immersion open-top light-sheet microscope for high-throughput imaging of cleared tissues. Nat Commun. 10, 2781 (2019).
27. M. G. Giacomelli, L. Husvogt, H. Vardeh, B. E. Faulkner-Jones, J. Hornegger, J. L. Connolly, J. G. Fujimoto, Virtual Hematoxylin and Eosin Transillumination Microscopy Using Epi-Fluorescence Imaging. PLOS ONE. 11, e0159337 (2016).
28. L. Fagerberg, C. Stadler, M. Skogs, M. Hjelmare, K. Jonasson, M. Wiking, A. Åbergh, M. Uhlén, E. Lundberg, Mapping the Subcellular Protein Distribution in Three Human Cell Lines. J. Proteome Res. 10, 3766–3777 (2011).
29. D. N. Itzhak, S. Tyanova, J. Cox, G. H. Borner, Global, quantitative and dynamic mapping of protein subcellular localization. eLife. 5, e16950 (2016).
30. S. Pahari, L. Sun, E. Alexov, PKAD: a database of experimentally measured pKa values of ionizable groups in proteins. Database. 2019 (2019), doi:10.1093/database/baz024.
31. Y. Chen, W. Xie, A. K. Glaser, N. P. Reder, C. Mao, S. M. Dintzis, J. C. Vaughan, J. T. C. Liu, Rapid pathology of lumpectomy margins with open-top light-sheet (OTLS) microscopy. Biomedical Optics Express. 10, 1257 (2019).
32. W. Xie, Y. Chen, Y. Wang, L. Wei, C. Yin, A. K. Glaser, M. E. Fauver, E. J. Seibel, S. M. Dintzis, J. C. Vaughan, N. P. Reder, J. T. C. Liu, Microscopy with ultraviolet surface excitation for wide-area pathology of breast surgical margins. Journal of Biomedical Optics. 24, 12 (2019).
33. E. D. Karagiannis, J. S. Kang, T. W. Shin, A. Emenari, S. Asano, L. Lin, E. K. Costa, IMAXT Grand Challenge Consortium, A. H. Marblestone, N. Kasthuri, E. S. Boyden, “Expansion Microscopy of Lipid Membranes” (preprint, Bioengineering, 2019), , doi:10.1101/829903.
34. D. Unnersjö-Jess, L. Scott, S. Z. Sevilla, J. Patrakka, H. Blom, B. Hjalmar, Confocal super-resolution imaging of the glomeruluar filtration barrier enables by tissue expansion. Kidney International (2017), doi:https://doi.org/10.1016/ j.kint.2017.09.019.
35. B. J. Beliveau, E. F. Joyce, N. Apostolopoulos, F. Yilmaz, C. Y. Fonseka, R. B. McCole, Y. Chang, J. B. Li, T. N. Senaratne, B. R. Williams, others, Versatile design and synthesis platform for visualizing genomes with Oligopaint FISH probes. Proceedings of the National Academy of Sciences. 109, 21301–21306 (2012).
36. B. Lehnertz, Y. Ueda, A. A. H. A. Derijck, U. Braunschweig, L. Perez-Burgos, S. Kubicek, T. Chen, E. Li, T. Jenuwein, A. H. F. M. Peters, Suv39h-Mediated Histone H3 Lysine 9 Methylation Directs DNA Methylation to Major Satellite Repeats at Pericentric Heterochromatin. Current Biology. 13, 1192–1200 (2003).

Chapter 3

Fluorescent Labeling of Abundant Reactive Entities (FLARE) for Cleared-Tissue and Super-Resolution Microscopy

3.1 Preface

After establishing and demonstrating the fluorescent analogs of classic histology stains, FLARE, in **Chapter 2**, we believe this labeling method that utilizes inexpensive reagents with a simple and robust procedure has a variety of applications. Therefore, we next sought to prepare a protocol paper that is based on several versions of the method published over the last three years as well as new variations created since our initial 2020 publication. In this chapter, I will present the prepared protocol paper that discusses the method in depth, includes step-by-step procedures for a range of samples, and addresses ways to customize and troubleshoot common problems. Moreover, data sets corresponding to each type of sample are also included to comprehensively assist researchers to adapt the method to their research.

I was heavily involved in this project at all stages. My contribution to this project was focused on the tissue part. I authored the procedures for expanded, unexpanded cleared, and unexpanded uncleared tissues. In addition, I performed all tissue-related experiments except the millimeter-thick mouse kidney tissue. Another co-first author, Dr. Min Yen Lee authored the procedure for expanded cells and drafted the manuscript which is adapted from a part of her dissertation. Dr. Min Yen Lee and I edited the manuscript. All other authors commented on the manuscript. This work was also in collaboration with members from the laboratory of Dr. Jonathan T.C. Liu who contributed to using open-top light-sheet microscopy to image thick tissues. Supplementary figures, as well as two supplementary protocols are provided in addition to the main text.

The following material in this chapter is reproduced with permission from:

Min Yen Lee[‡], **Chenyi Mao**[‡], Adam K. Glaser, Marcus A. Woodworth, Aaron R. Halpern, Jonathan T.C. Liu, Joshua C. Vaughan; “Fluorescent Labeling of Abundant Reactive Entities (FLARE) for Cleared-Tissue and Super-Resolution Microscopy”, *Nature Protocols*, accepted. Copyright 2021 Nature Publishing Group.

[‡] indicated equal contributions.

All material in this chapter has been reformatted to conform to the style of this thesis.

3.2 Key papers

- Feature-rich covalent stains for super-resolution and cleared tissue fluorescence microscopy (DOI: 10.1126/sciadv.aba4542);
- Rapid pathology of lumpectomy margins with open-top light-sheet (OTLS) microscopy (DOI: 10.1364/BOE.10.001257).

3.3 Abstract

Fluorescence microscopy is a vital tool in biomedical research but faces considerable challenges in achieving uniform or bright labeling. For instance, fluorescent proteins are limited to model organisms, and antibody conjugates can be inconsistent and are difficult to use with thick specimens. To partly address this challenge, we have developed a labeling protocol that can rapidly visualize many well-contrasted key features and landmarks on biological specimens in both thin and thick tissues or cultured cells. This method uses established reactive fluorophores to label a variety of biological specimens for cleared-tissue microscopy or expansion super-resolution microscopy (ExM) and is termed FLARE (Fluorescent Labeling of Abundant Reactive Entities). These fluorophores target chemical groups and reveal their distribution on the specimens; amine-reactive fluorophores such as hydroxysuccinimidyl esters target accessible amines on proteins while hydrazide fluorophores target oxidized carbohydrates. The resulting stains provide signals analogous to traditional general histology stains such as H&E (hematoxylin and eosin) or PAS (periodic acid-Schiff) but use fluorescent probes that are compatible with volumetric imaging. In general, the stains for FLARE are performed in the order of carbohydrates, amine, and DNA, and the incubation time varies from one hour to one day depending on the combination of stains and the type and thickness of the biological specimens. FLARE is easy and robust, and does not require specialized expertise.

3.4 Introduction

Fluorescence microscopy is a workhorse technique in the biomedical sciences. It offers the powerful ability to visualize structures or molecules in three dimensions within biological specimens and gives relevant context to the study of the functions of these structures. However, to practitioners, the success of fluorescence microscopy measurements often hinges on the use of fluorescent labels to illuminate the specimen. Immunolabeling of specimens using antibodies is popular due to its high specificity and contrast but it faces key challenges[1,2]. First, many biological molecules or structures of interest lack good commercially available antibodies, particularly for specimens that have been heavily fixed or processed. Second, the relatively large size of antibody molecules (~150,000 Daltons, or ~15 nm, for an immunoglobulin G) can often make staining of samples >100 μm in thickness prohibitively time consuming, with sample preparation times of up to weeks. Fluorescent proteins, which are also popular fluorescent probes, require genetic manipulation and are thus limited to a subset of laboratory model organisms.

To partially address these limitations, we developed a fluorescent labeling method that uses reactive probes to target abundant chemical groups on biological samples. We termed the method FLARE for Fluorescent Labeling of Abundant Reactive Entities[3]. FLARE operates analogously to classic histology stains such as H&E[4] that are widely used to reveal overall tissue or cell physiology. However, most histology

stains are either nonfluorescent or have poor fluorescence properties, making them ill-suited to volumetric imaging. Additionally, histology stains are typically affinity-based, such that they may be washed out of thick samples during multi-round processing used in some powerful, recently developed techniques in super-resolution microscopy and cleared-tissue microscopy. In contrast, FLARE utilizes covalent stains with good fluorescence properties that are compatible with volumetric imaging as well as a range of sample fixation and sample processing methods.

We designed FLARE to be compatible with a range of common sample processing methods including paraffin embedding, super-resolution expansion microscopy (ExM), and cleared-tissue microscopy. Paraffin-embedding of specimens, in the form of formalin-fixed paraffin-embedded (FFPE) blocks, is commonly used in pathology and research labs due to ease of tissue sectioning and the ability to store tissues for long periods of time, but the process may degrade specimen antigenicity for labeling with antibodies. FLARE provides histology-stain-like contrast in FFPE specimens while offering greater multiplexing capabilities and high-resolution, volumetric imaging capabilities for standard thin (5-10 μm) or moderately thick FFPE sections (10-100 μm, or thicker).

While a variety of innovative super-resolution microscopy methods have been developed to date[5–7], ExM uses a unique approach in which swellable polymer hydrogels grown within fixed specimens uniformly enlarge the sample in three dimensions[8–10]. This enables features to become resolvable in the enlarged state at ~70 nm resolution or better even when using conventional microscopes that have a physical diffraction-limited resolution of ~250 nm. Importantly, FLARE is able to brightly label many of the major structures within cells and tissues, which is particularly valuable for ExM since bright signals are required for reliable detection of fluorescence after expansion. In order to maximize the amount of protein available for staining via FLARE, we focus on a protein-retention variation of ExM termed MAP (Magnified Analysis of the Proteome)[11] that uses detergent and heat denaturation to homogenize specimens prior to expansion, although we do show that FLARE can also reveal major features for enzymatic digestion-based ExM[3].

Finally, tissue-clearing utilizes various methods to minimize light scattering for the volumetric study of thick intact specimens (100-1000 μm or more)[12,13], but labeling such thick specimens remains a persistent challenge particularly with large labels like antibodies. Because FLARE labels are small molecules, they can be easily tuned to rapidly penetrate thick specimens to produce uniform stains.

Currently, the chemical reactions used for FLARE to label biological specimens target amine groups, which are abundant on proteins, and oxidized carbohydrates, which are abundant on basement membranes and some other structures (**Fig. 3.1**). However, FLARE could also include targeting of other chemical groups (e.g. thiols, carboxylates, etc.) that are abundant in biological samples. This application can be conveniently performed using a range of fluorescent dyes that are commercially available across the visible and near-infrared ranges in order to suit a specific experiment or instrument. FLARE is generally easy to combine with other forms of stains, if desired, including immunolabeling and DNA fluorescence in situ hybridization (DNA FISH)[14].

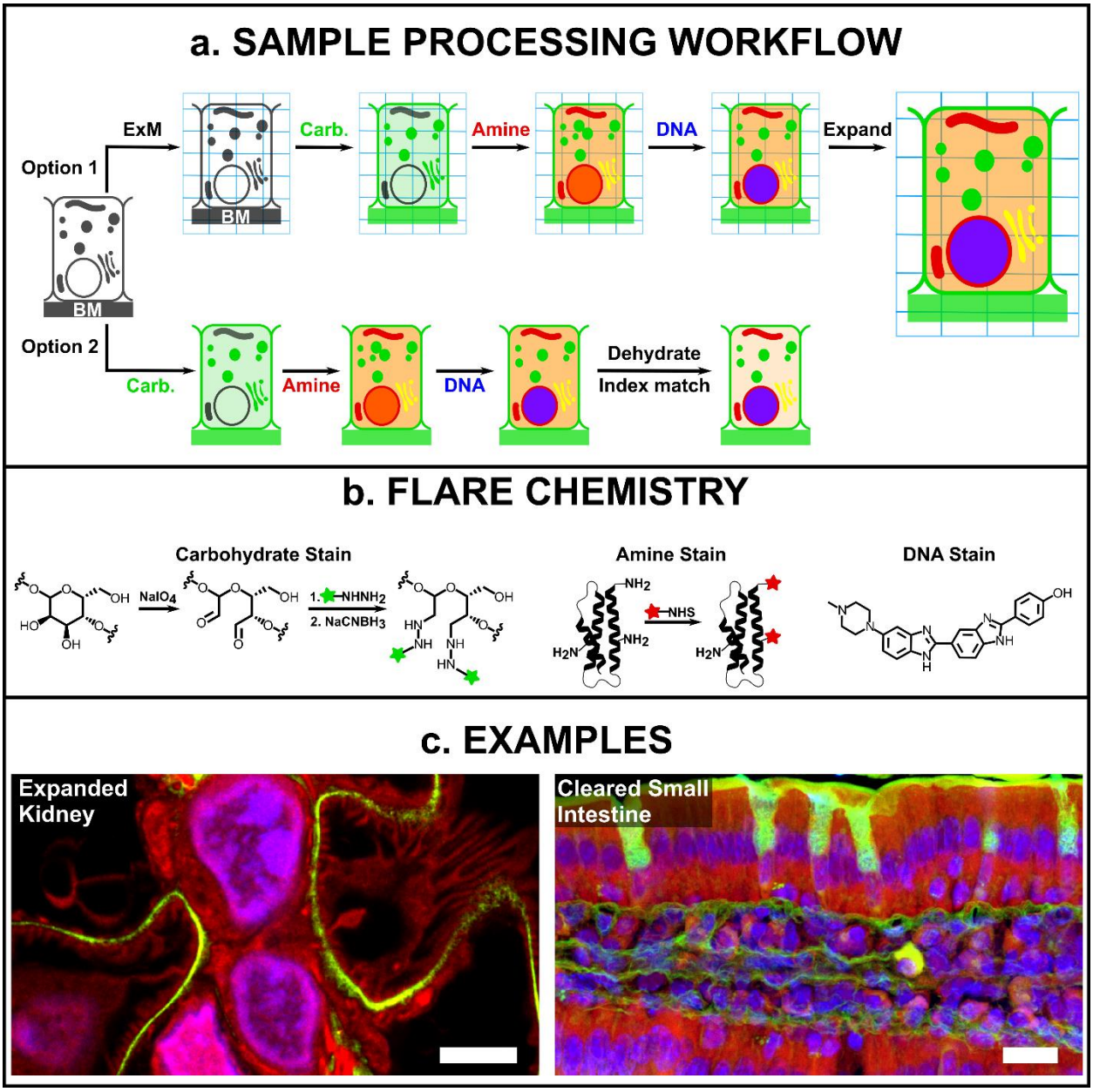

Fig. 3.1 | (a) General schematic for FLARE staining and sample processing workflow for ExM and cleared-tissue microscopy. (b) Details of FLARE chemistry. Carbohydrates are oxidized to aldehydes using sodium periodate, coupled to hydrazide-functionalized dyes, and stabilized by reduction with sodium cyanoborohydride. Then, N-hydroxysuccinimide (NHS)-functionalized dyes are used to label amine groups on proteins. DNA is labeled non-covalently using standard DNA-labeling dyes such as Hoechst. (c) Example confocal microscopy images of expanded kidney (100 µm) and optically cleared small intestine tissues (100 µm) that have been stained by FLARE (same color schemes as panel a). BM=basement membrane. Scale bars are 3 µm (left, pre-expansion units) and 10 µm (right).

3.4.1 Development of the protocol

In H&E staining, hematoxylin stains negatively charged components such as DNA blue while eosin stains positively charged protein components pink. With the inspiration from H&E staining, we employed N-hydroxysuccinimide (NHS) functionalized fluorophores to covalently label amines on proteins, and fluorescent DNA-staining dyes such as Hoechst or SYBR Green to stain nuclei[3]. In addition, we adapted the PAS stain to covalently label oxidized carbohydrates by first oxidizing the carbohydrates to aldehydes using sodium periodate and then subsequently reacting the aldehydes with hydrazide-functionalized fluorophores (**Fig. 3.1b**)[3]. The amine and carbohydrate-labeling reactions for FLARE are well-established in protein and carbohydrate conjugation but they are rarely used on intact biological samples for high resolution and high contrast fluorescence imaging purposes. During an early phase of the FLARE protocol development, we demonstrated the use of NHS-functionalized fluorophores to rapidly (<5 min) label the surface of unexpanded and uncleared clinical specimens to enable rapid diagnosis[15,16]. In addition, recently published papers by other groups also incorporated the use of NHS-functionalized fluorophores on expanded specimens[17,18]. Finally, a number of false-coloring algorithms have been developed to computationally render images of tissues, stained with fluorescent analogs of common pathology stains (e.g. H&E), in order to mimic the appearance of those (absorptive) pathology stains as viewed with a transmitted-light microscope[19,20].

3.4.2 Overview of the protocol

The main stages of the protocol are shown in **Fig. 3.2** and can be divided into two sections: labeling and sample processing. The labeling is done by FLARE which includes a carbohydrate stain (step 9 of Procedure 1 or step 1 of Procedure 2), an amine stain (step 10 of Procedure 1 or step 2 of Procedure 2), and a DNA stain (step 12 of Procedure 1 or step 3 of Procedure 2). Although FLARE does not have a specific requirement for sample fixation, paraffin-embedded samples or other dehydrated samples should be rehydrated prior to performing FLARE. The sample processing steps will depend on what kind of information the researchers wish to obtain. We recommend the use of ExM sample processing (steps 6-8, 11 of Procedure 1) if super-resolution visualization of nanoscale features is required. On the other hand, we recommend optical clearing sample processing (steps 4-6 of Procedure 2) for relatively thick samples where volumetric information is required. For ExM, FLARE can be performed before or after expansion processing, but when combining FLARE with optical clearing, FLARE must be performed first.

3.4.3 Comparison with other methods

Labeling of specimens with antibodies is a powerful approach that can visualize specific molecules of interest in biological specimens. However, antibodies face certain drawbacks such as poor penetration through thick complex specimens, lot-to-lot variability or sometimes inconsistent commercial availability. There can also be labeling difficulties with highly processed biological specimens, such as FFPE tissues, in which antigen targets may be degraded and not bound well by antibodies. In recent years, there has been substantial progress in improving the speed and penetration of antibody labeling for thick specimens, such as the use of sophisticated instruments[21], novel sample manipulation[22], optimized procedures[23], and new tissue permeabilization reagents[24], even though several of the other challenges remain. In general, if

the labeling of specific molecules is required, we suggest that practitioners should use, for instance, antibodies or perhaps small molecule probes that are specific for the desired target, etc., while if the labeling of general structures is desired, then FLARE offers many advantages, including a broad compatibility with other specific labeling methods.

Microscopists have, for many decades, stained specimens with a range of general contrast, small molecule labels that are typically examined using transmitted light (typically with thin sections), including H&E, PAS, and others[25]. While many of these stains are either nonfluorescent or have poor fluorescent properties (e.g., broad spectra or a tendency to photobleach, etc.), various reports over the years have utilized the fluorescence properties of the stains for microscopy, particularly with the eosin component of H&E[19,26–29], and less commonly with the PAS stain fuchsin[30,31]. These classical histology stains are viable options for fluorescent staining of unexpanded specimens, but care should be taken in some cases. First, eosin is an affinity-based stain and can be relatively easy to wash away, so there may be challenges with multi-step protocols. The classical PAS histology stain, fuchsin, is covalently bonded to the sample by means of a rather labile imine bond that may be hydrolyzed over time in solution and, additionally, the fluorescence emission spectrum of fuchsin is broad and can potentially hinder multiplexed imaging possibilities. On its own, eosin or fuchsin (PAS) staining may be sufficient for some experiments, particularly for thin specimens, but they are not easily used in combination. In contrast, the covalent reactions used in FLARE irreversibly bind fluorophores to amines and carbohydrates on the sample and thus, the labels are able to tolerate many of the subsequent steps (e.g., DNA FISH, immunolabeling, tissue clearing, etc.). At the same time, NHS- and hydrazide-functionalized fluorophores are commercially available for a large number of fluorophores with outstanding properties (brightness, resistance to photobleaching) in virtually any spectral band across the visible to near infrared in the range 400-800 nm.

The radically different approach to microscopy used by ExM has created some unique requirements for fluorescent probes compared to microscopy with unexpanded specimens. Expansion tends to dilute signals substantially (e.g., 4× linear expansion produces a 64× volumetric dilution) and it is challenging to retain affinity-based probes during the procedure due to the extensive washing and somewhat harsh digestion or denaturation procedures. It is therefore important to use bright fluorescent labeling and to take measures to retain probes introduced prior to expansion. There has recently been considerable innovation in the development of small-molecule probes for ExM. For example, Shi et al.[32], Karagiannis et al.[33], Wen et al.[34], and Götz et al.[35] developed small-molecule ExM probes that contain three chemical groups including (1) a group to target a small molecule (e.g. to a lipid, to the actin cytoskeleton using phalloidin, or to a genetically-encoded reactive protein), (2) a reporting group such as a fluorophore, biotin, or click-chemistry group, and (3) a label-retention group such as an acryloyl group that can be covalently linked to the polymer hydrogel. While these custom probes are very powerful, for instance in their ability to target specific molecules, their synthesis requires substantial chemical expertise beyond the scope of most biomedical researchers interested in using these tools. In contrast, FLARE only offers the ability to label relatively general structures, rather than specific molecules, but it is very bright, uses off-the-shelf reagents, and can be used to label a sample before or after expansion depending on the overall desired workflow (**Fig. 3.2**).

3.4.4 Applications and limitations

FLARE is currently applied only to fixed specimens, but is well suited to a range of specimen types and sample processing techniques. Expanded cultured cells and fresh-fixed tissue sections labeled using FLARE revealed major landmarks and sub-cellular organelles in great detail (**Fig. 3.1c** and **3.3**). During the development of FLARE, we focused on the use of retinal pigment epithelial cultured cells and mouse kidney tissue as model systems with ExM, although many ExM samples can be nicely labeled by FLARE. Recent work by others also showed that C. elegans[17] and other cultured cell lines18 are both nicely labeled by NHS-functionalized dyes after expansion. The protocol for C. elegans expansion was able to visualize important features using NHS-functionalized dyes with adequate contrast despite potential protein loss due to enzymatic digestion. M'Saad et al.[18] combined the MAP protocol[11] with iterative expansion[36], which allows expansion by ~18 fold, and labeled the resulting gels with NHS-ester functionalized dyes to study whole-cell protein distributions at very high resolution. Unexpanded tissue sections are easily labeled by FLARE either for highly processed FFPE specimens (**Fig. 3.4**) or specimens that are freshly fixed (**Fig. 3.5a and 3.5c**) or cryopreserved. Uniform tissue labeling can be achieved for thin sections (e.g., 5 μm thick FFPE sections) or thick ones (1 mm fresh-fixed sections, **Fig. 3.6**) although some tuning of the labeling protocol is required as described for thick specimens including optical clearing.

A further consideration with FLARE is the question of what features are stained in a given sample. For example, in expanded cultured cells, we found that many subcellular organelles were easily recognized, including mitochondria, lysosomes, the Golgi apparatus, nuclear pores, kinetochores, and centromeres, etc., but other structures, notably including the cytoskeleton, were not easily identified despite a relatively high protein abundance[3]. Sub-cellular organelles were not generally as easily discerned in relatively more complex 3D tissues, although we were able to observe details of nuclei and mitochondria in expanded mouse renal tubules in addition to details of basement membranes and interdigitated podocyte cells in expanded mouse renal glomeruli. Cell boundaries are brightly outlined in muscle cells in the carbohydrate stain (e.g., smooth muscle cells of the mouse small intestine3) but not in some other specimens, while bands of connective tissue tend to be enriched in both carbohydrates and amines in human prostate tissue, etc.

Taken together, the above observations suggest that the features that are revealed by FLARE depend on the distribution of the reactive groups in the specimen, the relative reactivity of those groups, and overall sample processing procedures (including fixation) which may consume or mask some reactive groups. Not surprisingly, classic histology stains, which were the inspiration for FLARE, also show contrast and features that depend prominently on the sample itself[37]. While FLARE will not stain every desired structure in every specimen of interest, published examples can in some cases help practitioners judge the likelihood of success. Additionally, since FLARE is easy and inexpensive, labs may begin to test it for their own specimens.

There may be structures or molecules that will simply not be possible to label with high contrast by using FLARE, alone. In such cases, researchers will need to use traditional specific labels, such as immunolabeling of proteins or labeling of nucleic acids by FISH. If desired, however, FLARE can often be combined with the use of these specific labels (e.g., antibodies or DNA oligonucleotides), and the FLARE dyes can be chosen in virtually any spectral region across the visible or near-infrared to accommodate other probes. In terms of antibody labeling, we found that 14 out of 16 tested antibodies were able to label their targets on cells or tissues after FLARE, and that the carbohydrate oxidation step appeared to

be the step that perturbed subsequent antibody labeling for 2 out of the 16 tests (amine labeling did not perturb antibody binding in any of the tests)[3]. If desired, it is possible to perform immunolabeling before FLARE to avoid oxidation-induced loss of antigenicity[2], and it may be possible to use milder oxidation that preserves antigenicity although we have not yet tested this thoroughly. For the combination of FLARE and DNA FISH, we performed FLARE after DNA FISH with good results (**Fig. 3.5b** and **3.5c**).

3.5 Experimental design

When designing FLARE labeling experiments, it is crucial that researchers consider the type of information they would like to obtain. First, researchers should determine whether they would like to use FLARE alone, or in combination with another labeling modality. Second, researchers should also decide if they need expansion in order to visualize the biological component of interest at high spatial resolution. While we focused on denaturation-based MAP in our protocol, we have also had success using enzymatic digestion-based ExM (see section FLARE with other modalities). These expansion methods were well described and validated in previous publications[8–11,17,18,38,39], and we advise researchers to choose an expansion method that works best for their specific sample. Third, researchers should plan control experiments for labeling, especially on new biological specimens that were not already tested and for experiments that seek to combine various labeling methods. For example, if immunolabeling is required in combination with FLARE, researchers should first establish whether or not the chemical stains perturb the desired immunolabel and determine if a shift in staining workflow is necessary. Lastly, in order to demonstrate FLARE's general utility, we described procedures on a wide variety of samples spanning from expansion to optical clearing, from 4 µm thickness to 1 mm thickness, from fresh fixation to FFPE preparation. Although several experimental parameters such as incubation times and dye concentrations vary, suggested parameters have been included for each procedure section. We recommend researchers begin with a procedure that most closely matches the thickness of their samples. Based on the outcome and issues encountered, researchers can improve the labeling using considerations discussed below, and the troubleshooting table (**Table 3.1**).

3.5.1 Sequence of labeling and combination with DNA FISH or immunolabeling

In general, the preferred sequence for using FLARE is: carbohydrate, amine, and DNA. It is preferred to label carbohydrates first because the periodate oxidation step (that converts carbohydrates to aldehydes) also tends to chemically bleach fluorophores already present on the specimen. By using this order, the amine-reactive fluorophores are introduced after the oxidation step that could otherwise bleach them (**Fig. 3.2a** and **3.2c**).

DNA FISH may be straightforwardly performed on FLARE-stained specimens using either tissue-clearing or ExM processing (**Fig. 3.2b** and **3.2d**). However, the harsh conditions used in DNA FISH procedures appear to dehybridize double-stranded DNA, leading to unsuccessful conventional DNA stains (e.g., DAPI). For the combination of immunolabeling with FLARE, immunolabeling can simply be performed after FLARE (**Fig. 3.2e**). In the event that an antibody does not label a sample well after FLARE, we recommend an alternative labeling sequence consisting of immunolabeling using a biotin-conjugated

primary or secondary antibody (biotin is resistant to sodium periodate oxidation), followed by FLARE, and then a final incubation with a fluorescent streptavidin conjugate (**Fig. 3.2f**).

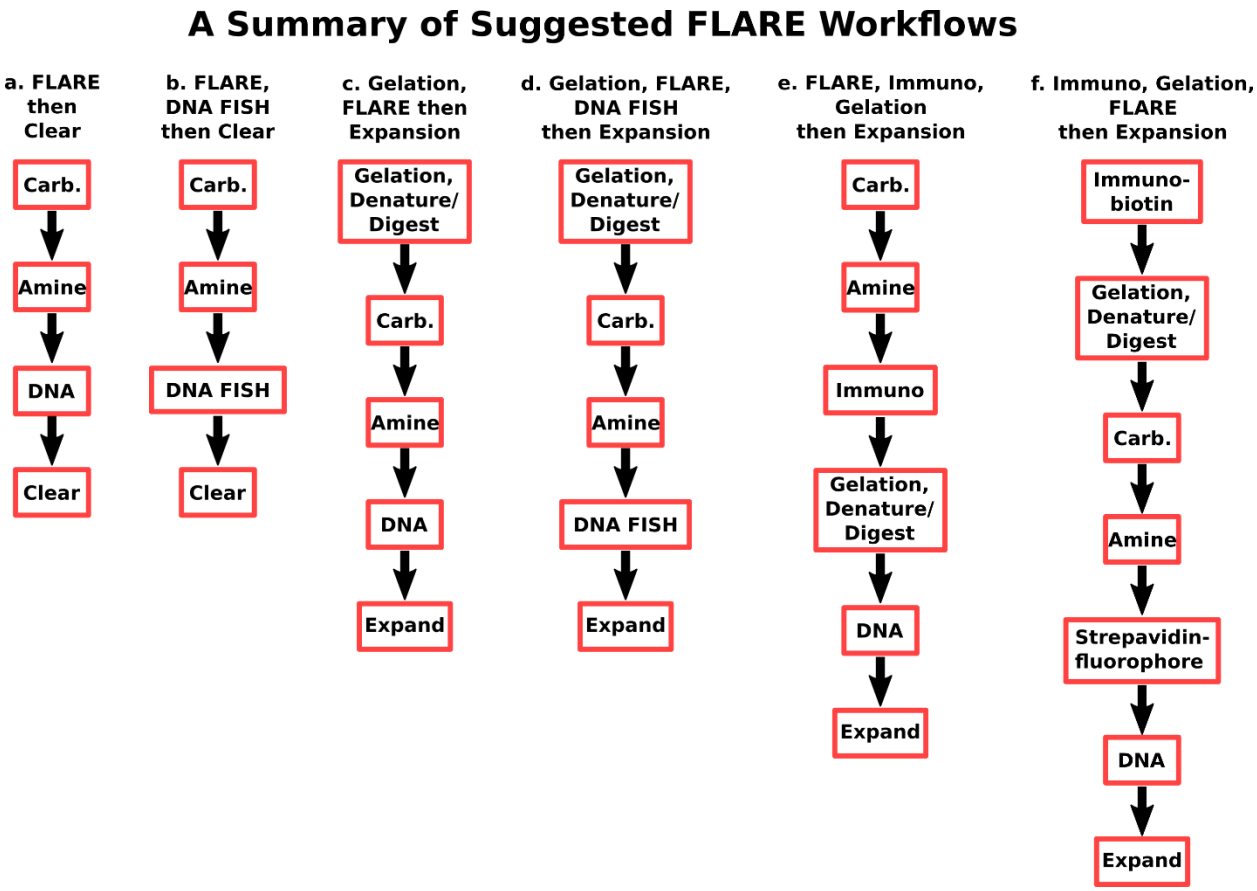

Fig. 3.2 | A summary of suggested workflows for FLARE. (a) A basic FLARE stain consists of carbohydrate, amine, and DNA labeling and may be followed by tissue clearing for unexpanded specimens. (b) DNA FISH may be added to workflow (a) after FLARE staining, although the noncovalent DNA stain is omitted since the stain is poor after the harsh conditions used for DNA FISH due to possible dehybridization of double-stranded DNA. (c) ExM and FLARE may be combined with gelation and denaturation (or digestion) of a sample, FLARE staining, and expansion by incubation in water. (d) DNA FISH may be added to workflow (c) after FLARE staining, again omitting the nonspecific DNA stain as in (b). (e) FLARE may be combined with immunostaining and ExM by labeling of carbohydrates, labeling of amines, immunolabeling, gelation and denaturation (or digestion), labeling of DNA, and then expansion in water. In case FLARE is found to perturb downstream immunolabeling, it is possible to use alternative protocol (f). Carb= carbohydrate stain; Amine= amine stain; DNA= DNA stain; Clear= organically cleared; Denature= protein denaturation using sodium dodecyl sulfate; Digest= enzymatic protein digestion; Expand= expansion in water; DNA FISH= DNA fluorescence in situ hybridization; Immuno= immunolabeling with standard primary and secondary antibodies; Immuno-biotin= immunolabeling with biotin-labeled primary antibodies or a combination of unlabeled primary and biotin-labeled secondary antibodies.

Integration of FLARE with ExM requires a few considerations. We generally perform FLARE either before all expansion procedures or after gelation and sample homogenization, but we have not observed

clear differences in the staining patterns, making either order a viable choice. However, slightly longer incubation times are required for FLARE stains after gelation and sample homogenization, possibly to give the dyes more time to transverse a thicker sample after partial (~two-fold) expansion. Unlike ExM approaches that use enzymatic digestion, MAP is able to allow post-gel immunostaining due to better preservation of protein epitopes[11]. Although we have not tested immunostaining after FLARE on expanded samples, we have previously tested a range of antibodies against non-expanded FLARE-processed samples, and we found that most antibodies worked well (14/16)[3]. We, therefore, suggest that FLARE-processed specimens are likely to still be stained well with antibodies after expansion for scenarios where the expansion procedure does not block antibody labeling.

3.5.2 Fluorophore choice

In this protocol, we typically use AT647N-NHS to label amines and AT565-$NHNH_2$ to target oxidized carbohydrates, but these may be easily substituted for other fluorophores that have the correct chemical functionality and non-overlapping spectra. If FLARE is done before gelation, then it is also important to choose fluorophores that survive the hydrogel polymerization step. AT488, AF488, AT565, AF568, and AT647N are all examples of dyes that survive the typical hydrogel polymerization process and are also good general-purpose fluorophores. If combining FLARE with immunolabeling or DNA FISH, then it is also important to make sure that the spectra of all channels are compatible.

For instance, FLARE could be performed with AT647N-NHS labeling of amines (664 nm emission maximum), AT565-hydrazide labeling of oxidized carbohydrates (590 nm emission maximum), Hoechst labeling of DNA (460 nm emission maximum), and an immunostain or DNA FISH stain could be performed using AF488 (525 nm emission maximum). The NHS- or hydrazide-functionalized dyes may be straightforwardly swapped for dyes in other spectral ranges by purchasing other commercially available dyes with the same reactive chemical groups. For instance, in **Fig. 3.5b and 3.5c**, we selected ATTO-488-NHS to label amines so that we could also use ATTO-647N oligonucleotides already on hand for DNA FISH. Although the electrical charge or hydrophobicity of different fluorophores could potentially result in stain differences, preliminary tests did not yield notable stain differences when using different fluorophores.

3.5.3 Tuning of the chemistry of uniform labeling

Some reaction conditions were tuned to improve FLARE labeling. First, for both expanded and unexpanded samples, we selected a pH of ~6.0 for the AT647N-NHS incubation buffer that promotes stain uniformity, in contrast with typical protein bioconjugation reaction conditions that use a higher pH (~8.4) to promote faster or more complete reactions[40]. This is because NHS-esters are less reactive and also hydrolyze (to a non-reactive state) more slowly at a lower pH; under these conditions, fluorophores are able to penetrate more deeply into the sample prior to reaction/hydrolysis[41,42]. Second, for expanded samples, due to the negative charge of the hydrogel, we used a relatively high salt concentration (1 M NaCl) in the 100 mM sodium acetate buffer to enable negatively charged molecules to penetrate better through the hydrogel network via electrostatic screening. Third, for unexpanded cleared samples, in addition to lowering the pH, we introduced the organic solvent THF as a co-solvent during the staining incubation in order to facilitate the dye diffusion process. Other organic solvents that are miscible with

water and do not interfere with the reaction may also be usable. The end result of these measures is to increase diffusion relative to the coupling reaction in order to produce a uniform stain, especially in thick specimens.

3.5.4 Level of expertise needed

FLARE does not require specific expertise for the implementation. However, researchers who are not familiar with the procedures for ExM are recommended to consult previously published expansion protocols[10,9,8,11,17,18,38,39].

3.5.5 Biological materials

- H-tert Retinal Pigment epithelium (H-tert RPE-1 cells, ATCC Cat# CRL-4000, RRID: CVCL_4388) !Caution frequently test for mycoplasma infection.
- Mouse tissue (two-month-old C57BL/6 male mice) !Caution All protocols involving animals used in this work were approved by the Institutional Animal Care and Use Committee (IACUC) of the University of Washington. Procedures involving animals were conducted according to the institutional guidelines that are in compliance with National Institutes of Health (NIH) policies.
- Human tissue microarray (US Biomax, Inc.)

3.5.6 Reagents

- 10× PBS, pH 7.4 (e.g., Fisher Bioreagents # L-5400)
- Sodium azide (NaN_3, Fisher Scientific #S227I)
- Sodium acetate, anhydrous (NaOAc, Fisher Scientific #S209)
- Sodium chloride (NaCl, Fisher Scientific #271)
- 4-Morpholineethanesulfonic acid (MES, Sigma-Aldrich, #M8250)
- Sodium periodate ($NaIO_4$, Sigma-Aldrich, #311448)
- Sodium cyanoborohydride ($NaCNBH_3$, Sigma-Aldrich, #156159) !Caution NaCNBH3 is toxic and releases flammable gas upon contact with water; wear appropriate PPE and handle with care.
- ATTO 647N NHS ester (AT647N-NHS, Sigma-Aldrich, #18373)
- ATTO 565 hydrazide (AT565-$NHNH_2$, ATTO-TEC GmbH, #AD565)
- Hoechst 33258 (Sigma-Aldrich, #B2883)
- SYBR Green I (Invitrogen, S7563)
- Deionized water (DI water)
- Ammonium persulfate (APS, Bio-Rad Laboratories, #161-0700)
- Tetramethylethylenediamine (TEMED, Bio-Rad Laboratories, #161-0800) !Caution TEMED is flammable, and a toxic respiratory hazard; handle in small amounts and work in a well-ventilated area.
- 32% (vol/vol) Paraformaldehyde (PFA, Electron Microscopy Sciences, #RT15714) !Caution PFA is a toxic respiratory hazard; handle in small amounts and work in a well-ventilated area.
- 50% (vol/vol) Glutaraldehyde (GA, Electron Microscopy Sciences, #16300) !Caution GA is a toxic respiratory hazard; handle in small amounts and work in a well-ventilated area.
- 1,4-Piperazinediethanesulfonic acid (PIPES, Sigma-Aldrich, #P6757)
- Triethylene glycol diamine tetraacetic acid (EGTA, Alfa Aesar, #ALFAA16086)

- Magnesium chloride ($MgCl_2$, Sigma-Aldrich, #M8266)
- 40% (wt/vol) Glyoxal (Sigma-Aldrich, #128465)
- Sodium borohydride ($NaBH_4$, Fisher Scientific, #AC189300050) !Caution $NaBH_4$ is toxic and releases flammable gas upon contact with water; wear appropriate PPE and handle it in small amounts.
- 40% (wt/vol) acrylamide (AA, Bio-Rad Laboratories, #161-0140) !Caution AA is carcinogenic and may cause nervous system damage; wear appropriate PPE and work in a well-ventilated area.
- 2% (wt/vol) bis-acrylamide (BA, Bio-Rad Laboratories, #161-0142) !Caution BA is carcinogenic and may cause nervous system damage; wear appropriate PPE and work in a well-ventilated area.
- Sodium acrylate (SA, Sigma-Aldrich, #408220)
- VA-044 (Thermo Fisher Scientific, NC0471397)
- Triton X-100 (Sigma-Aldrich, #X100)
- Poly-lysine (Sigma-Aldrich, #P8920)
- Sodium dodecyl sulfate (SDS, Sigma-Aldrich, #L3771)
- Tris base (Tris, Fisher Scientific, #BP152-500)
- Tetrahydrofuran (THF, Fisher Scientific, #T425) !Caution THF is volatile and flammable; wear appropriate PPE and work in a fume hood.
- Dichloromethane (DCM, Fisher Scientific, #D37) !Caution DCM is toxic, volatile, and flammable; wear appropriate PPE and work in a fume hood.
- Ethyl cinnamate (EC, Sigma-Aldrich, #112372)

3.5.7 Equipment

- Rectangular #1.5 glass coverslip (Fisher Scientific, #12544E, 24 x 50 mm)
- 12 mm round coverslip (Electron Microscopy Sciences, #72230-01)
- Forceps (Electron Microscopy Sciences, #78318-3)
- Parafilm M Bemis (VWR, #52858)
- Razor blade (American Line, #66-0089)
- 12-well plate (Pipette, #712011)
- 6-well plate (Pipette, #229106)
- Paint brush (Black Art Materials, #05130-1000)
- Scintillation vial, large enough (~28 mm diameter) to hold tissue section (Wheaton, #986546)
- 1.5 mL microcentrifuge tube (VWR, 76332-064)

3.5.8 Reagents set-up

1× PBS (pH 7.4): dilute 10× PBS 10 times with DI water. For instance, add 100 mL 10× PBS to 900 mL DI water. Store at room temperature.

20% (vol/vol) Triton X-100 solution: dilute pure Triton X-100 5 times with DI water. Note: Warm the pure Triton X-100 prior to use for easier handling. Store at 4 °C until use.

10× PEM buffer contains: 1 M aqueous PIPES buffer pH 7, 10 mM EGTA, 10 mM $MgCl_2$. Once prepared, sore at 4 °C until use.

Extraction solution contains: 100 mM aqueous PIPES buffer pH 7, 1 mM EGTA, 1 mM $MgCl_2$, 0.5% (vol/vol) Triton X-100 solution, and it can be prepared from above 10× PEM buffer and 20% (vol/vol) Triton X-100 solution. Prepare fresh each time.

PFA/GA fixation solution contains: 100 mM aqueous PIPES buffer pH 7, 1 mM EGTA, 1 mM $MgCl_2$, 3.2% (vol/vol) PFA, 0.1% (vol/vol) GA, and it can be prepared from 10× PEM buffer, 32% PFA stock, and 50%GA stock. Prepare fresh each time.

PFA fixation solution: use 10× PEM buffer and 32% PFA stock to prepare a PFA fixation solution that contains 100 mM aqueous PIPES buffer (pH 7), 1 mM EGTA, 1 mM $MgCl_2$, 4.0% (vol/vol) PFA. Prepare fresh each time.

3% (vol/vol) Glyoxal mixture solution (pH 5): the glyoxal mixture solution contains 0.75% (vol/vol) glacial acetic acid, 3% (vol/vol) glyoxal, 19.9% (vol/vol) absolute ethanol. The pH is adjusted to 5 using 1M NaOH. Prepare fresh each time.

NaOAc buffer: 100 mM NaOAc buffer is prepared from NaOAc powder, then pH is titrated to 5 using 1M HCl. Store at room temperature. It should be stable for at least two weeks.

NaOAc/NaCl buffer: NaOAc/NaCl buffer contains 100 mM NaOAc and 1 M NaCl. The pH is titrated to 5 using 1M HCl. Store at room temperature. It should be stable for at least two weeks.

MES buffer: prepare 100 mM MES, 150 mM NaCl in DI water; use 1M NaOH to adjust pH to 6; store at room temperature.

AT565-$NHNH_2$ master stock: prepare a master stock with a concentration of 5 mg/mL (6.65 mM) using anhydrous DMSO. Store at -20 °C until use.

AT647N-NHS ester master stock: prepare a master stock with a concentration of 5 mg/mL (5.93 mM) using anhydrous DMSO. Store at -20 °C until use.

SYBR Green master stock: prepare a master stock with a concentration of 10 mg/mL (19.6 mM) using anhydrous DMSO. Store at -20 °C until use.

Monomer solution (cells): use above reagents to prepare a monomer solution that contains 20% (w/v) AA, 10% (w/v) SA, 0.05% (w/v) BA, 4% (w/v) PFA, and 0.67% (w/v) TEMED. Store at 4 °C for up to 1 week, protected from light.

Monomer solution (tissues): use above reagents to prepare a monomer solution that contains 20% (w/v) AA, 10% (w/v) SA, 0.05% (w/v) BA, and 4% (w/v) PFA. Store at 4 °C for up to 1 week, protected from light.

Denaturing solution contains: 200 mM SDS, 200 mM NaCl, and 50 mM Tris. Its pH is adjusted to 9.3 using 1M HCl. Store at 37 °C until use.

PBST solution: prepare 0.1% Triton X-100 and 0.02%(wt/vol) NaN_3 using 1× PBS. Store at room temperature until use.

Hoechst 33258 master stock: prepare a master stock with a concentration of 10 mg/mL (23.4 mM) using anhydrous DMSO. Store at -20 °C until use.

THF/NaOAc solution: mix equal volumes of THF and above prepared NaOAc buffer. Prepare fresh each time.

THF/MES solution: mix equal volume of THF and above prepared MES buffer. Prepare fresh each time.

THF/PBS solution: mix equal volume of THF and 1× PBS buffer. Prepare fresh each time.

3.5.9 Procedure 1. FLARE for expanded specimens (see Supplementary Figure 3.1 and Supplementary Figure 3.2 for photos of key steps)

The following protocol for FLARE labeling of fixed and expanded specimens is described either for cultured cells or for thin (~100 µm) tissue sections, although instructions specific to tissue sections are indicated within solid boxes. The expansion part in this protocol is adapted and modified from "Multiplexed and scalable super-resolution imaging of three-dimensional protein localization in size-adjustable tissue"[11]. The bold numbers in brackets denote the quantities used during the experiment. We recommend that researchers follow the processing and staining procedures for either cell or tissue sections as a general starting point and then optimize, if needed, the labeling using the troubleshooting table (**Table 3.1**).

Specimen pre-processing •Timing **~12 hours (for cell cultures) or ~1-6 hours (for tissue)**

1. H-tert RPE-1 cells (H-tert Retinal Pigment Epithelium, ATCC CRL-4000) were grown to ~70–90% confluency and seeded (~30,000–70,000 cells/well) on #1.5 round coverslip in 24-well culture plates. After 12 hours, the cells were fixed using PFA/GA fixation solution for 10 minutes at room temperature (~20 °C). Fixed cells were stored in 1× phosphate buffered saline with 3 mM sodium azide (1× PBS azide) at 4 °C prior to use. ■Pause Point Able to store up to 6 months.

2. Mouse tissue specimens from two-month-old C57BL/6 male mice are typically obtained by cardiac perfusion with 1× PBS for 3 minutes followed by 4% PFA solution in 1× PBS for 5 minutes (7 mL/min); after removal of the organ of interest, the tissue is further fixed in 4% PFA at 4 °C depending on the thickness of the tissue (e.g., adult mouse kidney was immersion-fixed in 4% PFA for 1 hour, while adult mouse liver was fixed for 6 hr). The fixed tissue was then sliced on a vibratome into ~100 µm sections that were stored in a multiwell plate in 1× PBS buffer with 3 mM sodium azide at 4 °C until ready for further processing. ■Pause Point Able to store up to 6 months.

   OPTIONAL Reduction (for samples fixed with GA to quench remaining aldehydes from the fixation process and to lower the amount of GA-induced fluorescence; otherwise, may omit) •Timing 10 minutes

3. Prepare a fresh, aqueous 10 mM $NaBH_4$ solution [4 mg $NaBH_4$ in 10 mL DI H2O].

4. Incubate the fixed cells with the $NaBH_4$ solution prepared in Step 3 for 10 minutes [~0.5 mL per well, 24-well plate].

5. Wash cells with 1× PBS [0.5 mL per well, repeat three times]. ■Pause Point Store up to 6 months in 1× PBS azide, depending on your fixation conditions and cell sample stability.

6. **Monomer infusion •Timing 24 hours**

    a. Cell monomer solution infusion. Add the cell monomer solution to each well and incubate at room temperature (RT) for 24 hours [0.5 mL per well]. Protect the solution from light during the incubation.

> **Tissue sample monomer infusion procedure:** The sample is incubated in tissue monomer solution overnight at 4 °C while protected from light [**1 mL per well**].
>
> Note that for the relatively thin (~100 µm) tissue specimens focused on here, immersion of the sample within the monomer solution is sufficient for the production of uniform gels[46], whereas the original MAP procedure[11] used cardiac perfusion to enhance monomer infusion throughout relatively thick whole mouse organs. In any event, the FLARE labeling procedure is well-suited to either variation of the gelation procedure.

7. **Gelation •Timing 30 minutes for cells and 2 hours for mouse kidney tissue**

    a. Prepare a fresh, aqueous 10% (wt/vol) APS solution [10 mg APS in 100 µL DI H2O]. Keep the solution on ice until use.
    b. Pipette 98 µL of monomer stock solution into a microcentrifuge tube.
    c. Pipette 2 µL of 10% APS solution into the microcentrifuge tube, quickly mix, and add 70 µL of mixed solution onto a piece of Parafilm (~5 cm × 5 cm).
    d. Use the forceps to carefully take out the round coverslip with fixed cells from the well, and carefully place the coverslip with cells facing down onto the solution prepared from the previous step. ▲Critical Step Make sure the gelation is done on the side of the coverslip that is covered with cells.
    e. Wait 30 minutes for the solution to polymerize at RT. Protect the solution from light during polymerization. Note that any solution left in the microcentrifuge tube can be used to judge the progress of the gelation process.
    f. Use a ruler to measure the gel size to obtain the pre-expansion size for calculation of expansion factor later in step 11.

Tissue Sample Gelation (see **Supplementary Figure 3.2** for illustration**):** Using a paint brush, spread a 100 µm section of tissue on a rectangular #1.5 coverslip, place two stacked small pieces of #1.5 coverslip on either side of the sample to act as spacers, add one drop of monomer solution **[99 µL of fresh monomer solution + 1 µL of 10% (w/v) VA-44]** on the tissue surface, and place another rectangular #1.5 coverslip on top to create a tissue gelation chamber. The drop of monomer solution should cover the entire sample area (up to ~ 1 cm^2). Put the sample in a glass chamber and purge with nitrogen before shutting the airtight lid. Incubate the chamber at 45 °C for 2 hr.

8. **Denaturation** •Timing **60 minutes for cells and 48 hours for mouse kidney tissue**

   a. Use a razor blade to carefully peel off the gel from the Parafilm. Avoid peeling the gel off the coverslip at this point as this could damage the cells.
   b. Transfer the gel attached to the round coverslip into a 20 mL scintillation vial containing denaturing solution [10 mL solution each sample].
   c. Denature the cell sample for 60 minutes at 95 °C. Note that the hydrogel will typically expand ~2× during this process. The heating process can be done using heat blocks on an orbital shaker.
   d. Transfer the gel to a large volume of PBST solution to wash out denaturing reagents. This wash step should be repeated three times for 30 minutes each time. Next, use 1× PBS to wash away detergents prior to chemical staining. ■Pause Point Store up to a week in PBS azide at 4 °C.

Tissue Sample denaturation: For mouse kidney tissue samples, incubate in denaturing solution at 70 °C for 24 hours first, and then at 90 °C for an additional 24 hours. For more details, refer to "Confocal super-resolution imaging of the glomerular filtration barrier enabled by tissue expansion"[39].

9. **Carbohydrate stain of FLARE** •Timing **5 hours 45 minutes**

   a. Oxidation (oxidizes carbohydrates to aldehydes)
      i. Prepare a fresh, aqueous 20 mM $NaIO_4$ solution [43 mg $NaIO_4$ in 10 mL NaOAc/NaCl buffer].
      ii. Cut a piece of hydrogel to a suitable size (e.g., 1×1 cm^2) and transfer both the hydrogel and the 20 mM $NaIO_4$ solution [10 mL] into a 6-well plate.

iii. Let the oxidation reaction run for one hour while gently agitating the container on an incubator shaker at 37 °C. Protect the solution from light during the reaction.

b. Hydrazone formation (couples hydrazide dye to oxidized carbohydrate aldehydes)

i. Remove the solution from Step 9Aii and wash the sample with NaOAc buffer at room temperature for 10 minutes each with gentle agitation [10 mL per wash, repeat three times].
ii. Transfer the hydrogel sample into a well of a 12-well plate.
iii. Dilute AT565-$NHNH_2$ master stock in NaOAc buffer to final concentration 5 µg/mL and add to the well containing sample [1 µL dye in 1 mL NaOAC buffer, for 6.66 µM final concentration].
iv. Let the reaction run for 3 hours with gentle agitation on an orbital shaker.

c. Reduction (to form a stable bond between the oxidized carbohydrates and fluorophore)

i. Prepare a fresh 100 µL of 5 M $NaCNBH_3$ solution [31.4 mg $NaCNBH_3$ in 100 µL NaOAc buffer]. Note: $NaCNBH_3$ should be stored in an inert condition. $NaCNBH_3$ is a milder reductant than $NaBH_4$. $NaBH_4$ may adversely react with some fluorophores (such as cyanine dyes).
ii. Add 20 µL of the $NaCNBH_3$ solution directly to the sample well of Step 9Biii.
iii. Allow the sample to react for 30 minutes with gentle agitation.
iv. Wash the sample with the NaOAc buffer for 15 minutes [2 mL each, repeated twice]. Then allow the sample to remain in the NaOAc buffer for a longer period of time [1 hr or overnight depending on the sample] in order to remove excess unconjugated hydrazide dye.
v. Wash the sample with 1× PBS solution for 15 min. [2 mL]

10. **Amine stain of FLARE** •Timing **1 hour for cells and 6 hours for mouse kidney tissue**

a. Prepare 2.5 µg/mL AT647N-NHS from master stock [add 1 µL dye to 2 mL 1× PBS for 2.97 µM final concentration].
b. Incubate sample with AT647N-NHS solution for 1 hr with gentle agitation and while covered to protect from light.
c. Wash the sample with 1× PBS for 30 min [2mL each, repeated twice]. Then store in 1× PBS for further use.

> **Tissue Sample amine labeling:** A concentration of 5 µg/mL (5.9 µM) AT647N-NHS in MES with a reaction time of 6 hr is used for 100 µm thick expanded kidney tissue sections to help ensure a uniform stain. Faster stains can be achieved with a higher concentration of dye.

11. **Expansion •Timing 1 hour**

    a. Transfer the sample in an excess volume of DI H_2O enough to cover a 100 mm Petri Dish (~30 mL) and let it expand for at least 1 hr. Frequent DI H_2O change speeds up the expansion process. Note that the sample should be completely submerged in water.

    b. Remove water and use a ruler to measure the post-expansion size and divide the value by the pre-expansion size (found in step 7) to obtain the approximate expansion factor (4.5×-5×). ▲Critical This is the macroscopic expansion factor and should be the same as the microscopic expansion factor when the ExM procedure is done properly. However, one should keep an eye out for possible discrepancies between the two expansion factors, especially in specimens that have not been previously validated for expansion. OPTIONAL For DNA fluorescence in situ hybridization (FISH) general protocol, proceed to Supplementary information.

12. **DNA stain •Timing 35 minutes** ▲Critical Conventional DNA stain may not work after DNA FISH. This is due to the harsh conditions used in the DNA FISH protocol that potentially dehybridizes the double-stranded DNA leading to poor stain by DNA dyes subsequently.

    a. Prepare a 10 µg/mL SYBR Green solution from the master stock [add 1 µL master stock dye to 1 mL DI H_2O].

    b. Apply the solution directly to the surface of the gel side that contains the cells and incubate for 20 minutes.

    c. Rinse the sample three times with an excess of DI H_2O to remove unbound SYBR Green. Note that SYBR Green is a turn-on fluorescent dye with minimal background fluorescence. However, DNA dyes such as Hoechst require thorough washing of the hydrogel to minimize background fluorescence.

13. **Sample mounting •Timing ~5-15 minutes**

    a. Temporarily transfer the gel to a clean untreated coverslip and remove excess liquid by wicking the edges with tissue paper. Excess water beneath the gel may hinder the adhesion with poly-lysine later (Step 13B) and add unnecessary imaging depth. ▲Critical Be careful as the gel is prone to sticking to the tissue paper.

    b. To eliminate drift during imaging, carefully slide the gel from the untreated coverslip onto a poly-lysine coated coverslip to create strong adhesion between the gel and the poly-lysine surface. It is best to image the sample immediately. ▲Critical The poly-lysine coated coverslips for imaging may be prepared ahead of time and are stable for weeks. Evenly spread 2-3 µL of a 1 mg/mL poly-lysine solution on the surface of a hydrophilic coverslip and allow it to dry. Exposing the coverslip to an air plasma in a plasma cleaner for ~1 minute is the preferred way to render the slides hydrophilic prior to spreading the poly-lysine solution, but not required.

14. **Imaging and Image analysis •Timing Variable**

a. FLARE-labeled samples can be imaged using a variety of fluorescence microscopy modalities including widefield, confocal, and light-sheet microscopy (see **Supplementary Table 3.1** for a list of which of the three modalities was used for the data sets shown here). For expanded samples, we often use a widefield microscope to check sample usability, and we typically use confocal microscopy for routine experiments since confocal microscopy offers straightforward high-resolution 3D imaging with good optical sectioning. For high-resolution imaging of expanded specimens whose index of refraction is approximately the same as that of pure water, we use a water-immersion lens. Matching of the index of refraction of the specimen with the immersion medium of the objective lens is important to avoid serious optical aberrations. The objective lens should also have a large enough working distance to image into the specimen at the desired depth.

b. For all data sets from expanded samples, the free software package ImageJ was used for image visualization and processing, such as channel merge, image registration, and image smooth. Details regarding each figure can be found in **Supplementary Table 3.1**.

3.5.10 Procedure 2. FLARE for Unexpanded cleared tissue section (see Supplementary Figure 3.3 for photos taken from each step)

The following procedure is designed for 100 µm thick tissue sections. The bold numbers included in brackets are the quantities used during the experiment. Several modifications in the protocol are necessary when applying FLARE to thicker specimens (**Fig. 3.6**) or thinner tissue specimens, such as tissue microarrays (TMA) (**Fig. 3.4**). In this case, the modifications pertaining to TMA appear in solid boxes in the following text. We recommend that researchers follow the processing and staining procedure for 100 µm thick tissue sections as a general preliminary test. Based on the outcome, researchers can further optimize the labeling using the troubleshooting table (**Table 3.1**). For thicker specimens, due to the need for dyes to travel a longer distance, we recommend a longer incubation time. Following the protocol, below, researchers can use the conditions (found in **Supplementary Table 3.1**) for thick mouse kidney (**Fig. 3.6**) for their preliminary test, and then optimize from there if needed.

1. Carbohydrate stain of FLARE •Timing 4 hours

a. Oxidation (oxidizes carbohydrates to aldehydes)

i. Prepare a fresh, aqueous 100 mM $NaIO_4$ in pH 5.0 NaOAc buffer [42.8 mg $NaIO_4$ in 2 mL NaOAc buffer].

ii. Use a paint brush to gently transfer a tissue section into the above solution in a scintillation vial. Note that having the tissue section float, initially, at the surface of the solution in the well plate makes the transfer to a scintillation vial easier and helps avoid damage to the tissue section.

iii. Let the reaction run for 30 minutes while gently agitating the sample on an orbital shaker or rocker. Ensure that the tissue is in constant motion within the solution. Protect the solution from light during the reaction.

TMA sample oxidation: Use Parafilm M, instead of scintillation vial. A prepared 100 mM $NaIO_4$ solution is dropped onto TMA which is then covered by Parafilm M. Let the reaction run for 30 minutes.

b. Hydrazone formation (couples hydrazide dye to oxidized carbohydrate aldehydes)

i. Remove the solution in Step 1A and wash the sample with NaOAc buffer [10 mL per wash, 10 minutes each wash, repeat three times].

ii. Dilute AT565-$NHNH_2$ master stock in fresh THF/NaOAc solution to final concentration 2.5 µg/mL [1 µL of master stock dye in 2 mL THF/NaOAc solution, for 3.33 µM final concentration.

iii. Remove NaOAc washing buffer from Step 1Bi and add the diluted dye solution from Step 1Bii. Incubate the sample on the orbital shaker for 2 hours. Ensure that the tissue is in constant motion within the solution. Protect the solution from light during the reaction.

TMA sample hydrazine formation: prepare AT565-$NHNH_2$ solution by diluting AT565-$NHNH_2$ master stock in NaOAc solution to final concentration 2.5 µg/mL; drop the solution onto the washed TMA sample; cover the TMA sample with Parafilm M. Let the reaction run for 2 hours.

c. Reduction (to form a more stable amine bond)

i. Prepare 100 µL of fresh 5 M $NaCNBH_3$ solution [31.4 mg $NaCNBH_3$ in 100 µL NaOAc buffer]. ▲ Critical $NaCNBH_3$ should be stored in an inert condition. NaCNBH3 is a milder reductant than $NaBH_4$. $NaBH_4$ may react with certain fluorophores (such as many cyanine dyes).

ii. Add 10 µL of $NaCHBH_3$ solution directly into the reaction mixture in step 1Biii.

iii. Allow the sample to react for 30 minutes on an orbital shaker.

iv. Wash the sample with fresh THF/NaOAc solution [10 mL per wash, 10 minutes per wash, repeat two times].

v. Wash the sample with fresh THF/MES solution [10 mL, 10 min]. ■Pause Point Able to store overnight in THF/MES solution.

2. Amine Stain •Timing 2 hours (100 µm thick specimen)

a. Prepare 2.5 µg/mL AT647N-NHS from master stock [add 1 µL dye stock to 2 mL THF/MES solution, for 2.97 µM final concentration].

b. Incubate sample with AT647N-NHS solution from Step 2A for 2 hours with gentle rocking. Ensure that the tissue is in constant motion within the solution. Protect the solution from light during the reaction.

c. Wash the sample with fresh THF/MES solution [10 mL per wash, repeat two times].
d. Wash the sample with fresh THF/PBS solution [10 mL, 10 min]. ■Pause Point Able to store overnight in THF/PBS solution.

> **TMA sample amine stain:** prepare AT647N-NHS solution by diluting AT647N-NHS master stock in PBS solution to a final concentration 2.5 µg/mL. Drop the solution onto the washed TMA sample. Cover the TMA sample with Parafilm M. Let the reaction run for 30 minutes.

3. DNA Stain •Timing 30 minutes (100 µm thick specimen)

a. Prepare 5 µg/mL Hoechst 33258 solution [add 1 µL dye stock to 2 mL THF/PBS solution].
b. Incubate the sample in the solution prepared in Step 3A for 30 minutes with gentle rocking. Ensure that the tissue is in constant motion within the solution. Protect the solution from light during incubation.
c. Briefly wash the sample with fresh THF/PBS solution with gentle rocking [10 mL per wash, repeat twice, 5 min each].

> **TMA sample amine stain:** prepare 5 µg/mL Hoechst 33258 solution in PBS solution and drop the solution onto the washed TMA sample. Cover the TMA sample with Parafilm M. Let the reaction run for 30 minutes.

4. Dehydration and Refractive Index Matching •Timing ~3.5 hours (100 µm thick specimen)

a. Transfer the sample into fresh 50% (vol/vol) THF in DI water [4 mL].
b. Incubate the sample for 30 minutes with gentle rocking. Protect the solution from light during incubation.
c. Incubate the sample for 30 minutes in 80% THF (vol/vol) in DI water [3.2 mL THF and 0.8 mL DI water]. Protect the solution from light during incubation.
d. Incubate the sample for 30 minutes in 100% THF [4 mL THF]. Protect the solution from light during incubation.
e. Soak the sample in DCM until it sinks [4 mL DCM].
f. Finally, incubate the sample with EC to match the refractive index [1 mL EC]. The duration of the dehydration and index matching step will depend on the type of tissue and its thickness, but ~2 hours is a good starting point. It may be necessary to refresh the EC solution multiple times with longer incubation times for thicker samples to ensure good index-matching. The clarity of the cleared tissue is easy to judge by the unaided eye. ■ Pause Point Advisable to image as soon as possible but able to store in EC for a few days.

TMA sample dehydration: this step may be omitted as the TMA is very thin. The sample is imaged with an air and/or water-immersion objective lens directly.

5. **Sample mounting •Timing 5 minutes (100 µm thick specimen)**
    a. Use a paint brush to transfer the sample onto a rectangular #1.5 coverslip. Note that at this point, the sample is now rigid due to dehydration and thus would not entangle with the brush and can be easily transferred.
    b. Attach a piece of double-sided tape to the surface of each of the two short edges of the coverslip.
    c. Add one drop of EC to fully cover the sample.
    d. Press a second rectangular #1.5 coverslip onto the first to form a sandwich structure held together by the double-sided tape. Make sure that the sample is sitting very closely to the surface of the first #1.5 coverslip in the sandwich structure and that there are no air bubbles on the specimen surfaces.

6. **Imaging and Image Analysis •Timing Variable**
    a. There are some considerations in sample imaging that are similar to those mentioned in step #14A. A widefield microscope is typically used first to check for general sample quality and a confocal microscope is then used for routine experiments. For imaging of very thin (<10 µm) unexpanded specimens, we typically use a widefield microscopy with a 4× objective lens. For thicker unexpanded cleared specimens (10-200 µm), we typically use a confocal microscopy with an oil-immersion objective lens to avoid optical aberrations when imaging deeper into the EC-cleared specimens. For even thicker cleared specimens (>0.1 mm) we typically use light sheet microscopy[43–45].
    b. As described in step #14B, the free software package ImageJ is sufficient to analyze most data sets except for the large mouse kidney data set (**Fig. 3.6**) which was acquired by open-top light-sheet microscopy[29] and was volumetrically rendered using Imaris. Details regarding data processing for each figure can be found in **Supplementary Table 3.1**.

3.6 Troubleshooting

Troubleshooting advice can be found in Table 3.1.

Table 3.1. Troubleshooting Table

Step	Problem	Possible reason	Solutions
Procedure 1 step 8C.	Poor or uneven expansion	Easily visualized by sample tearing or under-expanded regions in the nuclei distribution and usually caused by inadequate	Extend the denaturation period and/or repeat the denaturation step at a higher temperature. In the case of enzymatic digestion, an addition of another category of

		denaturation or digestion of the sample. (**Fig. 3.7**)	enzyme may help with digestion.[46,47] (**Fig. 3.7**)
Procedure 1 steps 7D, 13, 14 OR Procedure 2 step 6	No signal	Lack of signal can arise due to several reasons:	
		Inappropriate microscope settings	Check that the microscope settings are appropriate to the fluorophores with a suitable positive control.
		Issues with sample gelation	Make sure that the hydrogel polymerization is done on the coverslip side coated with cells as it can be easy to lose track of which side of a coverslip the cells are adhered to (**Fig. 3.8a**). Make sure that the sample is positioned as close to the surface of the gel as possible in order to be within the working distance of the objective lens.
		Error with sample mounting	It is possible that the gel is upside down, and the surface of the hydrogel containing the sample is outside the working distance of the objective lens (**Fig. 3.8b**). Test this by imaging the other surface of the gel.
		Fluorophore bleaching	The $NaIO_4$ oxidation step will chemically bleach many fluorophores, and adequate removal of $NaIO_4$ is required prior to the hydrazide dye incubation. Repeat the procedure with more thorough washing. Importantly, the hydrazide labeling step should be performed before the NHS-dye coupling reaction, or any other fluorescent labeling reactions.
Procedure 1	Dim Signal	Dim signals can arise due to several reasons:	

steps 9C, 10, 12, 14 OR Procedure 2 steps 1C, 2, 3, 6		Reagent degradation can result in an inefficient reaction.	If the carbohydrate stain is dim, it could indicate that $NaCNBH_3$, which can become deactivated with prolonged exposure to moist air, has been hydrolyzed, leaving the hydrazide-dye conjugated to the specimen by a relatively labile hydrazone bond. If the amine channel is dim, it could indicate that the NHS groups on the NHS-dye have been hydrolyzed and thus the dyes were not efficiently coupled to the sample. In either of these cases, researchers can repeat the procedure using fresh aliquots or newly purchased reagents. In addition, proper storage can help slow down the degradation of these reagents (refer to the Stock Solutions section).
		Insufficient dye concentration	The sample staining intensity can be tuned to produce brighter signals by increasing the concentration of the reactive fluorophores used in the labeling reactions.
		Lack of sample exposure to chemicals	With respect to the hydrogel-embedded samples, make sure that the hydrogel surface containing the sample is placed face-up in a container during the labeling reaction, or the dyes may have a harder time accessing the sample resulting in dim signals (**Fig. 3.9**).
		Incorrect objective lens	It is essential to carefully choose the correct objective lens for a given type of sample: water-immersion objective lenses are well-suited to imaging specimens in hydrogels, whereas oil-immersion lenses are well-suited to imaging organic

			cleared oil refractive index matched EC specimens. The use of a mismatched immersion lens may lead to optical aberrations and loss of signal at substantial depths.
		Inner filter effect	See Uneven Signal.
Procedure 1 step 14 OR Procedure 2 step 6	Uneven Signal	Uneven signal is mostly an issue with thick sample labeling and could be a result of excess dye during a labeling reaction. A thick sample can be labeled so strongly at the surface that the excitation light in the microscope is substantially attenuated within the interior of the sample ("inner filter effect"), producing a very bright surface but an apparent dimmer interior, even if the sample itself is in fact labeled uniformly.	The researcher can section the hydrogel or the thick sample and image the cross-section to assess the sample uniformity without this complication. (**Fig. 3.10**) If the stain is indeed uniform, the researcher can stain a new sample with a more dilute dye to produce a dimmer stain that avoids this inner filter effect. (**Fig. 3.10**) If the stain is in fact enriched at the surface, the researchers should confirm that the NHS-dye coupling reaction is performed at a lower pH of 7.4 or could consider preparing the NHS-dye stock in ~100 mM MES buffer at pH 6.0 to slow down the hydrolysis and coupling reactions while also providing more time for the labeling reaction and dye penetration. In addition, to aid in the penetration of the dye through the negatively charged hydrogel, researchers can consider using NaCl to act as a shield to allow charged reactants to enter the gel. Researchers should also make sure that the bottom surface of the tissue sample is not attached to the surface of the container during incubation (**Fig. 3.9**) and to ensure continuous sample motion during gentle agitation. Using a lower concentration of dye may also help

			improve the uniformity of labeling, but possibly at the cost of decreasing the brightness of the stain.
Procedure 1 steps 9B, 10 OR Procedure 2 Steps 1B, 2	Overly Bright Signals	Crosstalk from an overly bright signal in a channel could swamp a weaker signal from a different spectral channel. In addition, an overly bright signal can produce inner filter effect. (see Uneven Signal) Overly bright signals can arise due to several reasons:	
		First, insufficient washing could prevent unconjugated dyes from being removed from the sample resulting in very bright signals.	Washing the sample extensively can fix this problem and improve contrast.
		Second, if the dye concentration is too high, an overly bright sample may be produced.	Lowering the concentration of dye(s) in the coupling reaction(s) can help tune the signal.
Procedure 2 step 4	Poor Transparency in Refractive Index Matched Samples	Improper or insufficient tissue clearing can arise due to several reasons:	
		Inadequate dehydration prior to incubation with ethyl cinnamate (EC) or other common refractive index oil.	A thorough dehydration is crucial to achieve a uniform refractive index match throughout the entire specimen thickness and extending the dehydration periods at each stage may help improve the clarity.
		Insufficient incubation with EC	Researchers can try to refresh the EC a couple of times, followed by waiting ~30-60 minutes or more (depending on the size of the

			tissue) for the tissue to become fully cleared and index-matched.

3.7 Anticipated results

We have applied FLARE to a wide variety of samples including cultured cells, mouse organs, human specimens, as well as different sample processing procedures such as fresh fixation, FFPE preparation, clearing, or expansion. In this section, we show some results of these FLARE applications in order to give researchers a general idea of FLARE labeling with a range of samples (**Fig. 3.3 - 3.6**). We also include figures and data to illustrate possible issues associated with FLARE labeling (**Fig. 3.7 – 3.10**).

3.7.1 Effects of fixatives

Fixation is a critical part of many imaging experiments. Because FLARE is able to show the general physiology of samples extremely well, it can be a useful tool for revealing potential perturbations in fixation or other sample processing steps. For example, we compared fixation using paraformaldehyde and glutaraldehyde (**Fig. 3.3a-d**) with fixation using glyoxal48 (**Fig. 3.3e-h**) in expanded RPE cells. We found that cells fixed with paraformaldehyde and glutaraldehyde revealed mitochondria, lysosomes, the Golgi apparatus, nuclear pores, and portions of the cytoskeleton (**Fig. 3.3a-d**) while glyoxal-fixed cells showed major perturbations to many of these structures (**Fig. 3.3e-h**).

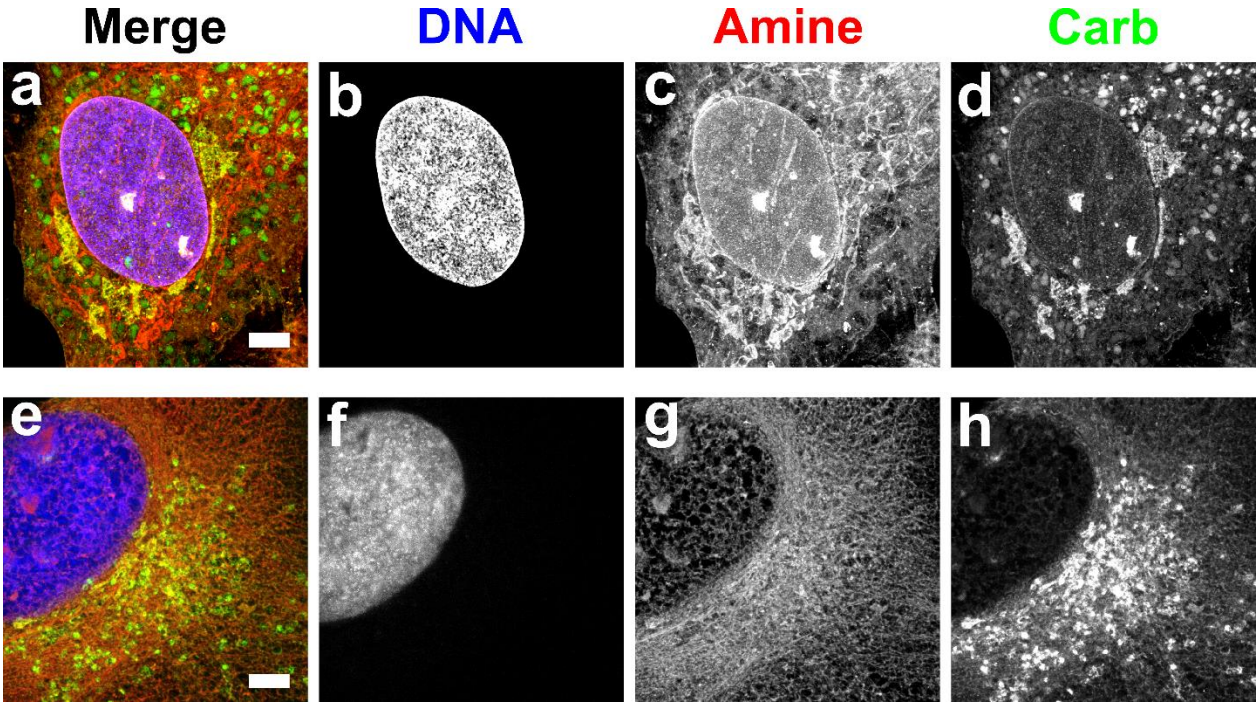

Fig. 3.3 | Comparison of fixation conditions for expanded RPE cells stained by FLARE. Red corresponds to amine stain, green corresponds to carbohydrate stain, and blue corresponds to nuclear stain. (a-d) Fixation with paraformaldehyde and glutaraldehyde generally preserved membrane-bound organelles and other structures

while (e-h) fixation with glyoxal showed substantial perturbations. Scale bar (pre-expansion): 3 µm (a-h). Panels a-d were adapted from Mao et al.3 Science Advances. AAAS Publishing Group.

3.7.2 FLARE on tissue microarrays

FLARE's simplicity and robustness make the staining method appealing for use with diverse types of samples, such as in the fluorescent staining of FFPE sections in tissue microarrays that have been embedded and stored for ~13 months (**Fig. 3.4a-g**) or 5 years (**Fig. 3.4h-n**) prior to staining. FLARE is able to present the general physiology of these tissues similar to H&E (**Fig. 3.4b, 3.4e, and 3.4i-k**) with an additional benefit of showing abundant multicolor details with high contrast (**Fig. 3.4c-d, 3.4f-g, and 3.4l-n**). Since FLARE reveals the accessible amine and carbohydrate groups, extensive fixation or different processing procedures or storage conditions could in principle alter the staining pattern of FFPE sections.

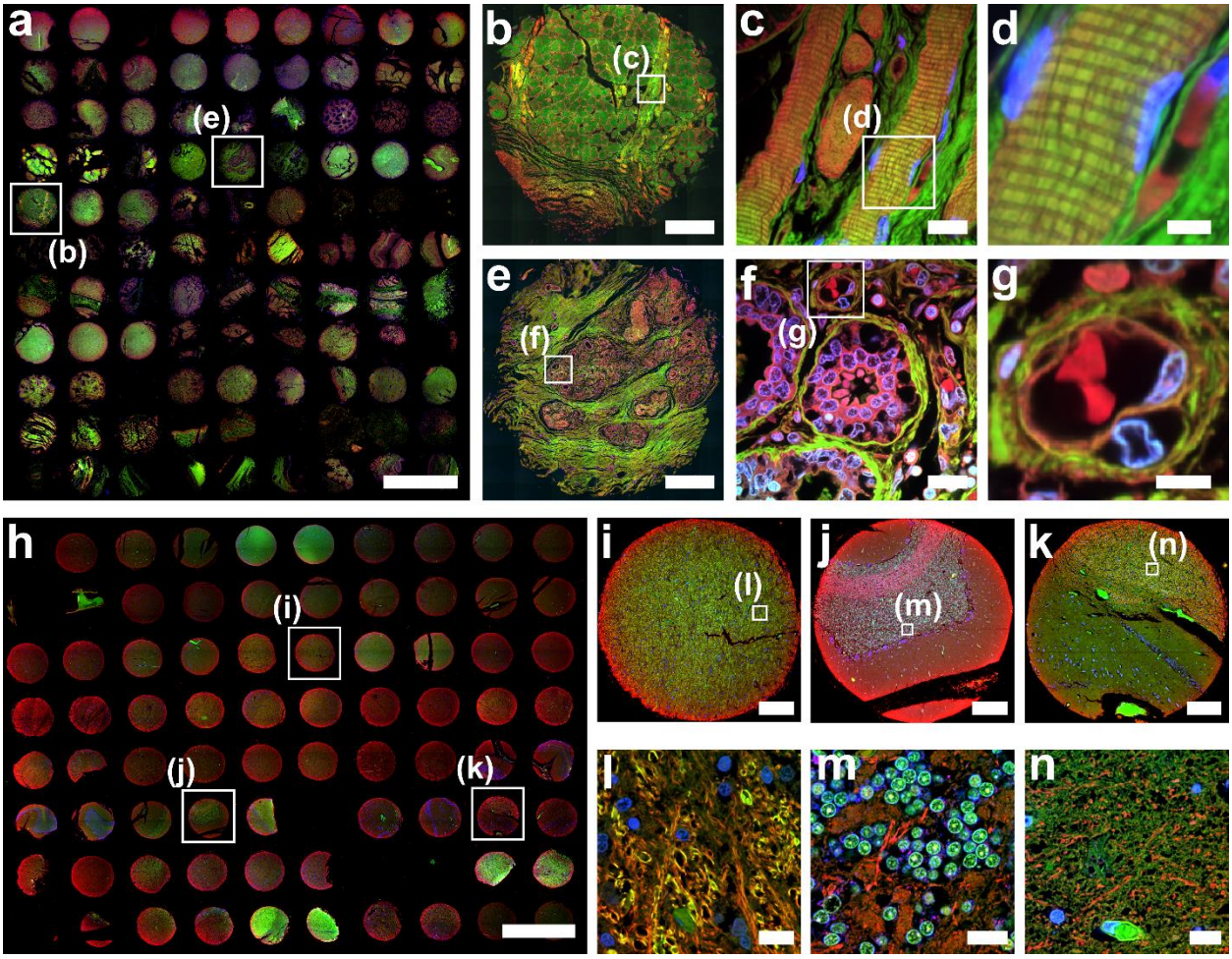

Fig. 3.4 | FLARE staining of 5 µm thick FFPE human tissue microarrays. (a) Overview image of 96 human organ tissue cores that were FLARE-stained for amines (red), carbohydrates (green), and DNA (blue), and then tiled using a 4× objective lens on a widefield microscope. See also **Supplementary Figures 3.4 – 3.5** for a larger version of a) as well as a diagram of which cores represent which tissues. Zoom-in views of a tonsil core from the boxed region in panel a) were recorded by confocal microscopy with (b) tiling using a 20× objective lens and (c-d) single-region

imaging using a 60× objective lens. The cross-striations of skeletal muscle fibers were well-visualized in c-d) and fibrocytes and erythrocytes were distinctively labeled in panel d). Zoom-in views of the breast core from the boxed region in panel a) were recorded by confocal microscopy with (e) tiling using a 20× objective lens and (f-g) single-region imaging using a 60× objective lens. Breast lobules surrounded by carbohydrate-rich connective tissue were well-visualized in e-g), as were details of secretory alveoli and nearby blood vessels. (h) Overview image of 75 human brain tissue cores that were FLARE-stained for amines (red), carbohydrates (green), and DNA (blue), and then tiled using a 4× objective lens on a widefield microscope. See also **Supplementary Figures 3.6 – 3.7** for a larger version of h) as well as a diagram of which cores represent which regions of the brain. Cores for (i) midbrain, (j) cerebellum, and (k) hippocampus, selected from panel h), highlight the variable distribution of amines and carbohydrates within the brain. Zoom-in views (l-n) of the regions indicated in boxes of (i-k) were imaged using a 60× objective lens, revealing highly distinct tissue morphologies such as the cell bodies of cerebellar granule cells that are brightly labeled by the carbohydrate stain in (m). Scale bars are 3 mm (a, h), 300 µm (b,e,i-k), 15 µm (c, f, l-n), 6 µm (d, g).

3.7.3 FLARE with other modalities

If desired, FLARE can be optimized to combine with other modalities such as immunolabeling on fresh mouse kidney tissue (**Fig. 3.5a**, see **Supplementary Table 3.2** for a summary), DNA FISH on FLARE-stained expanded mouse kidney (**Fig. 3.5b**) and cleared unexpanded mouse kidney (**Fig 3.5c**). It is prudent to keep in mind that while the labeling order in combination with such modalities may face challenges, FLARE is flexible and can often be applied at different steps in a protocol (**Fig. 3.2**). As mentioned above, FLARE also reveals major features in combination with enzymatic digestion-based ExM (**Fig. 3.5d**), however, digestion-induced protein loss may alter the labeling to some extent.

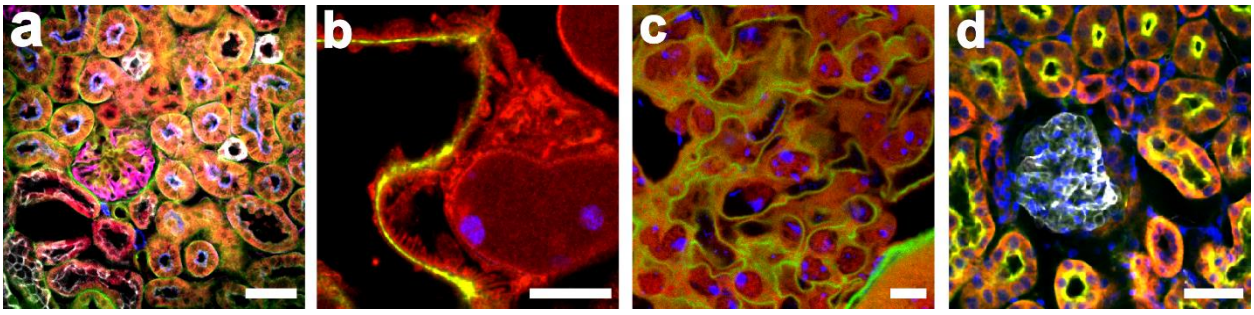

Fig. 3.5 | FLARE-stained 100 µm thick mouse kidney sections prepared using various procedures that include two different ExM variants, tissue clearing, and the combination with either immunostaining or DNA FISH. (a) 5-color confocal microscopy image of unexpanded mouse kidney tissue that was stained for carbohydrates (green), amines (red), and then immunostained for podocalyxin (magenta), aquaporin-1 (blue), and cytokeratin 8+18 (grey). (b) Confocal microscopy image of expanded mouse kidney tissue that was treated by the detergent-based protocol and stained for carbohydrates (green), amines (red), and then DNA FISH (blue) against pericentromeric major satellite (MaSat) DNA. (c) Confocal microscopy image of unexpanded cleared mouse kidney tissue that was stained for carbohydrates (green), amines (red), and then DNA FISH (blue) against MaSat DNA. (d) Confocal microscopy image of enzyme digested expanded mouse kidney tissue that was stained for carbohydrates (green), amines (red), DNA (blue) and then immunostained for podocalyxin (grey). Scale bars are 50 µm (a, d), 3 µm (b, pre-expansion units) and 5 µm (c). Panels a-b were adapted from Mao et al.3 Science Advances. AAAS Publishing Group.

3.7.4 FLARE on thick tissue

We used FLARE to label a relatively thick (~1 mm) kidney tissue specimen and we were able to uniformly stain the specimen by tuning of buffer conditions (**Fig. 3.6** and **Supplementary Movie 3.1**). Bioconjugation with NHS-esters tends to be very quick especially at a reaction-optimized buffer pH of ~8-9. However, this may result in most of the reactions happening on the tissue surface thus creating uneven labeling because hydrolysis is also rapid at this pH and competes with bioconjugation. By using a lower buffer pH of ~6 and a mixed aqueous and organic solvent, we were able to slow down the bioconjugation reaction while also increasing the rate of dye diffusion, thereby allowing the dye to infiltrate the sample fully before bioconjugation could happen, resulting in a more uniform stain. An advantage of the FLARE stain for such a thick specimen is that the labeling can be done in < 24 hr, while the use of immunolabels could take days or weeks.

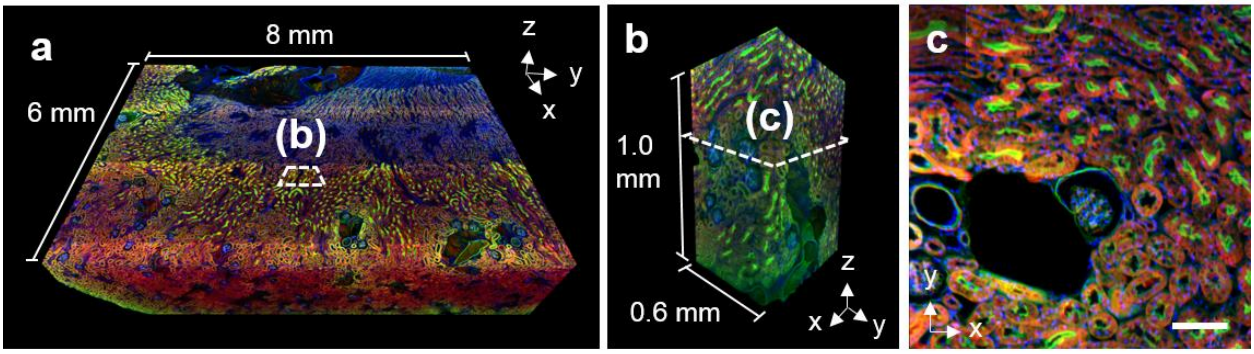

Fig. 3.6 | (a) Volumetric imaging of a large mouse kidney section (8 mm × 6 mm × 1 mm) imaged with open-top light-sheet microscopy. Amines (red), carbohydrates (green), and DNA (blue) reveal unique structures throughout the tissue. (b) The zoom-in view from the boxed region in panel a) shows that there is uniform labeling of structures through the full ~1 mm tissue thickness. (c) A single optical section from the boxed region in panel b) demonstrates highly specific amine, carbohydrate, and DNA staining of kidney tissue microstructure. Scale bar, 100 µm (c).

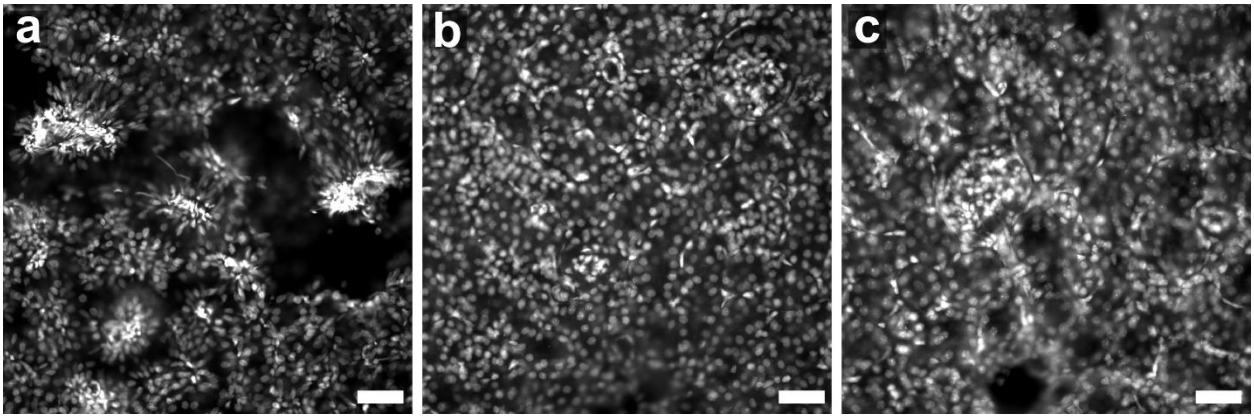

Fig. 3.7 | Epifluorescence images showing nuclei (DNA) stained by Sybr Green in expanded 100 µm thick mouse kidney tissue sections that were homogenized using a MAP-based protocol. (a) Incomplete homogenization leads to abundant tears (empty areas) and under-expanded regions (high-density clusters) exhibiting relatively small or abnormally stretched nuclei. (b) Extending the homogenization period (~5 times longer than in panel a) leads to

uniform sample expansion that lacks obvious distortions in the expanded state. (c) A further extension of the homogenization period (~25 times longer than in panel a) does not cause a larger expansion factor or damage DNA. Scale bars 200 µm (a,b,c) in pre-expansion units.

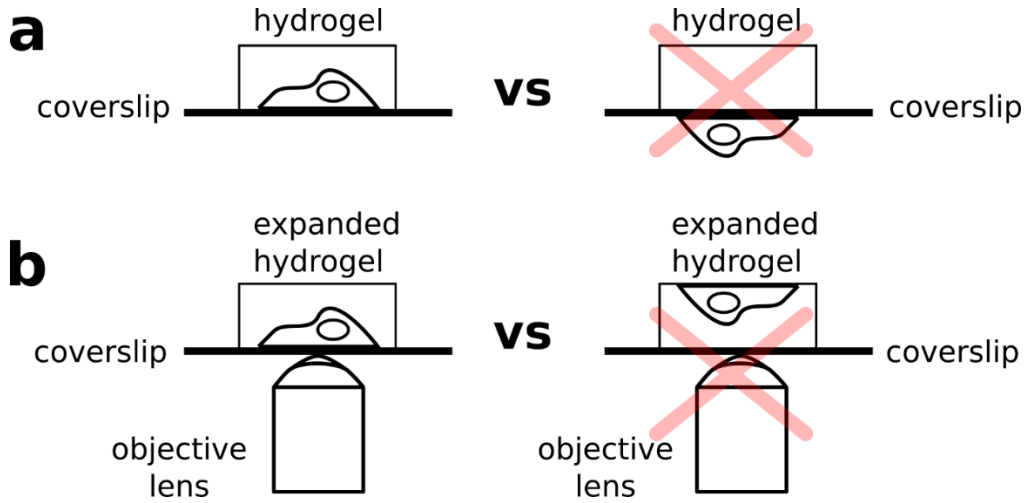

Fig. 3.8 | Figure showing cell sample orientation in hydrogel. (a) Hydrogel polymerization on the side coated with cells (left) vs polymerization on the incorrect side (right). If polymerization is performed on the side without the cells, then the subsequent hydrogel would not have any cells embedded, resulting in no signal under the microscope. (b) Expanded hydrogel mounted on poly-lysine coated coverslip, where cell sample is within the working distance of the objective (left) and the cell sample on the opposite side of coverslip (right). If the hydrogel is mounted as seen on the right, the cell sample might not be within the working distance of the objective lens.

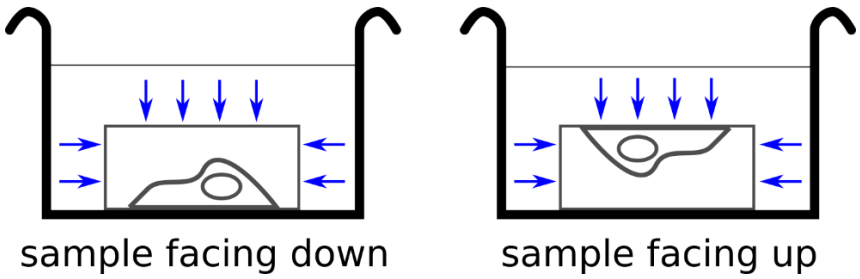

Fig. 3.9 | Figure showing the orientation of hydrogel in a dye incubation container. If the cell sample is facing down (left), the dyes often have lower accessibility to the sample (blue arrows), resulting in dimmer stains. If the cell sample is facing up (right), the dyes have higher accessibility to the sample (blue arrows), resulting in brighter stains.

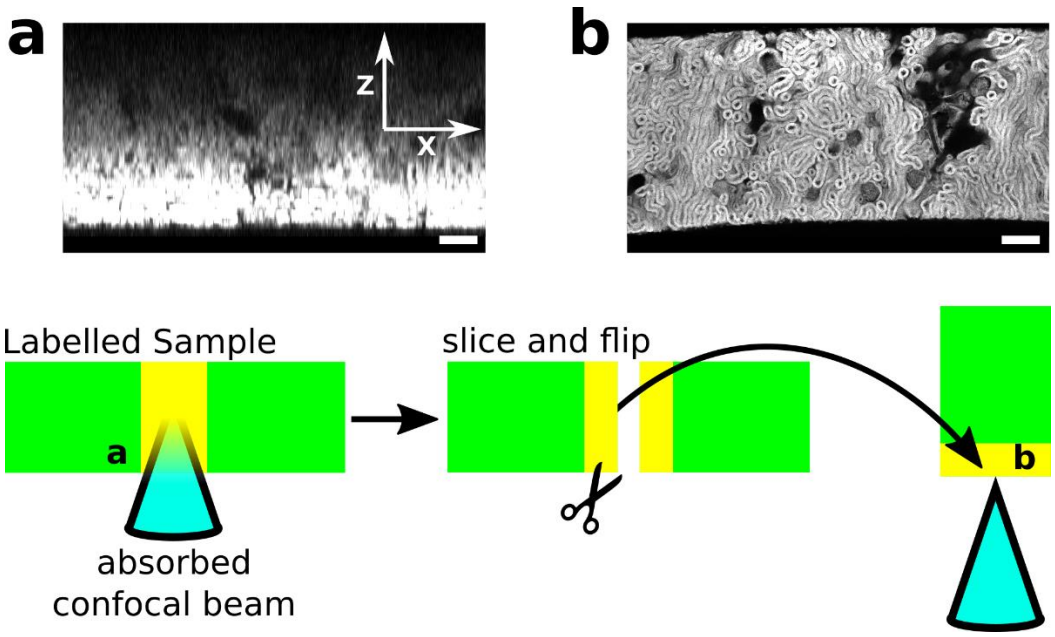

Fig. 3.10 | Confocal images of densely labeled 500 µm human kidney stained with AT647N-NHS ester in MES/THF co-solvent showing prominent inner filter effect, with a figure showing imaging procedure. The inner filter effect results from substantial absorption of the excitation light through the depth of a strongly labeled specimen, giving the impression that labeling is stronger at the surface of a specimen. (a) Cross-sectional view of kidney slice z-stack showing strong signal close to the coverslip with decaying intensity at depth (increasing z distance). The kidney slice was then cut, flipped on edge, and (b) reimaged to show the newly revealed surface. The revealed face showed that the stain was uniform across the sample depth (~500 µm), confirming that the artifact in panel a indeed resulted from the Inner Filter Effect. See **Troubleshooting Table 3.1**. Scale bar: 100 µm (a,b).

3.8 Conclusion

FLARE is a valuable addition to the fluorescent labeling toolkit. It produces bright, well-contrasted, and reliable stains using commercially available reagents. The fluorescence spectra of the FLARE probes can be easily tuned to meet experimental constraints or preferences by choice of commercial fluorophore, with many examples spanning the entire visible spectrum and into the near-infrared region. We have described detailed procedures for FLARE that are compatible with a variety of types of specimens, sample formats, and applications, including examples shown for expanded cells and tissues, cleared thick tissues, and thin uncleared tissue sections. The step-by-step procedures are accompanied by a guide to troubleshooting of potential problems that practitioners may face when implementing FLARE. Although FLARE is good for obtaining relatively general contrast in order to quickly explore the general physiology of specimens, researchers who wish to selectively stain specific structures or molecules would be better off using traditional, specific labels. In those situations, it may nonetheless still be useful to combine FLARE with specific labels in order to gain the best of both worlds.

3.9 Acknowledgments

This work was supported by the University of Washington, NIDDK Diabetic Complications Consortium grants DK076169 and DK115255 (J.C.V.), NIH grants R01 MH115767 (J.C.V.), R01 CA244170 (J.T.C.L.), and K99 CA240681 (A.K.G.), and DoD PCRP grant W81XWH-18-10358 (J.T.C.L.). NW BioTrust, a core service for patient consenting, and NWBioSpecimen, a core service for procurement and annotation of research biospecimens, are supported by National Cancer Institute grant P30 CA015704 (G. Gilliland, principal investigator [PI]), Institute of Translational Health Sciences grant UL1 TR000423 (M. Disis, PI), the University of Washington School of Medicine and Department of Pathology, and Fred Hutchinson Cancer Research Center.

3.10 Supporting Information

Supplementary Protocol 1: General Immunostaining Protocol

General reagents

- RPE cells (H-tert Retinal Pigment Epithelium, ATCC CRL-4000)
- Bovine Serum Albumin (BSA), IgG-free (Jackson ImmunoResearch, #001-000-161)
- Primary antibodies, depending on the desired protein targets
- Fluorophore-conjugated secondary antibodies

Chemical reagents

- 10× PBS, pH 7.4 (e.g., Fisher Bioreagents # L-5400)
- Sodium azide (NaN_3, Fisher Scientific #S227I)
- Deionized water (DI water)
- 32% paraformaldehyde (PFA, Electron Microscopy Sciences, #RT15714) **!Caution**
- 50% glutaraldehyde (GA, Electron Microscopy Sciences, #16300) **!Caution**
- Triton X-100 (Sigma-Aldrich, #X100)
- Poly-Lysine (Sigma-Aldrich, #P8920)
- Sodium chloride (NaCl, Fisher Scientific #271)
- Sodium borohydride ($NaBH_4$, Fisher Scientific, #AC189300050)

Caution: Researchers should consult the safety data sheets (SDSs) for these chemicals prior to use. PFA and GA are toxic and volatile. Procedures using PFA, GA should be performed in a fume hood and researchers are advised to be cautious.

Other materials

- 12 mm round coverslip (Electron Microscopy Sciences, #72230-01)
- Forceps (Electron Microscopy Sciences, #78318-3)
- Parafilm M Bemis (VWR, #52858)
- 24 well-plate (Pipette, #229106)

Stock solutions

- 1× PBS (pH 7.4)
- 1× PBS azide (pH 7.4)
    - Add 19.5 mg of Sodium Azide to the 100 mL 1× PBS.
- 20% Triton X-100 solution (v/v)

- Add 2 mL of Triton X-100 to 8 mL of H_2O.
- Store at 4 °C until use.

- Block/Perm solution: 1× PBS containing 3% BSA (wt/v) and 0.5% Triton X-100.
  - Add 3 g of BSA and 2.5 mL of 20% Triton X-100 solution to 100 mL of 1× PBS.
  - Store at 4 °C until use. Add 19.5 mg of Sodium Azide to the 100 mL Block/Perm solution to extend shelf-life in 4 °C.
- Post-fixation solution: 1× PBS containing 0.25% GA
  - Add 5 µL of 50% GA solution into 995 µL of 1× PBS.
  - Prepare fresh each time.

Procedure

The following procedure is written as a general procedure for the immunostaining of fixed RPE cells on a coverslip in a 24-well plate. This serves as a starting guide and may require further optimization depending on the specific antibodies or specimens being used.

Blocking and Permeabilization •Timing ~30 min

1. Add Block/Perm solution to each well and incubate at room temperature (RT, ~22 °C) for 30 minutes **[0.3mL per well].**

Primary Antibody Incubation •Timing ~90 min

2. Prepare a fresh diluted stock of desired primary antibodies **[~2-5 µg/mL]** in Block/Perm solution **[0.3 mL per well].** Keep the solution on ice until use.
3. Remove the solution in **Step 1** and add the solution made in **Step 2** to the fixed cells in a 24-well plate **[0.3 mL per well]**. Incubate for ~90 min at RT. ▲**Critical** For immunostaining of fixed tissues, the incubation time is typically several days or longer at 4 °C.
4. Remove primary antibody solution and wash in Block/Perm solution three times. **[0.3mL per well]**.

Secondary Antibody Incubation •Timing ~45 min

5. Prepare a fresh diluted stock of desired fluorophore (or biotin)-conjugated secondary antibodies **[~2-5 µg/mL]** in block/perm solution **[0.3 mL per well]**.
6. Remove the Block/Perm solution in **step 4** and add the solution made in **Step 5** to the fixed cells in a 24-well plate **[0.3 mL per well]** and incubate for ~90 min. ▲**Critical** For

immunostaining of fixed tissues, the incubation time is typically several days or longer at 4 °C.

7. Remove secondary antibody solution and wash with 1× PBS solution three times. **[0.3mL per well]**. ■**Pause Point** May be able to store immunostained cells in PBS azide for up to a month depending on the binding affinities of the antibodies. To prepare for post-fixation, add 1× PBS solution again and let the solution sit for 5 minutes before post-fixation.

OPTIONAL Post-fixation •**Timing ~10 min**

8. Prepare a fresh 0.25% GA in 1× PBS **[5 µL of 50% GA stock in 995 µL PBS**].
9. Remove the 1× PBS solution in **step 7** and add the solution prepared in **Step 8** to the fixed immunostained cells in a 24-well plate **[0.3 mL per well]**. Incubate for ~10 min at RT.
10. Wash each well three times with 1× PBS solution. **[0.3 mL per well]** ■**Pause Point** Able to store immunostained cells in PBS azide for up to a month.

OPTIONAL Post-expansion Streptavidin-Fluorophore Incubation (for biotin secondary antibodies) •**Timing ~1 hr (expanded cells)**

11. Prepare a fresh diluted stock of desired fluorophore-conjugated streptavidin **[~2-5 µg/mL]** in 1× PBS **[>0.5mL per well]**.
12. Remove the 1× PBS solution that the ~2× expanded gel is suspended in and add the solution prepared in **Step 11** to the side of the gel containing the cells in a 12-well plate **[>0.5 mL per well]** and incubate for ~1 hr.
13. Wash each gel three times with 1× PBS solution **[>0.5 mL per well, 10 minutes each wash]**.

Supplementary Protocol 2: DNA-FISH on Expanded Kidney tissue

General reagents

- 10 µM Major Satellite (MaSat) DNA oligonucleotide probe **(**5'-GGAATATGGC GAGAAAACTG AAAATCACGG AATGATACGG CGACCACCGA ACTGCTACAG-3'**,** IDT).
- 10 µM Fluorescent oligonucleotide reporter probe (5'-/5ATTO647NN/CTGTAGCAGT TCGGTGGTCG CCGTATCATT-3', IDT).

Chemical reagents

- 10× PBS, pH 7.4 (e.g., Fisher Bioreagents # L-5400)
- Sodium azide (NaN_3, Fisher Scientific #S227I)
- Deionized water (DI water)
- Triton X-100 (Sigma-Aldrich, #X100)
- Formamide (Fisher Chemical, F84-1) **!Caution**
- 20× SSC (Sigma-Aldrich, S6639)
- 50% OmniPur Dextran Sulfate (EMD Millipore, 3730)
- Tween 20 (Sigma-Aldrich, P9416)

Caution: Researchers should consult the safety data sheet (SDS) for these chemicals prior to use. Formamide is toxic. Procedures using formamide should be performed in a fume hood and researchers are advised to be cautious.

Other materials

- 1.5 mL microcentrifuge tubes (e.g., Fisher Scientific**,** 05-408-129)
- Razor blade (American Line, #66-0089)

Stock solutions

- 1× PBS (pH 7.4)
- 300 mM sodium azide:
    - Add 1.95 g of sodium azide to 100 mL of H_2O.
- 20% Triton X-100 solution (v/v)
    - Add 2 mL of Triton X-100 to 8 mL of H_2O.
    - Store at 4 °C until use.
- 20% Tween-20 solution (v/v)
    - Add 2 mL of Tween-20 to 8 mL of H_2O.
    - Store at 4 °C until use.
- 20× SSC (pH 7.0)
- 2× SSC (pH 7.0)
- 2× SSCT: 2× SSC containing 0.1% Tween 20 (v/v).
    - Add 5 µL of 20% Tween 20 solution into 995 µL of 2×SSC.
- 20% Triton X-100 solution (v/v)

    - Add 2 mL of Triton X-100 to 8 mL of H_2O.
    - Store at 4 °C until use.
- DNA-FISH perm solution: 1× PBS containing 0.5% (v/v) Triton X-100.
    - Add 25 µL of 20% Triton X-100 solution to 975 µL of 1× PBS.
    - Store at 4 °C until use.
- Hybridization buffer solution: 2× SSC with 50% (v/v) Formamide and 0.1% (v/v) Tween-20.
    - Add 10 µL of 20% Tween-20 solution, 1000 µL of Formamide, 200 µL of 20× SSC to 790 µL of H_2O.
    - Prepare fresh each time.
- Hybridization mixture solution: 2× SSC with 50% Formamide, 10% Dextran Sulfate, 0.1% (v/v) Tween-20, 3mM sodium azide, 100 nM MaSat probe, 100 nM fluorescent reporter probe.
    - Add 1 µL of 20% Tween-20 solution, 1 µL of 300 mM sodium azide, 100 µL of Formamide, 20 µL of 20× SSC, 40 µL of 50% dextran sulfate, 2 µL of 10 µM of MaSat probe, 2 µL of 10 µM fluorescent reporter probe, 34 µL H_2O.
    - Prepare fresh each time.

Procedure

The following procedure is written as a general procedure for DNA Fluorescence *in situ* hybridization (FISH) labeling of Major Satellite genomic DNA in MAP-expanded mouse Kidney tissue nuclei. This serves as a starting guide and could be further optimized to target other genomic regions.

Permeabilization and equilibration •Timing ~3 hours

1. Incubate MAP-expanded mouse Kidney sample in 1×PBS **[50 mL per sample]** for 10 min.
2. Remove excess buffer and, using a razor blade, slice a small section of MAP-expanded mouse kidney sample and weigh the sliced sample **[~ 40 mg per gel slice].** ▲**Critical** When removing the excess 1× PBS, avoid aspirating close to the gel, then carefully slice the gelled sample on a clean surface.
3. Prepare a fresh stock of hybridization mixture so that the approximate volume of the mixture is twice that of the sliced sample **[> 0.1 mL per gel slice]** and place the mixture into a 1.5 mL tube.
4. Place weighed sliced sample into a 1.5 mL tube and incubate in DNA Perm solution **[1 mL per tube]** for 120 min. ▲**Critical** Sliced samples must be gently slid into the tube without breaking the gel apart.

5. Carefully remove DNA Perm solution and incubate sample in 1× PBS **[1 mL per tube]** for 10 min. ▲**Critical** To avoid puncturing or ripping the gel, aspirate liquid with a micropipette by slowly sliding pipette tip down the inner wall of the tube until reaching the bottom, then slowly aspirate liquid.
6. Carefully remove 1× PBS and incubate sample in 2× SSCT **[1 mL per tube]** for 10 min. ▲**Critical** To avoid puncturing or ripping the gel, aspirate liquid with a micropipette by slowly sliding pipette tip down the inner wall of the tube until reaching the bottom, then slowly aspirate liquid. ■**Pause Point** Able to store gel sample in 2× SSCT for up to a week.
7. Carefully remove 2× SSCT and incubated in hybridization buffer **[1 mL per tube]** for 10 min at room temperature. ▲**Critical** To avoid puncturing or ripping the gel, aspirate liquid with a micropipette by slowly sliding pipette tip down the inner wall of the tube until reaching the bottom, then slowly aspirate liquid.

DNA denaturation and *in situ* hybridization •**Timing** **~20 hr**

8. Carefully remove hybridization buffer and add pre-heated hybridization buffer **[1 mL per tube],** and incubate for 25 min at 60 °C. ▲**Critical** To avoid puncturing or ripping the gel, aspirate liquid with a micropipette by slowly sliding pipette tip down the inner wall of the tube until reaching the bottom, then slowly aspirate liquid.
9. Incubate hybridization mixture made in **Step 1** for 5 min at 92.5 °C as the sliced sample remains in hybridization buffer for another 5 min at 60 °C.
10. Carefully remove hybridization buffer from the sliced sample, then slide sample with a disposable plastic tip into the preheated tube with hybridization mixture. ▲**Critical** To avoid puncturing or ripping the gel, aspirate liquid with a micropipette by slowly sliding pipette tip down the inner wall of the tube until reaching the bottom, then slowly aspirate liquid.
11. Denature sample in hybridization mixture for 10 min at 92.5 °C.
12. Incubate tube overnight (~18 hr) at 37 °C.

Wash and expansion •**Timing** **~1 hr**

13. Carefully remove hybridization mixture and rinse gels with a pre-heated 2× SSCT **[0.5 mL per tube].**
14. Carefully remove 2× SSCT and incubate in pre-heated 2× SSCT **[0.5 mL per tube]** for 15 min at 60 °C. ▲**Critical** To avoid puncturing or ripping of the gel, aspirate liquid with a micropipette by

slowly sliding pipette tip down the inner wall of the tube until reaching the bottom, then slowly aspirate liquid.

15. Carefully remove 2× SSCT from the tube and incubate in pre-heated 2× SSCT **[0.5 mL per tube]** for 15 min at 37 °C. ▲**Critical** To avoid puncturing or ripping the gel, aspirate liquid with a micropipette by slowly sliding pipette tip down the inner wall of the tube until reaching the bottom, then slowly aspirate liquid.
16. Carefully remove 2× SSCT from the tube and incubate in 2× SSCT **[0.5 mL per tube]** for 15 min at room temperature. ▲**Critical** To avoid puncturing or ripping of the gel, aspirate liquid with a micropipette by slowly sliding pipette tip down the inner wall of the tube until reaching the bottom, then slowly aspirate liquid.
17. Carefully remove 2× SSCT from the tube and incubate in 0.2× SSCT **[0.5 mL per tube]** for 15 min at 4 °C. ▲**Critical** To avoid puncturing or ripping the gel, aspirate liquid with a micropipette by slowly sliding pipette tip down the inner wall of the tube until reaching the bottom, then slowly aspirate liquid. ■**Pause Point** Able to store gel sample in 0.2× SSCT for up to a week.
18. Carefully remove 0.2× SSCT from the tube and incubate in DI water for 15 min at 4 °C. ▲**Critical** To avoid puncturing or ripping the gel, aspirate liquid with a micropipette by slowly sliding pipette tip down the inner wall of the tube until reaching the bottom, then slowly aspirate liquid.
19. Proceed to **Procedure 1 Step 13** of the main manuscript for sample mounting.

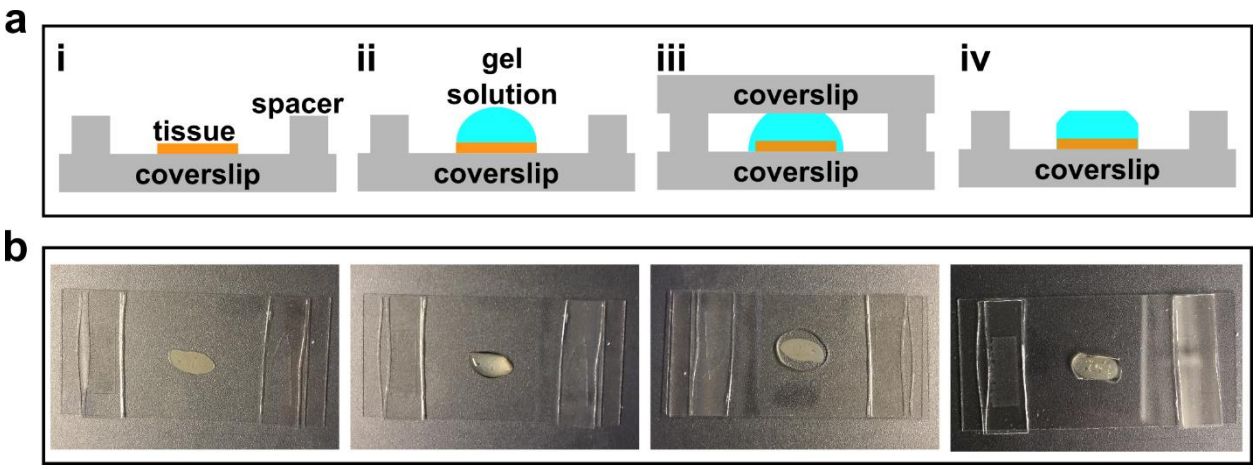

Supplementary Figure 3.1 | Gelation chamber setup. (a) Schematic of tissue sample gelation: i. spread a tissue sample on a coverslip (24mm × 50mm) and construct a spacer on each side using a stack of two #1.5 cover glass (~160 µm each); ii. Add a few drops of the freshly prepared gel solution to cover the entire sample area; iii. Place another coverslip (24 mm × 50 mm) on the top; iv. Once the gel has formed, peel off the top glass slide and trim off the excess gel. (b) Step-by-step photos correspond to i-iv in panel (a).

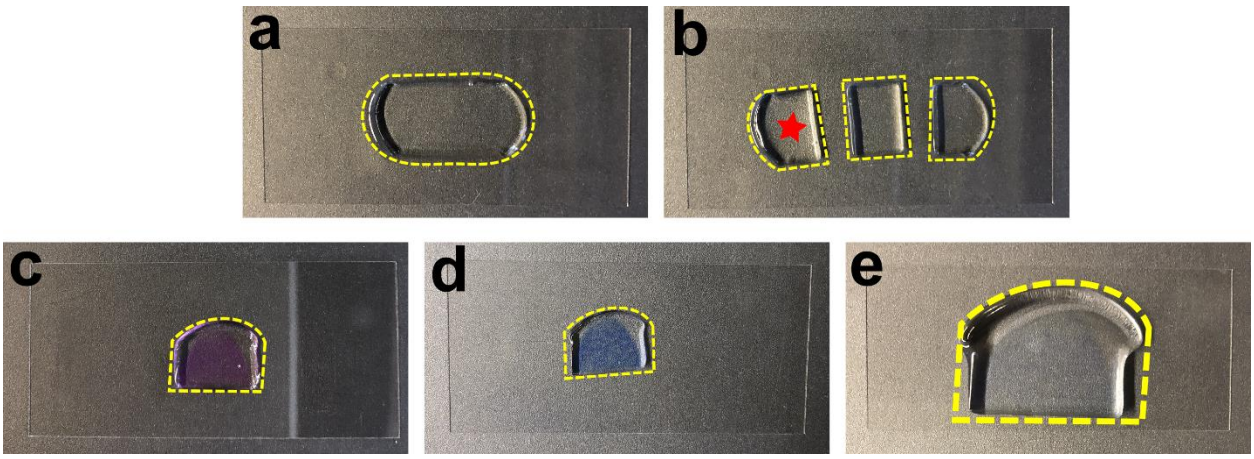

Supplementary Figure 3.2 | A step-by-step illustration of the FLARE procedure for the expanded sample. (a) The gel embedded tissue section shown in **Supplementary Figure 3.1b** partially expanded after the denaturation and became transparent. (b) The tissue section was cut into three pieces. One piece (star) was used for FLARE staining and the other two were saved for other purposes. (c) The tissue section was stained pink after using ATTO 565 hydrazide for the carbohydrate stain. (d) Subsequently, the amine stain performed by using ATTO 647N-NHS ester made the tissue section light violet. (e) The tissue section was slightly colored even after the full expansion, demonstrating the characteristic of intense labeling of FLARE. The gel was laying down on a coverslip (24 mm × 50 mm) while taking step-by-step photos.

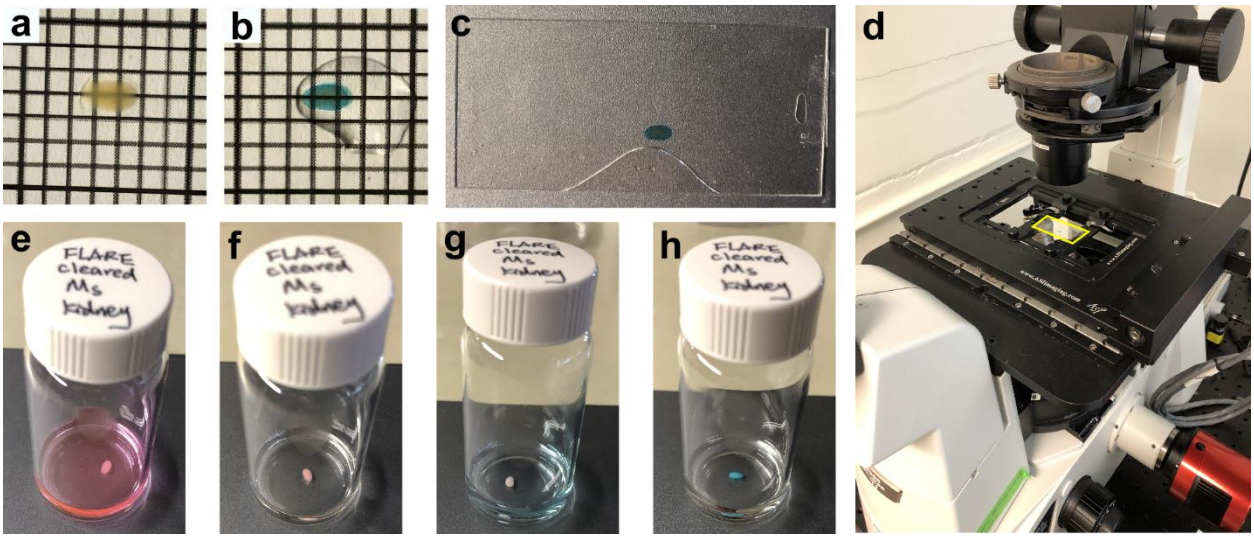

Supplementary Figure 3.3 | A step-by-step illustration of the FLARE procedure for the optically cleared sample. (a) A flat, 200 µm mouse kidney section was placed on a #1.5 coverslip. (b-c) The same section was performed with FLARE, optically cleared, and incubated in ethyl cinnamate and sandwiched between two #1.5 coverslips. (d) The mounted sample (yellow box) was directly placed on a widefield microscope. (e-h) A scintillation vial was used to perform the FLARE procedure, including (e) carbohydrate stain, (f) wash, (g) amine stain, (h) DNA stain. The grid lines are separated by ~2 mm. The amine labeling was not uniform on purpose to demonstrate the result of without using MES/THF co-solvent mixture.

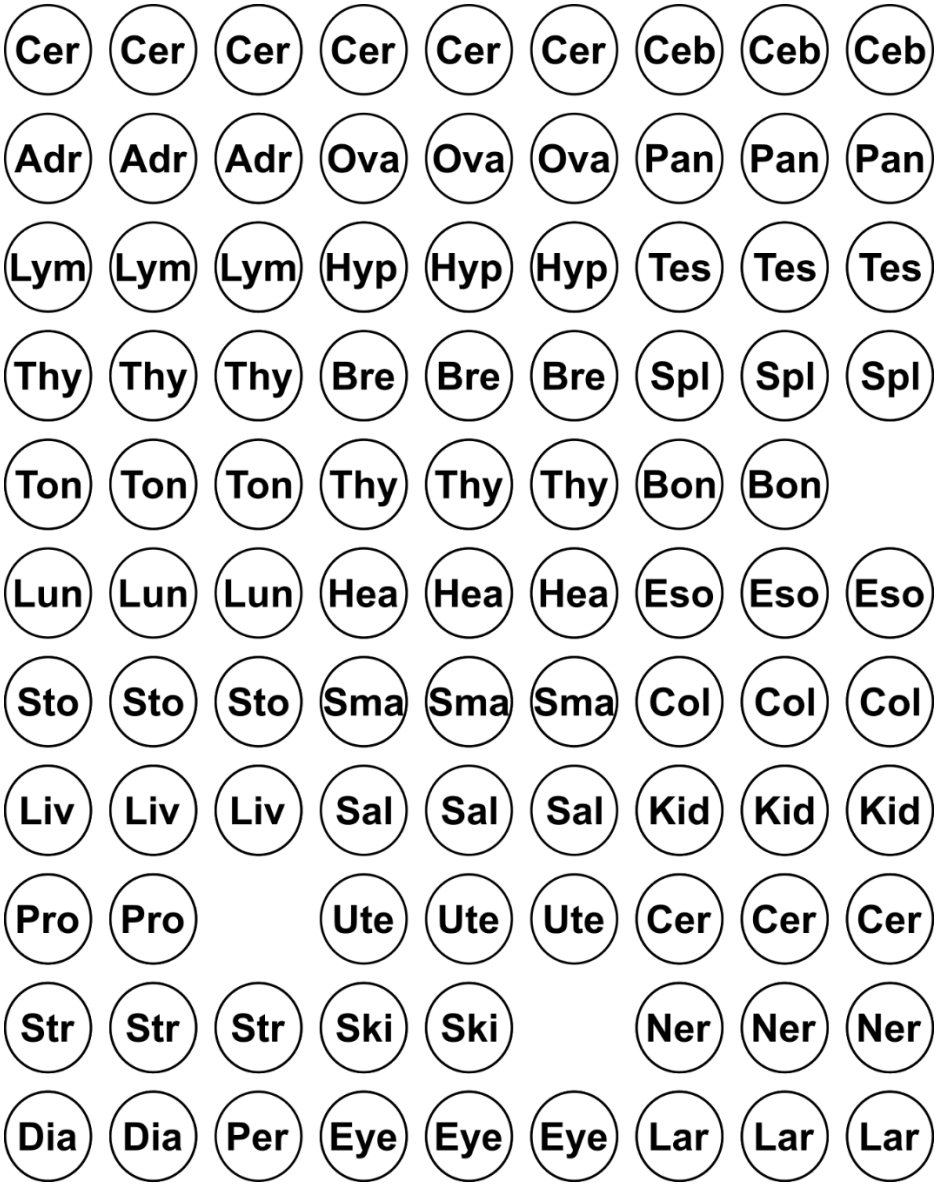

Supplementary Figure 3.4 | Map and identity of each core of the FFPE tissue microarray (TMA) used for Figure 3.4a-g. The slide contains 96 human tissue cores of 30 different organs (US Biomax FDA999rt). Each core is 1.5 mm in diameter and 5 µm in thickness. Bon: bone marrow; Bre: Breast; Ceb: Cerebellum tissue; Cer: Cervix; Col: Colon; Dia: Diaphragm; Eso: esophagus; Eye: Eye; Hea: Heart; Hyp: Hypophsis; Kid: Kidney; Lar: Larynx; Liv: Liver; Lun: Lung; Lym: Lymph node; Ner: Nerve; Ova: ovary; Pan: Pancreas; Per: Pericardium; Pro: Prostate; Sal: Salivary Gland; Ski: Skin; Sma: Small intestine; Spl: Spleen; Sto: Stomach; Str: Striated muscle; Tes: Testis; Thy: Thymus gland; Ton: Tonsil; Ute: Uterus. Note, some cores were missing from the array and their identities are not included in the map.

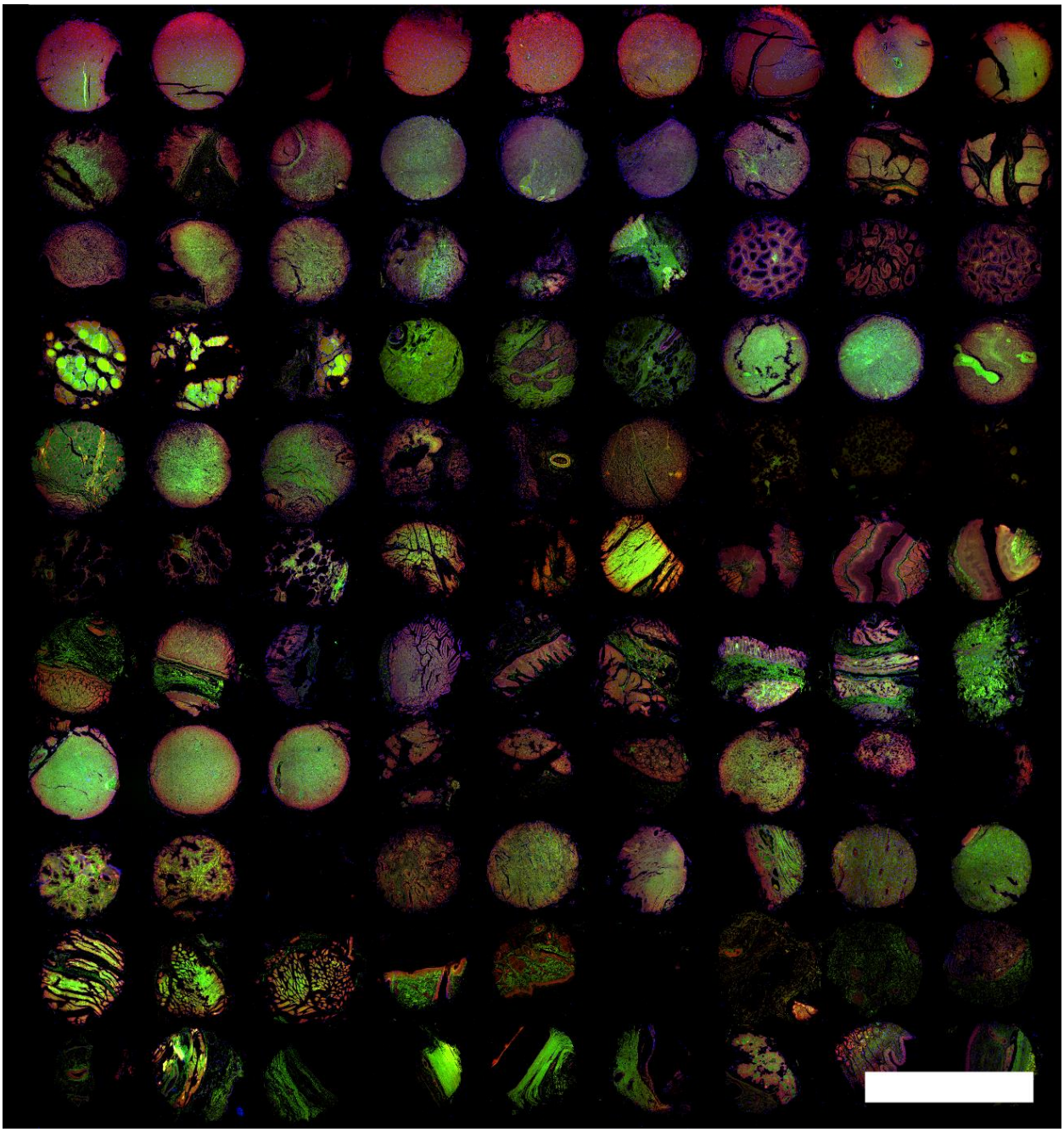

Supplementary Figure 3.5 | A larger view of the FFPE human tissue microarray from Fig. 3.4a. Scale bar is 3 mm.

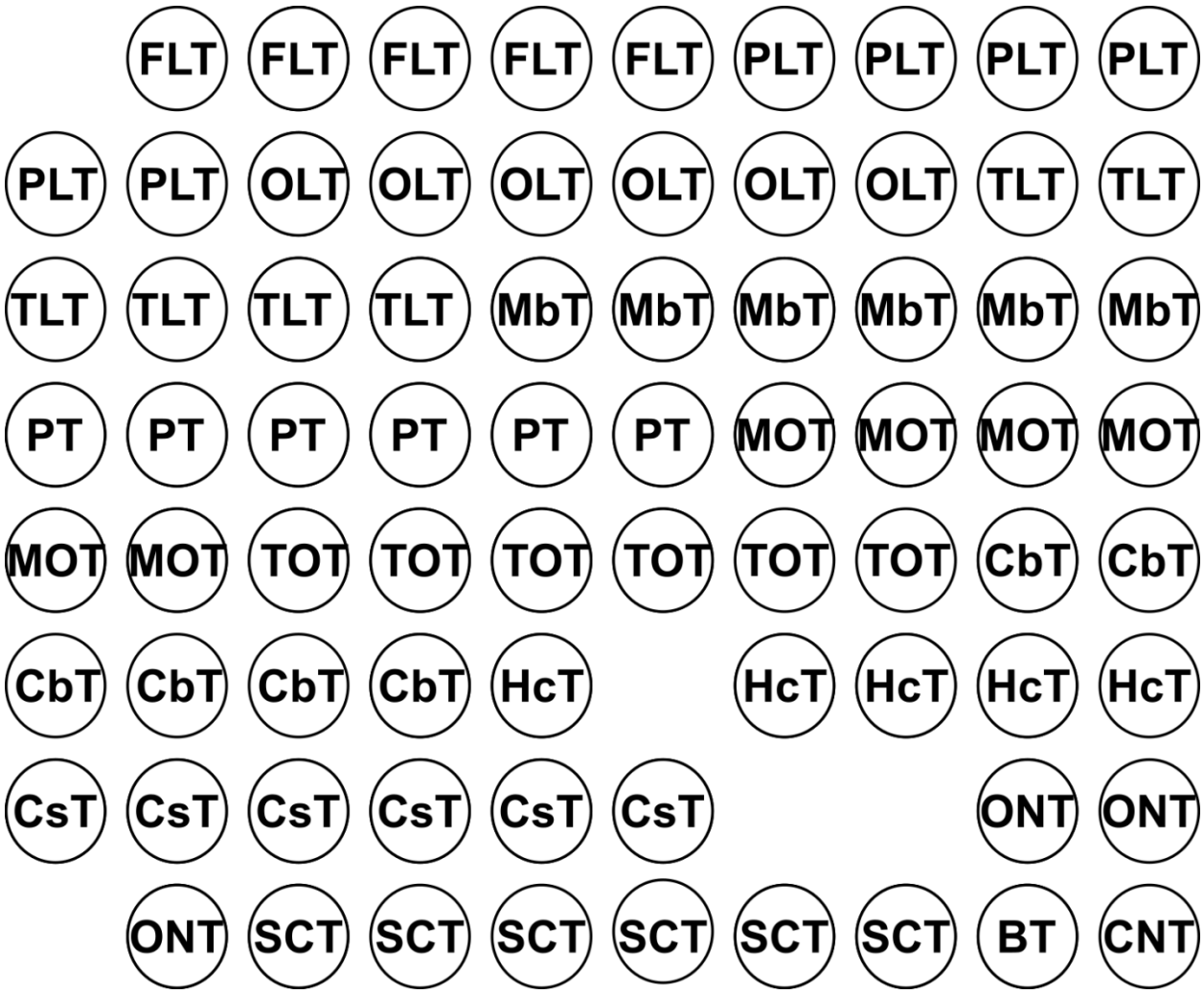

Supplementary Figure 3.6 | Map and identity of each core of the FFPE tissue microarray (TMA) used for Figure 3.4h-n. The slide contains 75 human brain cores of 15 different brain regions (US Biomax BNC17011at). Each core is 1.5 mm in diameter and 5 µm in thickness. FLT: Frontal lobe tissue; PLT: Parietal lobe tissue; OLT: Occipital lobe tissue; TLT: Temporal lobe tissue; MbT: Midbrain tissue; PT: Pons tissue; MOT: Medulla oblongata tissue; TOT: Thalamus opticus tissue; CbT: Cerebellum tissue; HcT: Hippocampus tissue; CsT: Callositas tissue; ONT: Optic nerve tissue; SCT: Spinal cord tissue; BT: Brain tissue; CNT: Caudate nucleus tissue. Note, some cores were missing from the array and their identities are not included in the map.

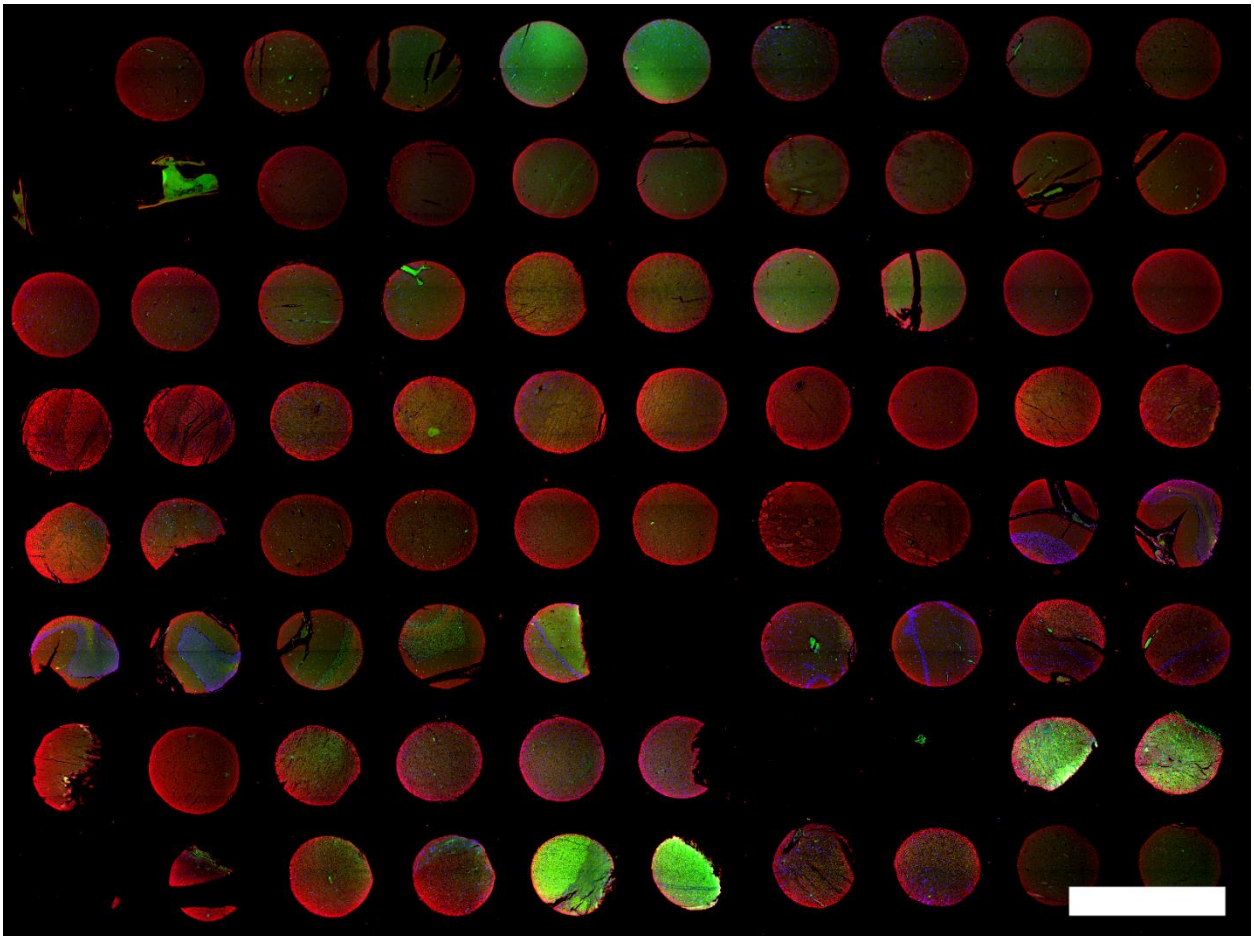

Supplementary Figure 3.7 | A larger view of the FFPE human brain tissue microarray from Fig. 3.4h. Scale bar is 3 mm.

Supplementary Table 3.1: summary of sample preparation and imaging conditions

Figure	Sample	Fixation	Tissue Format	Carbohydrate Stain	Amine Stain	Other Stain(s) and Stain Order	Expansion or Clearing	Imaging
Fig. 1c	Mouse kidney	PFA 1hr	100µm vibratome sections	1hr, 20mM $NaIO_4$ in 100mM NaOAc with 1M NaCl, pH5; then 3hr, 6.65µM hydrazide-AT565 in 100mM NaOAc, pH5; then 30 min, 50mM $NaBH_3CN$ in 100mM NaOAc, pH5.	6hr, 5.9µM NHS-AT647N in 100mM MES, pH6.	DNA: 30min, 1.87µM Hoechst 33258 in PBS, pH7.4. Order: gel, covalent stains, DNA, expand.	Expansion	Confocal, 63× 1.2NA water lens. Image thickness: 92.3nm. Filter: 2.
Fig. 1c	Mouse intestine	PFA 1hr	100µm vibratome sections	30min, 100mM $NaIO_4$ in 100mM NaOAc, pH 5; then 2hr, 3.33µM hydrazide-AT565 in THF:NaOAc (1:1); then 30min, 100mM $NaBH_3CN$ in THF:NaOAc (1:1).	2hr, 5.9µM NHS-AT647N in THF:MES (1:1).	DNA: 30min, 1.87µM Hoechst 33258 in THF:PBS (1:1). Order: covalent stains, DNA, clear.	Clearing	Confocal, 63× 1.4NA oil lens. Image thickness: 2.26µm Filter: none
Fig. 3a-d	RPE cell	PFA/GA 10min	---	Same as Fig 1c mouse kidney.	1hr, 3.0µM NHS-AT647N in PBS.	DNA: 30min, 1.96µM SYBR Green in DI water Order: gel, covalent stains, expand, DNA.	Expansion	Confocal, 63× 1.2NA water lens. Image thickness: a-d) 738nm. Filter: none.
Fig. 3e-h	RPE cell	Glyoxal solution mix 10min rt	---	Same as Fig. 3a-d.	Same as Fig. 3a-d.	Same as Fig. 3a-d.	Expansion	Confocal, 63× 1.2NA water lens. Image thickness: e-h) 3680nm. Filter: none.
Fig. 4	TMAs	Formalin overnight	5µm microtome sections	30min, 100mM $NaIO_4$ in 100mM NaOAc, pH 5; then 2hr, 3.33µM hydrazide-Al568 in NaOAc; then 30min, 100mM $NaBH_3CN$ in NaOAc.	30min, 3.0µM NHS-AT647N in PBS.	DNA: 30min, 1.87µM SYBR Green in PBS. Order: covalent stains, DNA	Neither	Wide-field epifluorescence, a, h) tiling with 4× 0.2NA air lens. i-k) 4× 0.2NA air lens. Homebuilt spinning-disk confocal, b,e) tiling with 20× 0.45NA air lens, c-d,f-g, l-n) 60× 1.2NA water lens. Image thickness: single plane. Filter: none.
Fig. 5a	Mouse kidney	PFA 1hr	100µm vibratome sections	Same as Fig. 4	1hr, 3.0µM NHS-AT647N in PBS	Immuno: 2µg/mL G×PODXL, Rb×AQP-1, Gp×CK8+18 18h; 2µg/mL D×G-AFdye405, D×Rb-AF488, D×Gp-AF750 18h; at ~4°C. Order: covalent stains, immuno	Neither	Homebuilt spinning-disk confocal, 20× 0.45NA air lens; imaging cocktail was tris 200mM pH8.0, 10% glucose, 1mM Trolox, 0.4mg/mL glucose oxidase, 0.2% catalase. Image thickness: single plane. Filter: none.
Fig. 5b	Mouse kidney	PFA 1hr	100µm vibratome sections	Same as Fig. 1c mouse kidney.	Same as Fig. 1c mouse kidney.	DNA FISH: denature 10min at 92.5°C; hybridize 18hr at 37°C with 100nM MaSat oligo + 100nM AT647N oligo. Order: gel, covalent stains, DNA FISH, then expand	Expansion	Confocal, 63× 1.2NA water lens. Image thickness: 92nm. Filter: 2.
Fig. 5c	Mouse kidney	PFA 1hr	100µm vibratome sections	Same as Fig. 1c mouse intestine.	Same as Fig. 1c mouse intestine.	DNA FISH: same as Fig 5b. Order: covalent stains, DNA FISH.	Clearing	Confocal, 63× 1.4NA oil lens. Image thickness: 92.3 nm Filter: none
Fig 5d	Mouse kidney	PFA 1hr	100µm vibratome sections	Same as Fig. 5a.	Same as Fig. 5a	Immuno: 2µg/mL G×PODXL, 18h; 2µg/mL D×G-AF488, 18h; at ~4°C. Order: covalent stains, immuno, DNA	Expansion	Confocal, 20× 0.7NA air lens. Image thickness: 776 nm. Filter: none.
Fig. 6	Mouse kidney block	PFA 1hr	1mm vibratome section	5hr, 100mM $NaIO_4$ in 100mM NaOAc, pH5; then 6hr, 3.33µM hydrazide-AT565 in THF:NaOAc (1:1); then 1hr, 100mM $NaBH_3CN$ in THF:NaOAc (1:1).	8hr, 5.9µM NHS-AT647N in THF:MES (1:1).	DNA: 15hr, 20µM SYBR green in H_2O: PBS (1:1). Order: covalent stains, DNA, clear.	Clearing	Light sheet microscope, 20× 0.43NA multi-immersion lens from ASI and Special Optics. Image thickness: f-h) 446nm. Filter: none.
Fig. 7	Mouse kidney	PFA 1hr	100µm vibratome sections	---	---	DNA: 30min, 1.87µM Hoechst 33258 in DI water, pH7.4.	Expansion	Wide-field epifluorescence, 4× 0.2NA air lens. Image thickness: single plane. Filter: none.
Fig. 10	Human kidney	PFA 1hr	500µm vibratome sections	---	15hr, 1.2µM NHS-AT647N in THF:MES (1:1).	---	Neither	Confocal, 10× 0.4NA air lens. Image thickness: single plane Filter: none

Acronyms: Ab=antibody; AF=Alexa Fluor; AT=ATTO-TEC; DI=deionized; NA=numerical aperture; rt = room temperature (~22 °C); RPE=retinal pigment epithelium cell line; TMA=tissue microarray.

Additional notes: filter in the Imaging column indicates the number of pixels used for the application of 3D median filter if used on confocal data sets. Image thickness refers to the thickness of the data displayed in terms of the pixel sizes of the data set, where distances are in pre-expansion units for expanded tissues.

Supplementary Table 3.2. Summary of Biological Structures Validated with Independent Stains						
Sample	**Expansion or Clearing**	**Structures**	**Used markers for validation (vendor)**	**Carbohydrate Stain (green)**	**Amine Stain (red)**	**remarks**
RPE cell	**MAP expanded**	Mitochondria	Anti-TOMM20 (Santa Cruz Biotechnology, sc-11415)	✓	✓	Red > Green
		Lysosomes	Anti-LAMP1 (Abcam, 24170)	✓	✓	Green > Red
		Golgi Apparatus	Anti-GM130 (BD Biosciences, 610822)	✓	✓	Green ≈ Red
		Nuclear pores	SYBR Green II (Invitrogen S7563)	✓	✓	Green ≈ Red
Mouse kidney	**Clearing**	Glomerulus	Anti-podocalyxin (R&D Systems INC., AF1556)	✓	✓	Green ≈ Red
		Proximal tubule	Anti-AQP-1 (Abcam, ab15080)	✓	✓	Green > Red
		Collecting duct	Anti-CK8+18 (Abcam, ab194130)	✓	✓	Red > Green

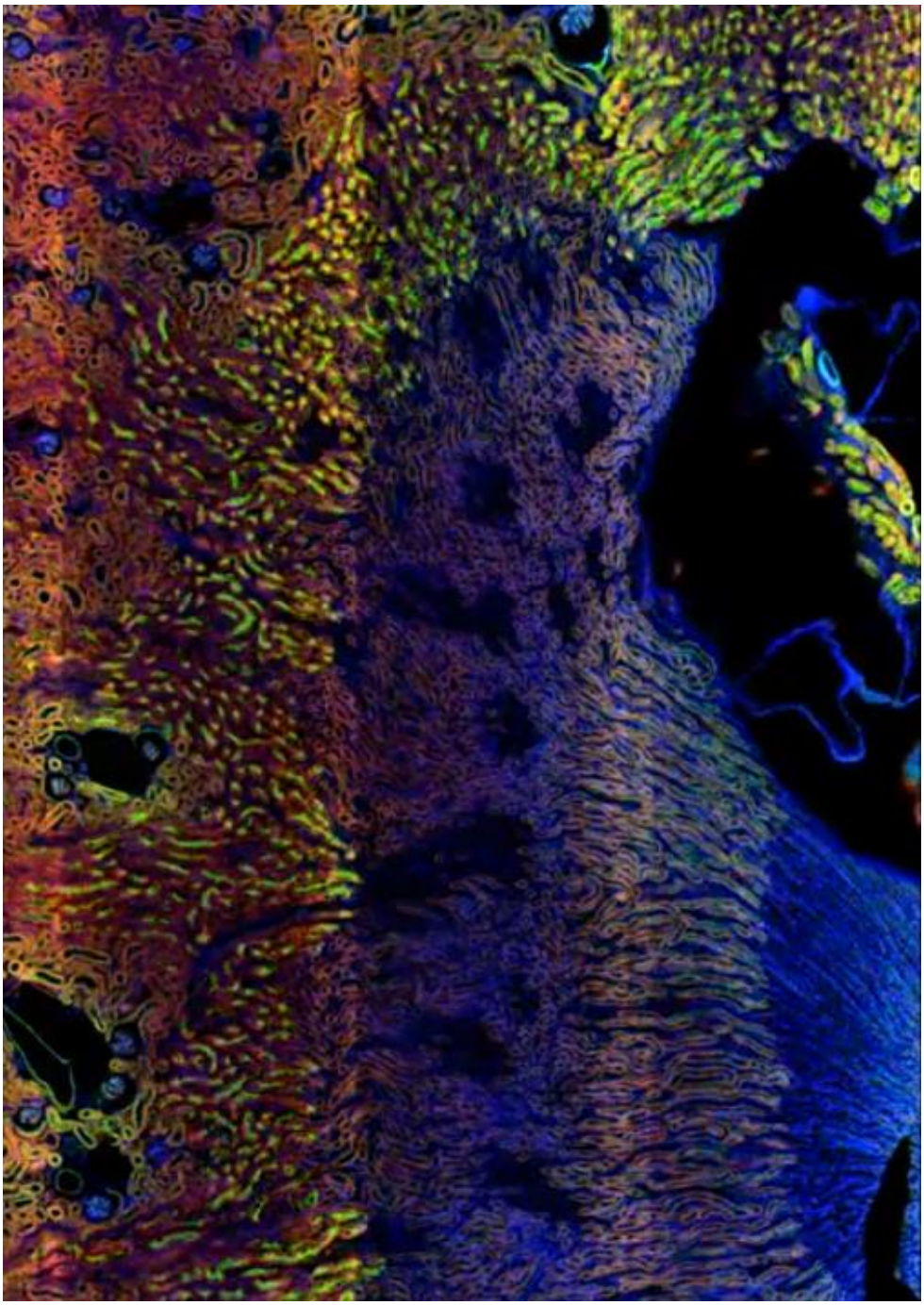

Supplementary Movie 3.1 | Open-top light-sheet imaging of a ~1-mm-thick mouse kidney section (slice) labeled with amines (red), carbohydrates (green), and DNA (blue). An animated 2D z-stack through the tissue volume is shown, followed by a 3D volumetric visualization and zoom-in fly-through. Residual vertical seams in the dataset arise from the microscope scanning, stitching, and fusion, and are not due to non-uniform FLARE staining.

3.11 References

1. Bradbury, A. & Plückthun, A. Reproducibility: Standardize antibodies used in research. Nature 518, 27–29 (2015).
2. Schnell, U., Dijk, F., Sjollema, K. A. & Giepmans, B. N. G. Immunolabeling artifacts and the need for live-cell imaging. Nat. Methods 9, 152–158 (2012).
3. Mao, C. et al. Feature-rich covalent stains for super-resolution and cleared tissue fluorescence microscopy. Sci. Adv. 6, eaba4542 (2020).
4. Titford, M. Progress in the Development of Microscopical Techniques for Diagnostic Pathology. J. Histotechnol. 32, 9–19 (2009).
5. Sigal, Y. M., Zhou, R. & Zhuang, X. Visualizing and discovering cellular structures with super-resolution microscopy. Science 361, 880–887 (2018).
6. Schermelleh, L. et al. Super-resolution microscopy demystified. Nat. Cell Biol. 21, 72–84 (2019).
7. Sahl, S. J., Hell, S. W. & Jakobs, S. Fluorescence nanoscopy in cell biology. Nat. Rev. Mol. Cell Biol. 18, 685–701 (2017).
8. Chen, F., Tillberg, P. W. & Boyden, E. S. Expansion microscopy. Science 347, 543–548 (2015).
9. Chozinski, T. J. et al. Expansion microscopy with conventional antibodies and fluorescent proteins. Nat. Methods 13, 485–488 (2016).
10. Tillberg, P. W. et al. Protein-retention expansion microscopy of cells and tissues labeled using standard fluorescent proteins and antibodies. Nat. Biotechnol. 34, 987–992 (2016).
11. Ku, T. et al. Multiplexed and scalable super-resolution imaging of three-dimensional protein localization in size-adjustable tissues. Nat. Biotechnol. 34, 973–981 (2016).
12. Richardson, D. S. & Lichtman, J. W. Clarifying Tissue Clearing. Cell 162, 246–257 (2015).
13. Tainaka, K., Kuno, A., Kubota, S. I., Murakami, T. & Ueda, H. R. Chemical Principles in Tissue Clearing and Staining Protocols for Whole-Body Cell Profiling. Annu. Rev. Cell Dev. Biol. 32, 713–741 (2016).
14. Beliveau, B. J. et al. Versatile design and synthesis platform for visualizing genomes with Oligopaint FISH probes. Proc. Natl. Acad. Sci. 109, 21301–21306 (2012).
15. Chen, Y. et al. Rapid pathology of lumpectomy margins with open-top light-sheet (OTLS) microscopy. Biomed. Opt. Express 10, 1257 (2019).
16. Xie, W. et al. Microscopy with ultraviolet surface excitation for wide-area pathology of breast surgical margins. J. Biomed. Opt. 24, 12 (2019).
17. Yu, C.-C. (Jay) et al. Expansion microscopy of C. elegans. eLife 9, (2020).
18. M'Saad, O. & Bewersdorf, J. Light microscopy of proteins in their ultrastructural context. Nat. Commun. 11, 3850 (2020).
19. Elfer, K. N. et al. DRAQ5 and Eosin ('D&E') as an Analog to Hematoxylin and Eosin for Rapid Fluorescence Histology of Fresh Tissues. PLOS ONE 11, e0165530 (2016).
20. Serafin, R., Xie, W., Glaser, A. K. & Liu, J. T. C. FalseColor-Python: A rapid intensity-leveling and digital-staining package for fluorescence-based slide-free digital pathology. PLOS ONE 15, e0233198 (2020).
21. Yun, D. H. et al. Ultrafast immunostaining of organ-scale tissues for scalable proteomic phenotyping. http://biorxiv.org/lookup/doi/10.1101/660373 (2019) doi:10.1101/660373.
22. Ku, T. et al. Elasticizing tissues for reversible shape transformation and accelerated molecular labeling. Nat. Methods 17, 609–613 (2020).
23. Susaki, E. A. et al. Versatile whole-organ/body staining and imaging based on electrolyte-gel properties of biological tissues. Nat. Commun. 11, 1982 (2020).
24. Zhao, S. et al. Cellular and Molecular Probing of Intact Human Organs. Cell 180, 796-812.e19 (2020).
25. Theory and practice of histological techniques. (Elsevier Churchill Livingston, 2013).

26. Apgar et al. Fluorescence microscopy of rat embryo sections stained with haematoxylin-eosin and Masson's trichrome method: FLUORESCENCE MICROSCOPY USING HAEMATOXYLIN-EOSIN AND MASSON'S TRICHROME. J. Microsc. 191, 20–27 (1998).
27. Giacomelli, M. G. et al. Virtual Hematoxylin and Eosin Transillumination Microscopy Using Epi-Fluorescence Imaging. PLOS ONE 11, e0159337 (2016).
28. Glaser, A. K. et al. Light-sheet microscopy for slide-free non-destructive pathology of large clinical specimens. Nat. Biomed. Eng. 1, 0084 (2017).
29. Glaser, A. K. et al. Multi-immersion open-top light-sheet microscope for high-throughput imaging of cleared tissues. Nat. Commun. 10, 2781 (2019).
30. Kasten, F. H., Burton, V. & Glover, P. Fluorescent Schiff-Type Reagents for Cytochemical Detection of Polyaldehyde Moieties in Sections and Smears. Nature 184, 1797–1798 (1959).
31. Li, Z. et al. Application of periodic acid-Schiff fluorescence emission for immunohistochemistry of living mouse renal glomeruli by an 'in vivo cryotechnique'. Arch. Histol. Cytol. 69, 147–161 (2006).
32. Shi, X. et al. Label-retention expansion microscopy. http://biorxiv.org/lookup/doi/10.1101/687954 (2019) doi:10.1101/687954.
33. Karagiannis, E. D. et al. Expansion Microscopy of Lipid Membranes. http://biorxiv.org/lookup/doi/10.1101/829903 (2019) doi:10.1101/829903.
34. Wen, G. et al. Evaluation of Direct Grafting Strategies via Trivalent Anchoring for Enabling Lipid Membrane and Cytoskeleton Staining in Expansion Microscopy. ACS Nano 14, 7860–7867 (2020).
35. Götz, R. et al. Nanoscale imaging of bacterial infections by sphingolipid expansion microscopy. http://biorxiv.org/lookup/doi/10.1101/2020.05.06.080663 (2020) doi:10.1101/2020.05.06.080663.
36. Chang, J.-B. et al. Iterative expansion microscopy. Nat. Methods 14, 593–599 (2017).
37. Ross, M. H. Histology: a text and atlas with correlated cell and molecular biology. (Lippincott Williams & Wil, 2006).
38. Bucur, O. et al. Nanoscale imaging of clinical specimens using conventional and rapid-expansion pathology. Nat. Protoc. (2020) doi:10.1038/s41596-020-0300-1.
39. Unnersjö-Jess, D. et al. Confocal super-resolution imaging of the glomeruluar filtration barrier enables by tissue expansion. Kidney Int. (2017) doi:https://doi.org/10.1016/ j.kint.2017.09.019.
40. Hermanson, Greg. Bioconjugate Techniques, 2nd Edition.
41. Mujumdar, R. B., Ernst, L. A., Mujumdar, S. R., Lewis, C. J. & Waggoner, A. S. Cyanine dye labeling reagents: sulfoindocyanine succinimidyl esters. Bioconjug. Chem. 4, 105–111 (1993).
42. Murray, E. et al. Simple, Scalable Proteomic Imaging for High-Dimensional Profiling of Intact Systems. Cell 163, 1500–1514 (2015).
43. Power, R. M. & Huisken, J. A guide to light-sheet fluorescence microscopy for multiscale imaging. Nat. Methods 14, 360–373 (2017).
44. Santi, P. A. Light Sheet Fluorescence Microscopy: A Review. J. Histochem. Cytochem. 59, 129–138 (2011).
45. Liu, J. T. C. et al. Harnessing non-destructive 3D pathology. Nat. Biomed. Eng. (2021) doi:10.1038/s41551-020-00681-x.
46. Chozinski, T. J. et al. Volumetric, Nanoscale Optical Imaging of Mouse and Human Kidney via Expansion Microscopy. Sci. Rep. 8, (2018).
47. Jiang, N. et al. Superresolution imaging of Drosophila tissues using expansion microscopy. Mol. Biol. Cell 29, 1413–1421 (2018).
48. Richter, K. N. et al. Glyoxal as an alternative fixative to formaldehyde in immunostaining and super-resolution microscopy. EMBO J. e201695709 (2017) doi:10.15252/embj.201695709.